SEEBECK EFFECT AND ELECTRICAL CONDUCTIVITY

OF STANNIC OXIDE AS A FUNCTION OF TEM-

PERATURE AND AMBIENT PRESSURE

By

JAMES LUTHER RUTLEDGE

Bachelor of Science
Oklahoma State University
Stillwater, Oklahoma
1963

Master of Science
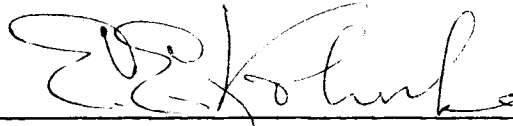Oklahoma State University
Stillwater, Oklahoma
1966

Submitted to the Faculty of the Graduate College
of the Oklahoma State University
in partial fulfillment of the requirements
for the degree of
DOCTOR OF PHILOSOPHY
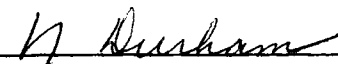May, 1968

There
is no
print on
copy.

SEEBECK EFFECT AND ELECTRICAL CONDUCTIVITY

OF STANNIC OXIDE AS A FUNCTION OF TEM-

PERATURE AND AMBIENT PRESSURE

Thesis Approved:

_____

Thesis Adviser

_____

_____

_____

Dean of the Graduate College

ii

ACKNOWLEDGMENTS

TABLE OF CONTENTS

LIST OF TABLES

LIST OF FIGURES

CHAPTER I

INTRODUCTION

Background Information

In recent years the study of the electrical properties of oxide
systems has grown tremendously[1,2,3]. As yet, however, these systems are
only partially understood[4]. One of the major experimental problems is
the lack of samples suitable for precise measurements. The variation in
the available samples has led to significant differences in the experi-
mental parameters associated with defect structure. Since conductivity
theories for compound materials are still evolving, much use is made of
the theory developed for the simpler elemental semiconductors such as
silicon and germanium.

Stannic oxide (SnO_2) has been used commercially for several appli-
cations[5,6,7], but a detailed understanding of its electronic processes
is still lacking in many respects. Reports of electrical measurements
on stannic oxide have been made by several authors. Most of this work
has been on thin films[8,9], pressed powders[10], sintered samples[11,12] and
natural crystals[13]. Recently, work on the electrical properties of
grown single crystals has been reported by Kunkle[14], Houston[15], Marley
and MacAvoy[16], Morgan and Wright[17], Nagasawa, Shionoya and Makishima[18],
and Marley and Dockerty[19]. These studies show limited quantitative
correlation, as might be expected due to differences in the nature and
number of defects in the samples and to the temperature ranges of in-

1

terest to the different groups.

Stannic oxide has the following properties which increase the difficulty of obtaining good experimental data:

a) Large pure single crystals are not available.

b) Crystal growth occurs at high temperatures leading to a large number of defects.

c) Chemical bonding is largely, but not completely, ionic.

d) Stoichiometry at high temperatures is dependent upon temperature and the partial pressure of oxygen in the ambient atmosphere.

e) The forbidden energy gap is large.

f) Defect activation energies appear to be comparable to the binding energies of the constituent ions.

As a consequence of these properties, many of the effects studied in the past are due to defects contained in the lattice of the particular sample being studied.

Scope of the Present Study

It has been the primary purpose of this study to determine which properties are inherent to the material itself and are not dependent upon crystal defects.

Intrinsic behavior predominates at high temperatures when the active, permanent defect density may be neglected. Two properties which may be conveniently measured at high temperatures are the Seebeck effect (thermoelectric power) and electrical conductivity.

In the absence of defect-controlled conductivity at high temperatures these measurements are sufficient to determine the mobility ratio

of holes and electrons, the intrinsic thermal band-gap and its varia-
tion with temperature, and the ratio of the effective mass of holes to
that of electrons[20,21]. At high temperatures thermal formation of de-
fects is possible by either stoichiometric or non-stoichiometric mechan-
isms. In the non-stoichiometric case evidence of oxygen ion motion is
available if the conductivity is dependent upon the ambient oxygen pres-
sure[22]. This dependence could occur in the region of defect formation,
in which case the activation energy would include the defect formation
energy, or might manifest itself at lower temperatures by providing a
different fixed defect structure and a higher conductivity level than
observed in untreated specimens.

An attempt has been made to determine the true nature of intrinsic
electronic behavior of stannic oxide and to correlate this behavior
with that of other materials having similar properties.

At lower temperatures the mechanisms controlling the defect struc-
ture have been studied by the use of both crystalline and polycrystal-
line samples. In this region the conductivity depends both on the den-
sity of bulk defects resulting from reduction at high temperatures and
the density of surface acceptor states associated with the chemisorption
of oxygen. The use of polycrystalline samples made possible studies of
surface controlled behavior through their larger surface-to-volume
ratio.

A model has been developed to explain the importance of past his-
tory of temperature and ambient pressure treatment for determining the
electrical properties of the ceramic samples in the region of surface
controlled conductivity. This model has been extended to non-equilib-
rium cases which occur following admission of air to a previously evacu-

ated sample.

Included also are certain suggestions for further study which should extend the understanding of the basic transport mechanisms associated with compound semiconductors.

CHAPTER II

THEORY OF SEMICONDUCTOR STATISTICS

General Aspects

This review of semiconductor statistics is designed only to touch upon salient points particularly pertinent to the measurements performed. The background and theoretical development of these concepts are presented in most introductory texts on solid state physics[21,23,24].

In general, according to the band theory of solids, there exist, separated by a forbidden energy gap, two bands in which free carriers (electrons in the conduction band, and holes in the valance band) are mobile and thus may be influenced by external or internal fields. In the simplest cases, in which the bands are not degenerate and the density of states can be approximated by a spherically symmetric parabolic function, $(N(E) \propto E^{\frac{1}{2}})$, these bands are characterized as having a fixed energy and a temperature dependent density of allowed states. The free carriers are characterized as having an effective mass and a temperature dependent mobility. These concepts are the result of appropriate averages of complex processes over space, time and energy.

In addition to these bands there exist impurity or defect levels (states) within the forbidden gap which are due to imperfections in the crystal. In these levels the carriers are normally not free to move under the influence of external fields, but the presence of the levels does affect the equilibrium densities of the mobile carriers. These

5

levels are normally classed as donors or acceptors depending upon whether they are positively or negatively charged upon ionization[21].

At equilibrium there exists a Fermi energy, E_F, such that the density of electrons in any state, j, is given by:

$$n_j = N_j \ \frac{1}{1 + \exp{(E_F - E_j)}/kT}$$ (1)

where: n_j = electron density of level j

N_j = state density of level j

E_j = energy of an electron in level j

k = Boltzmann's constant

and   T = absolute temperature.

This form is appropriate if energy is measured downward on the energy level schemes. In the further analysis the conduction band energy is taken to be zero. Thus all the energies to be treated in this review will be non-negative. For a visual representation the electron energy is plotted as a function of position in order to show the relative positions in energy space of all energies involved. Thus, in an energy level scheme, the electrons have a lower energy if they are in a state lower in the plot and holes have a lower energy if they are raised to a higher level. The lowest energy state then occurs when levels below the Fermi level are filled with electrons and those above are empty.

For the sake of simplicity, such factors as degeneracy of the electron gas, spin degeneracy of the state and the complexities of more than one ionization level of the defect are omitted for the present. Further details in these matters may be found in Semiconductor Statistics by Blakemore[24].

The electron occupation of the level is often approximated by Boltzmann statistics when the level lies more than 3kT in energy above the Fermi level. In this case:

$$n_j \approx N_j \exp \left[-(E_F - E_j)/kT\right].$$ (2)

When the level lies more than 3kT below the Fermi level it is usually convenient to speak of hole (or lack of electron) densities, p_j, since:

$$p_j = N_j - n_j = N_j \left(1 - \frac{1}{1 + \exp \ (E_F - E_j)/kT}\right)$$

$$= N_j \frac{1}{1 + \exp \left[- (E_F - E_j)/kT\right]}$$ (3)

$$\approx N_j \exp \ (E_F - E_j)/kT$$

which is a much easier form for mathematical manipulation. These forms are also correct for calculating the density of free carriers in either band provided that the proper density of state term (as given later) is used. The appropriate energies are those of the bottom of the conduction band or the top of the valence band in this case.

Figure 1 represents a simple energy level scheme in which the mathematical parameters are associated with the visual representation. In this case the densities are given by the Boltzmann approximation to the Fermi function.

Before leaving this introductory section it is to be noted that many of the above parameters are temperature dependent. A partial listing of these dependences are[23]:

$$N_{c,v} = 2 \left(\frac{2\pi m_{n,p} kT}{h^2}\right)^{3/2} = 4.82 \times 10^{15} \ (m_{n,p}^{*} T)^{3/2}$$ (4)

where: $m_{n,p}$ = effective mass of the electron, hole.
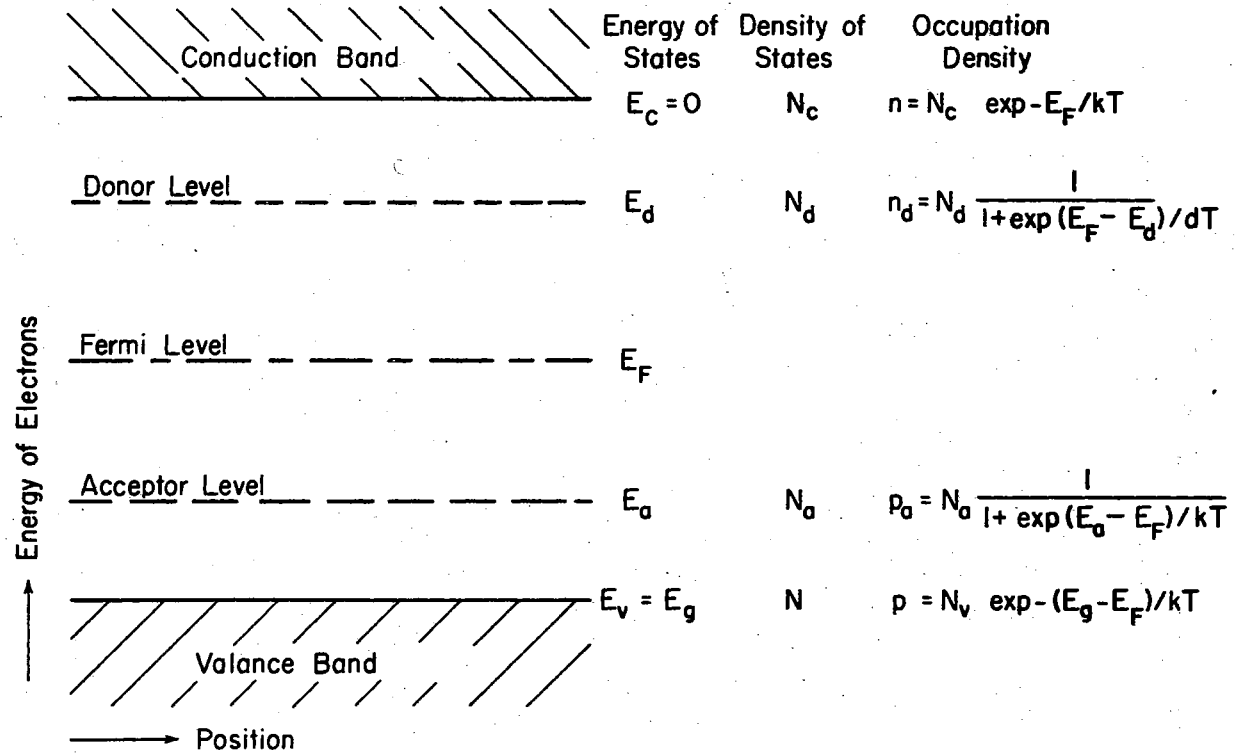
Figure 1. Energy Level Scheme for Simple Model

$m^{*}_{n,p}$ = effective mass of electron, hole, divided by the true electron mass

h = Plank's constant

$$E_g = E_{go} - \alpha T \tag{5}$$

where α and E_{go} are constants.

Relationship of Electrical Conductivity and
Seebeck Coefficient to the Fermi Energy

Since this study is primarily related to the measurement of electrical conductivity and thermoelectric power (Seebeck effect), the dependence of these properties upon the Fermi energy must be understood. As there are two sets of free carriers the effect of each type will be analyzed and then summed in the appropriate manner to give the desired relations for comparison to experiment.

The total electrical conductivity, σ, is composed of two components, that due to electrons, σ_n, and that due to holes, σ_p. These two conductivities are the products of the respective carrier densities their mobilities, μ_n and μ_p, and the electronic charge e. The mobilities are the average velocities per unit field strength of the free carriers. This property is temperature dependent and, for the case of simple lattice scattering, is proportional to $T^{-3/2}$.

Including the dependence of the carrier densities upon the Fermi energy one obtains:

$$\sigma_n = n \, e \, \mu_n = N_c \, e \, \mu_n \exp \left[- E_F/kT \right] \tag{6}$$

$$\sigma_p = p \, e \, \mu_p = N_v \, e \, \mu_p \exp \left[- (E_g - E_F)/kT \right] \tag{7}$$

and σ (measured) $= \sigma_n + \sigma_p$.

The thermoelectric power for electrons is related to the Fermi level and in non-degenerate cases is given by[20]:

$$Q_n = \frac{-E_F}{eT} - \frac{2k}{e} \tag{8}$$

in the case of simple lattice scattering. The term on the right is due the scattering mechanism and varies from this value to twice this value for several simple models.

A similar relation holds for holes and is given by[20]:

$$Q_p = \frac{E_g - E_F}{eT} + \frac{2k}{e}. \tag{9}$$

It is to be noted that these differ in sign and cannot be added quite so simply as the conductivities.

Upon application of the temperature gradient necessary for the measurement of this property the thermoelectric fields induce current flows which require the weighted sum[20],

$$Q = \frac{\sigma_n Q_n + \sigma_p Q_p}{\sigma_n + \sigma_p}, \tag{10}$$

for the total (or measured) thermoelectric power.

Single Donor Level Case

In many simple cases it is possible to calculate directly the Fermi energy which will in turn give the desired values for the experimental properties as seen in the previous section.

The simplest of all cases is the one in which a single donor level lies near the conduction band[24]. At low temperatures all the electrons participating in the conduction process arise from the donor level and

the valence band is completely filled so that the number of holes is negligible. Thus $\sigma_p = 0$ so $\sigma = \sigma_n$ and $Q = Q_n$.

One may determine the position of the Fermi level in non-degenerate cases by solving simultaneously the charge neutrality equation,

$$n + n_d = N_d, \tag{11}$$

the equation giving the density of conduction electrons,

$$n = N_c \exp - E_F/kT \tag{12}$$

and the equation giving the density of electrons in the donor level,

$$n_d = N_d \ \frac{1}{1 + \exp \ (E_p - E_d)/kT} \tag{13}$$

in which the use of Fermi statistics has been employed.

The solution for E_F is readily seen to be:

$$E_F = \frac{E_d}{2} + \frac{kT}{2} \ \ln \ (N_c/N_d) \tag{14}$$

Upon proper substitution one finds:

$$\sigma = e \ [N_c \ N_d]^{1/2} \mu_n \ \exp \ [- E_d/kT] \tag{15}$$

and

$$Q = \frac{-E_d}{2kT} - \frac{k}{2e} \ \ln \ N_c/N_d - \frac{2k}{e}, \tag{16}$$

which are the desired results.

At higher temperatures the donor level is completely exhausted and if $E_g \gg E_d$ no intrinsic electrons will contribute to the conductivity. This temperature region is termed the exhaustion region and the conductivity is given by:

$$\sigma = N_d \ e \ \mu_n \tag{17}$$

and the Fermi energy and thermoelectric power are given by:

$$E_F = kT \ln N_c/N_d \quad \text{and} \quad Q = \frac{-k}{e} \ln \frac{N_c}{N_d} + 2 \quad . \tag{18}$$

At still higher temperatures, significant numbers of electrons are thermally excited completely across the forbidden energy gap. When this density becomes much larger than the donor density the sample is said to be intrinsic. In this case the number of free holes is very nearly equal to the number of conduction electrons. Thus the set of equations:

$$n = p \tag{19}$$

$$n = N_c \exp -E_F/kT \tag{20}$$

$$p = N_v \exp (E_F - E_g)/kT \tag{21}$$

completely defines the system.

The solution for the Fermi level is:

$$E_F = \frac{E_g}{2} + \frac{kT}{2} \ln N_c/N_v = \frac{E_g}{2} + \frac{3}{4} kT \ln \frac{m_n}{m_p}, \tag{22}$$

where use is made of the relations for N_c and N_v.

This gives for the electrical conductivity:

$$\sigma = \sigma_n + \sigma_p = e(N_c N_v)^{\frac{1}{2}} \exp [- E_g/2kT] (\mu_n + \mu_p). \tag{23}$$

The thermo-electric power is given by:

$$Q = \frac{\sigma_n Q_n + \sigma_p Q_p}{\sigma_n + \sigma_p} = \frac{\mu_n Q_n + \mu_p Q_p}{\mu_n + \mu_p} = \frac{c Q_n + Q_p}{c + 1} \tag{24}$$

$$= \frac{-k}{e} \left\{ \frac{c - 1}{c + 1} \frac{E_g}{2kT} + \frac{2(c - 1)}{(c + 1)} + \frac{3}{4} \ln \frac{m_n}{m_p} \right\},$$

where c is the ratio of electron mobility to hole mobility.

Thus even such a simple model as that assuming a single donor

level gives three limiting regions of conductivity. Assuming that the pre-exponential temperature terms cancel, as in the case of simple lattice scattering, an Arrhenius plot ($\ln \sigma$ vs $1/T$) will show three slopes, one of which is related to $E_d/2$, another of zero slope, and the third related to $E_g/2$.

Similar, but more complex changes, occur in plots of the thermo-electric power which is also normally plotted against $1/T$.

As an example of this behavior, the thermoelectric power has been calculated and plotted (Figure 2) in three regions for a simple two-donor-level model. For this calculation the following parameters have been used:

$$E_g = 2 \text{ eV}, \quad E_{d1} = 0.4 \text{ eV}, \quad N_{d1} = 10^{16}/\text{cm}^3,$$

$$m_n = m_p = m_o, \quad E_{d2} = 0.8 \text{ eV}, \quad N_{d2} = 10^{18}/\text{cm}^3,$$

$$\mu_n/\mu_p = 10.$$

As the temperature is changed, the thermoelectric power must move along one curve, then move to another. As the behavior in the transi-tion region is unknown, it should be possible in certain cases for the slope to approach zero or even change sign. It is for this reason that care must be used in interpreting these curves over short temperature regions.

Heavily Compensated Donor Case

Real samples have many defects, and it is nearly impossible to produce a real sample which follows single donor level statistics. In general there may be several donor levels and several acceptor levels. The solution of such systems is very complex but they may often be
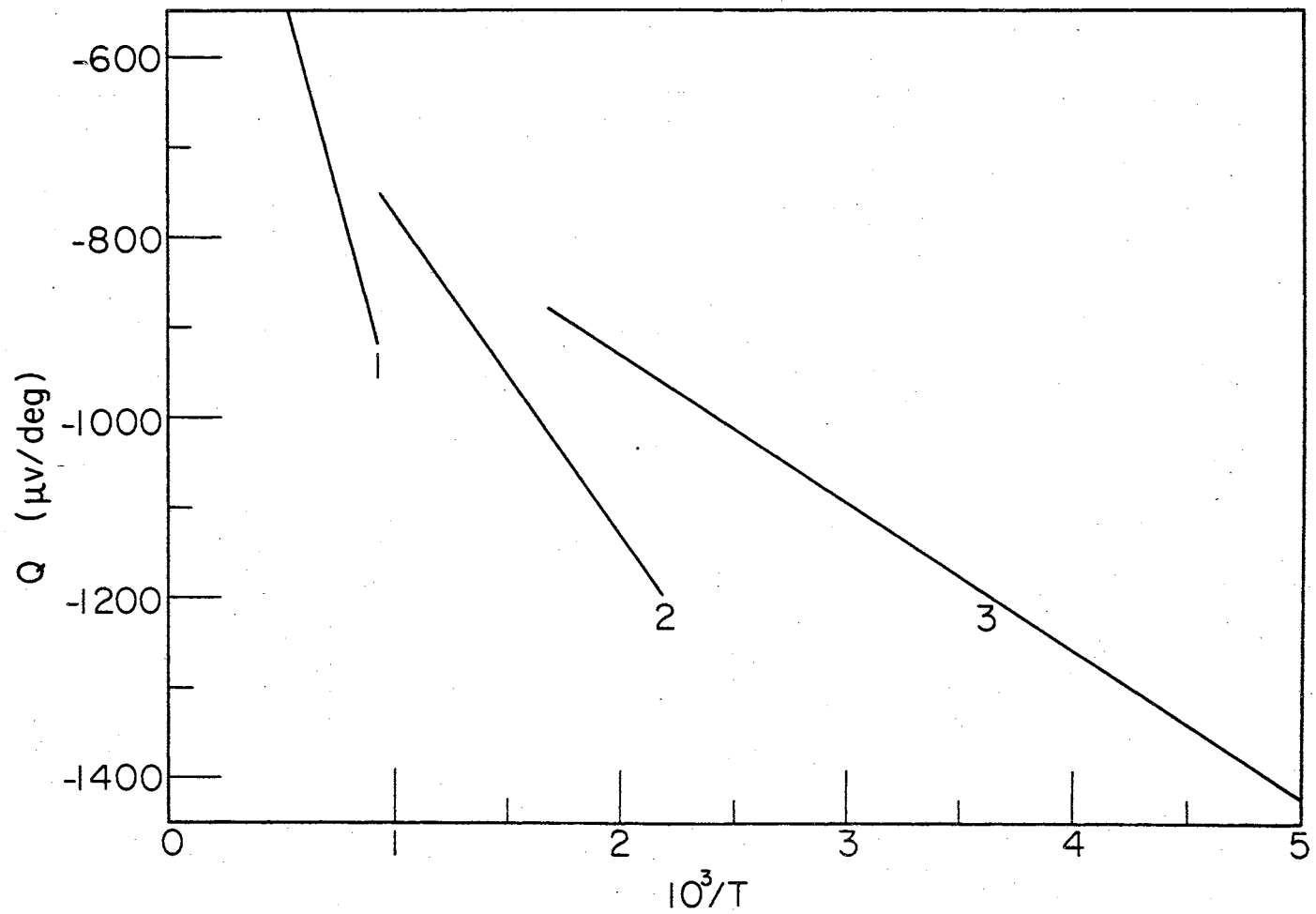
Figure 2. Thermopower Calculated From Simple Model

solved by graphical means by following the outline given by Shockley[23].

Blakemore[24] gives a solution to the case of a dominating donor level and several low-lying acceptor levels. The behavior associated with this model may qualitatively be applied to more complicated systems. This solution is based on the following relations:

1) $N_d > \Sigma N_a$ (25)

2) $\sigma_p = p = p_a = 0$ (26)

3) $n + n_d = N_d - \Sigma N_a.$ (27)

His result for a heavily compensated semiconductor, including the spin degeneracy factor, β, gives:

$$E_F = E_d - kT \ln \beta \frac{N_d - N_a}{N_a} , \qquad (28)$$

$$\sigma = \sigma_n = e\mu_n N_c \beta \frac{N_d - N_a}{N_a} \exp - E_d/kT , \qquad (29)$$

and

$$Q = Q_n = \frac{-E_d}{eT} + \frac{k}{e} \ln \frac{N_d - N_a}{N_a} - \frac{2k}{e} \qquad (30)$$

when $n \ll N_a < N_d.$

Due to the complexities of the solution, which includes an approximate Fermi distribution function, and the restrictions upon validity, it is wise to consult the original work for details and for solutions not restricted to this limiting case.

General Aspects of a Variable Defect Density

The concepts just discussed are applicable to many semiconducting materials. However, these results are appropriate only to systems in

which the defect density is constant with respect to all variables.

There are several mechanisms by which the defect concentration can vary with space, time or treatment. A space variation is commonly associated with the surface, at which intrinsic levels may exist[23] (due to a discontinuity in the nature of the system) and where there may be other levels arising from local chemical reactions[25]. Of particular interest in the latter case are levels with a time variation of density following the change of any parameter which affects the equilibrium chemisorption density.

The bulk density may vary with temperature alone if the major defect is an equilibrium thermal defect[26]. Also possible are bulk reactions in which the defect density is in equilibrium with the composition and pressure of the surroundings. Such reactions are commonly used for changing the nature of a material as in the reduction of oxides by a vacuum heat treatment[27].

In addition the very act of measuring a property, such as electrical conductivity, may affect the defect structure due to interactions with the measuring field.

It is normally expected that processes ocurring in the bulk would predominate at higher temperatures. Effects associated with the surface are normally expected at lower temperatures although these are only rough criteria as the energies involved in the different processes vary considerably from material to material.

Only in certain restricted cases have the effects of variable defect density been adequately treated. Some of these are included in the following sections.

Variable Defect Density at the Surface

In the study of semiconductors and insulators the surface is espe-
cially important, for here the material may chemically react with the
surroundings. It is also at the surface that a discontinuity of the
lattice potential occurs.

Surface states which arise from this discontinuity may be termed
intrinsic surface states[23]. Another important class of surface states
arising from interaction with the ambient atmosphere are chemisorption
states[25]. In either case it is possible for the surface to be charged[23],
and as a consequence the charge neutrality condition is valid only when
averages are taken over the whole sample and not at each point as was
assumed previously in equation 11.

The common effect of surface charge is to create a space charge
region near the surface[23]. When this exists, bands and other levels
within the sample are curved and do not lie everywhere equidistant from
the Fermi energy. As a consequence the occupation of a state depends
upon its distance from the surface. When a suitable model can be found
for calculating the band curvature, it is possible to average in an
appropriate manner so that theory and experiment will agree[23]. More
often the effect of a space charge region is neglected or included in
another term relating the bulk density of carriers to the measured para-
meters.

Quantitative calculations of the space charge region have been
given by several authors[29,30,31]. These are normally based on models
which unfortunately do not have general applicability. In work on
single crystals it is often possible to neglect the effects of a space
charge region since it usually comprises only a minor fraction of a

large sample in geometrical extent. In thin films and polycrystalline ceramic materials, however, this region may play a particularly important role.

In this study the effects of a space charge region have been only qualitatively included and no account has been taken of possible spatial variations of conduction electron densities. This is tantamount to treating the surface acceptor levels associated with chemisorbed oxygen as if they are equally distributed throughout the bulk and assuming that the other effect of a space charge region is to reduce the effective cross-sectional area of the sample.

Chemisorption Transients

The oxygen chemisorbed acceptor model has been used by several investigators[25,32,33] of oxides to explain their results. Quantitative calculations of transients have till now been less than satisfactory.

To determine the dynamics of a current transient due to formation of chemisorption sites upon a change of ambient, it is necessary to know the conduction mechanism applicable to the sample, the nature of the chemisorption sites, and the rate of formation of these sites.

The following model is applicable to heavily compensated semiconductors (i.e. $n \ll N_a < N_d$) upon which chemisorbed gas states exist as filled acceptor levels. For stannic oxide it is believed that oxygen is the active component of the ambient forming acceptor centers upon chemisorption.

Since the semiconductor in question is heavily compensated, the current for a fixed temperature and applied voltage is given by:

$$i = C \ (N_d - N_a)/N_a \qquad (31)$$

which is easily obtained from equation 29, where N_d and N_a are donor

and acceptor densities and C a constant including other material and

geometric parameters. In the limiting case where $n \ll N_a \approx N_d$

$$i \approx C \ (N_d - N_a)/N_d = C - C^\prime \ N_a. \tag{32}$$

In another limiting case in which $n \ll N_a \ll N_d$ the current is

given by:

$$i \approx C^{\prime\prime} \ (1 - N_a/N_d)/(N_a/N_d) \approx C^{\prime\prime} \ N_d/N_a \tag{33}$$

and
$$1/i \approx C^{\prime\prime\prime} \ N_a \tag{34}$$

To proceed further it is necessary to re-interpret N_a as being

composed of three components: a fixed bulk concentration, an initial

surface concentration, and a surface concentration which varies with

time. By defining x as the surface-to-volume ratio, q_o as the initial

surface density of acceptors, $q(t)$ as the time dependent density of

acceptors, one obtains:

$$N_a(t) = N_a^\prime + xq_o + x \ q(t) = N_a^* + x \ q(t). \tag{35}$$

At this point one needs to know the correct relation for chemi-

sorption rate, $q(t)$. In many cases it is found that the chemisorption

process obeys an Elovich rate law[34] i.e.

$$q(t) = A \ \ln \frac{t + t^\prime}{t^\prime} \tag{36}$$

where t is time and $t^\prime$ a constant. As yet this relationship does not

have a unique theoretical basis so care needs to be taken in the inter-

pretation of the constants involved.

Inserting this relation into Equations 32 and 34 yields

$$i(t) \approx C - C' \left\{ N_a^* + A \ln \frac{(t + t')}{t'} \right\}$$

$$\text{(37)}$$

$$\approx a - b \ln \frac{t + t'}{t'} \quad (n \ll N_a \approx N_d)$$

and

$$\frac{1}{i(t)} \approx C''' \left\{ N_a + x A \ln \frac{t + t'}{t'} \right\}$$

$$\text{(38)}$$

$$\approx c + d \ln \frac{(t + t')}{t'} \cdot \quad (n \ll N_a \ll N_d)$$

The intermediate case can also be easily developed but is less useful for simple comparison with experimental data.

Care must be taken in using these relations to insure that only one donor level is active during the process and that the electron occupation of the levels is essentially in "equilibrium" with the varying acceptor density.

In summary, the current should be proportional to $\ln(t + t')$ when the sample is very closely compensated. In this case the Fermi level lies somewhat below the active donor level. The current should be inversely proportional to $\ln(t + t')$ when the surface is relatively clean and the acceptor density is somewhat lower than the donor density. When this dependence occurs the Fermi level lies above the active donor level.

Self-Activated Conductivity

At constant temperature the Helmholtz free energy is a minimum for the equilibrium state. This free energy is given by:

$$F = U - TS$$

where U is the internal energy, T the absolute temperature and S the entropy. Since the entropy is a measure of the disorder there will always be some deviation from perfection in all crystalline systems at any finite temperature.

In certain cases the crystalline lattice may not be in equilibrium and still be "stable" in that the times involved in reaching the equilibrium state are very large. In other cases these times are short, and as the temperature of the system is changed a "new" set of defects is formed. If these defects are electrically active, then each temperature requires new values for the donor (or acceptor) density. Consequently, the previous discussion of the temperature dependence of conductivity is not complete as it has required that the defect concentration remain constant.

The term "self-activated-conductivity" (SAC) has been coined to specify the case in which the defects are equilibrium thermal defects[26].

The following analysis of SAC is extracted from the work of Vinetskii and Kholodar[26] and is only intended to exhibit the method of solution and to quote the results.

Consideration of the case restricted to Frenkel defects in a binary crystal in which only one sublattice is active greatly simplifies the calculations. In this case the defect is formed by the motion of an atom or ion from its lattice position to an interstitial position. This results in a donor and an acceptor state. (The vacancy is a donor if the active element is the anion sublattice.) This type of defect leads to the following energy scheme:

$$E_c = 0$$
$$E_a$$
$$E_d$$
$$E_v = E_g$$
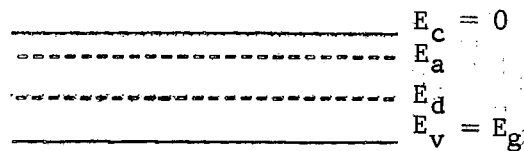
where E_c, E_a, E_d, and E_v are the energies of the conduction band, the acceptor level, the donor level, and the valence band. If the donor and acceptor levels are not interacting, then the grand cannonical ensemble probability of state, P, is given by:

$$P = \frac{N_c^n}{n!} \frac{N_c^p}{p!} \frac{N_d!}{n_d!(N_d - n_d)!} \frac{N_a!}{n_a!(N_a - n_a)!} \frac{N!}{N_d!(N - N_d)!} \frac{N'!}{N_a!(N' - N_a)!} \times$$

$$\text{(39)}$$

$$\exp\left[- \{N_d W + E_d(n - p) + (E_d - E_a)n_a + E_g p\}/kT\right]$$

where: N_c = density of states in the conduction band,

N_v = density of states in the valence band,

N_d = density of donors,

N_a = density of acceptors,

N = density of lattice sites (if a vacancy is a donor),

N' = density of interstitial sites,

n = density of conduction electrons,

p = density of free holes,

n_d = density of electrons in the donor level,

n_a = density of electrons in the acceptor level,

W = energy of formation of a Frenkel defect,

k = the Boltzmann constant,

and T = the absolute temperature.

The stoichiometry condition requires that the number of donors be the same as the number of acceptors. A further simplification is obtained by letting the number of lattice sites and interstitial sites be

equal. The most probable state is found by maximizing the probability of state which is most conveniently done by maximizing its logarithm (obtained by Stirling's approximation) with respect to n, n_d, n_a, and N_d, utilizing the charge neutrality condition:

$$n + n_d + n_a = N_d + p. \tag{40}$$

This gives, with some manipulation, the following system of equations:

$$np = N_c N_v \exp [- E_g/kT], \tag{41}$$

$$N^2 \exp [- W/kT] \exp (E_a - E_d)/kT = n_a (N_d - n_d), \tag{42}$$

$$N^2 \exp [- W/kT] = n_d (N_d - n_a), \tag{43}$$

$$pN^2 \exp (E_g - E_d - W)/kT = N_c (N_d - n_d) (N_d - n_a). \tag{44}$$

Elimination of n_a, n_d, N_d and p from equations 40, 41, 42, 43 and 44 gives the following equation for n:

$$n + N \exp [- W/2kT] \left\{ \frac{n(n + N_c \exp [- E_d/kT])}{N_c \exp [- E_a/kT] (n + N_c \exp [- E_a/kT])} \right\}^{\frac{1}{2}} = \tag{45}$$

$$\exp [- E_g/kT] + N \exp [- W/2kT] \left\{ \frac{n + N_c \exp [- a/kT]}{n N_c \exp [- E_a/kT](n + N_c \exp [- E_d/kT])} \right\}^{\frac{1}{2}}.$$

At this point it is readily noticed that if the defect formation energy is extremely large the second terms on the right and on the left are very small. This gives for n the expected relation:

$$n = (N_c N_v)^{\frac{1}{2}} \exp [- E_g/kT], \tag{46}$$

which is the result obtained earlier for intrinsic conductivity.

If the formation energy of defects is small, then these two terms are large and the first term on either side may be neglected. In this case:

$$n = N_c \exp \left[- (E_a + E_d)/2kT \right]. \tag{47}$$

Considering two other cases when only one term on each side is dominant gives:

$$n = (N \, N_c)^{\frac{1}{2}} \exp \left[- (W + E_d)/2kT \right] \tag{48}$$

and

$$n = (N^2 N_c)^{1/3} \exp \left[- (2W + E_d)/3kT \right]. \tag{49}$$

In these latter three cases the number of conduction electrons, n, is greater than the intrinsic value given in equation 46. It is to be further noted that if a material exhibits both intrinsic conductivity and SAC, then the intrinsic conductivity must occur at a lower temperature than SAC. The order in which the three cases of SAC occur is dependent upon the densities and energies involved.

Vinetskii and Kholodar[26] also treat the case of a frozen donor defect of density N_o in addition to the above system. This yields six relations for n of which only two are not given above. They are:

$$n = (N_c N_d)^{\frac{1}{2}} \exp \left[\frac{-E_d}{2kT} \right] \tag{50}$$

and

$$n = N_o \tag{51}$$

which are identical to relations for a donor level not involving thermal production of defects.

As a consequence several different activation energies may be cal-

culated from an Arrhenius plot of electrical conductivity. It is then necessary to ascertain which region of conductivity is prevalent (or even if the region is a transition region) if the calculated activation energy is to be correctly interpreted.

Oxygen Pressure Dependence of Conductivity

Electrical conductivity is known to vary with the partial pressure of oxygen in many metal oxides. This phenomena is normally associated with the formation of defects and a good general treatment is given by Kroger and Vink[35]. The analysis reviewed here is that of Kevane[22] and is restricted to pure metal oxides.

In this treatment the only source of conduction electrons is the ionization of oxygen vacancies. It is further assumed that the only carriers are electrons and that they have only one conduction state. As a consequence the only reactions to be considered are

$$O^{--} \rightleftharpoons V_A^{\cdot\cdot} + 2e^- + \tfrac{1}{2} (O_2)_g, \tag{52}$$

$$V_A^{\circ} \rightleftharpoons V_A^{\cdot\cdot} + e^-, \tag{53}$$

and

$$V_A \rightleftharpoons V_A^{\circ} + e^- \tag{54}$$
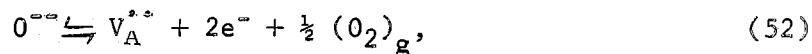
where e^- is a conduction electron, V_A, V_A°, $V_A^{\cdot\cdot}$ are un-ionized, singly ionized, or doubly ionized oxygen vacancies, O^{--} the oxygen ion in the lattice and $\tfrac{1}{2}(O_2)_g$ an oxygen atom in the ambient gas.

If the law of mass action leads to relations involving concentrations of the above quantities and equilibrium constants, they are:

$$[e^-]^2 \, [V_A^{\cdot\cdot}]P^{\frac{1}{2}} = K_2 \, (T), \tag{55}$$

$$[e^-] \, [V_A^{\bullet\circ}] = K_3 \, (T) \, [V_A^{\bullet}], \qquad (56)$$

and

$$[e^-] \, [V_A^{\circ}] = K_4 \, (T) \, [V_A] \qquad (57)$$

where [ ] denotes concentration and P is the oxygen partial pressure.

The charge neutrality equation

$$[e^-] = [V_A^{\bullet}] + 2 \, [V_A^{\bullet\bullet}] \qquad (58)$$

is used with equations 55, 56 and 57 to solve explicitly for the density of conduction electrons ($[e^-] \equiv n$).

The solution as taken from Kevane's[22] paper is given in figure 3. It is to be noted that in the high pressure region $[e^-] \, \alpha \, P^{-1/6}$ while in the low pressure region $[e^-] \, \alpha \, P^{-1/4}$. In the transition region, which is slow changing, it is possible to obtain a good fit of $[e^-] \, \alpha \, P^{-1/5}$ over six orders of magnitude of change in oxygen pressure. As a consequence it is possible to experimentally observe any power dependence between these two limiting values and still be concerned with the oxygen vacancy mechanism. Unfortunately, other mechanisms of defect formation predict rather similar behavior and consequently it is practically impossible to uniquely identify the actual defect mechanism of conductivity as a function of oxygen pressure.

By considering the limiting cases, i.e. $[e^-] \, \alpha \, P^{-1/6}$ and $[e^-] \, \alpha \, P^{-1/4}$, it is possible to extract a temperature dependence of conductivity at constant pressure. For this calculation it is necessary to obtain the temperature dependence of K_2 and K_3. Kevane[22] gives the following:

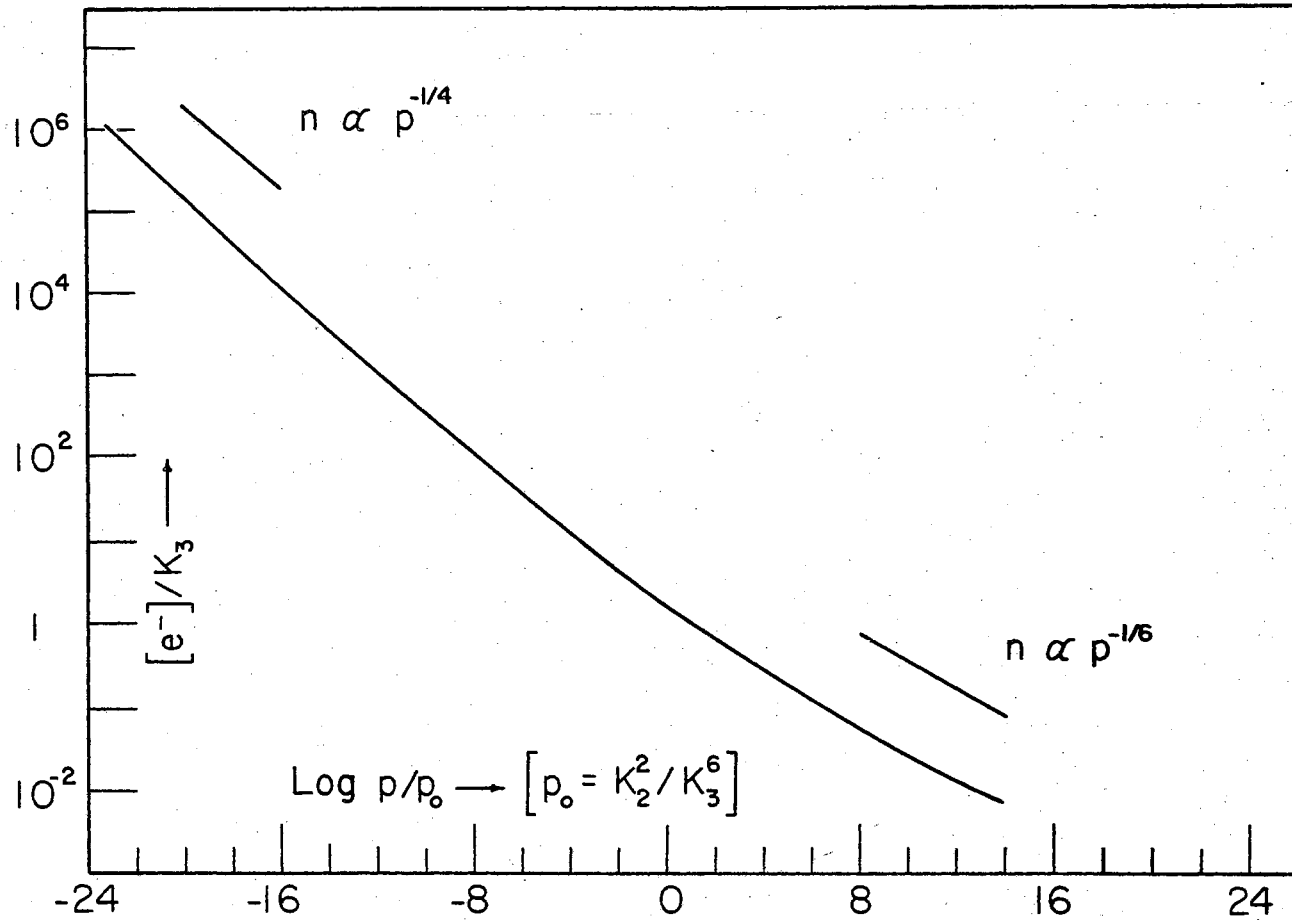$$K_3 \, (T) = N_c \, \exp \, [- \, eV_2/kT] \qquad (59)$$

and

Figure 3. Dependence of Carrier Density Upon Pressure

$$K_2 (T) = K_{20} \exp [-eV_{fi}/kT] \tag{60}$$

where eV_2 is the second ionization energy of the vacancy, K_{20} a constant, and eV_{fi} the energy necessary to form a doubly ionized oxygen vacancy.

Consequently, for the higher pressure region

$$n \propto \exp [\frac{-eV_{fi}}{3kT}], \quad P = \text{const.} \tag{61}$$

and at lower pressures

$$n \propto \exp [- \frac{(eV_{fi} - eV_2)}{2kT}], \quad P = \text{const.} \tag{62}$$

As indicated in Figure 3, these pressures are relative and the actual pressure required to be in either region depends upon K_2 and K_3. Since K_2 and K_3 are temperature dependent, the temperature dependence of conductivity at constant pressure is more complicated in the intermediate region.

Field Induced Transients

It is to be noted that any electrical field exerts a force on all charged particles, and, as a consequence, electrical conductivity may also result from ionic motion. In certain ionic materials such as the alkali halides the conduction is due entirely to ions[4]. In other substances conductivity may be a mixture of electronic and ionic conduction. Some materials, e.g. MgO^{36}, conduct at different temperatures by either ionic or electronic mechanisms.

Ionic conductivity is similar to electronic conductivity in that there is an intrinsic conductivity at high temperatures and an extrinsic ionic conductivity at low temperatures[4]. Studies made on mixed

conductors normally include galvanic cell measurements by which transport numbers for specific current carriers are determined[36,37]. (The transport number for species "i" is defined as the ratio of the conductivity due to species "i" to the total conductivity.)

It is to be expected that all conductors whose bonding is partially ionic exhibit some ionic conductivity, and as a consequence the effects of ionic conduction must be taken into consideration if there is any evidence of ionic motion. Treatments of ionic conductivity and the determination of transport numbers have been given by Vest[38], Kingery[4], Mitoff[36] and Wagner[37].

Of interest, at this point, is a more subtle aspect of ionic conductivity which can occur even if the transport number for ions is very small. By considering an electronic conductor with a small contribution due to ions, one may easily calculate that the rate at which ions of species i cross a unit plane perpendicular to the field is:

$$\frac{dN_i}{dt} = \frac{1}{q_i} \frac{V}{L} \sigma_i \qquad (63)$$

where V is the applied potential, q_i the valence state of the ionic species, L the length of the sample and σ_i the conductivity due to the ionic species. For a unit field and an ionic conductivity (σ_i) of 10^{-6} $(\Omega\ cm)^{-1}$ this equation implies that around 10^{12} ions/second cross a unit (1 cm^2) plane perpendicular to the field. In semiconductor statistics this number is too large to be neglected.

If the electrodes cannot accept and replace via an electrolysis reaction the ions at the required rate they are termed blocking or partially blocking electrodes. In this case, there develops a concentration gradient of the mobile ionic species which induces a diffusion

current in the opposite direction. If the applied field is small enough, a steady state condition will be reached for blocking electrodes with a concentration gradient given by

$$\frac{\overrightarrow{dN}}{dx} = \frac{qe}{kT} \cdot \frac{\overrightarrow{E}(x)}{D(x)}, \tag{64}$$

where $\overrightarrow{E}(x)$ is the electric field vector and $D(x)$ the diffusion constant of the ionic species. This gradient must now be considered as a defect level in calculating the desired electrical properties. The solution is difficult due to the dependence of $\overrightarrow{E}(x)$ upon the externally applied field, the density of conduction electrons (n), ionic species (N), and all other charges in the material (P, N_d^+, N_a^-, ...).

At even higher voltages $\frac{dN}{dx}$ may become so large that the material is no longer stable and decomposition occurs[38].

In view of the lack of a satisfactory solution to this problem it is advisable to reduce it to a minimum when making experimental measurements. This may be accomplished by the use of low D.C. fields which should not greatly perturb the sample, or the use of A.C. or pulsed D.C. measurements which do not allow enough time for the ionic motion to occur.

As this mechanism gives rise to a field dependence of conductivity it may easily be mistaken for space charge conduction. In view of the present state of the theoretical treatment of both cases care must be taken to avoid making the incorrect identification.

CHAPTER III

EXPERIMENTAL DETAILS

Sample Description and Properties

Experimental measurements were taken on three types of samples:
single crystals, porous ceramics, and dense ceramics. The methods were
initially restricted to those which would be applicable to the single
crystals since the analysis of polycrystalline ceramic specimens is
complicated by the possible presence of additional conduction mechan-
isms.

The single crystals were grown by the flux growth technique re-
ported by Kunkle[39]. They were grown from a cuprous oxide melt in a
platinum crucible at a temperature around 1225°C. After a period of
one week, crystals in the form of needles, platelets, and rods were re-
moved from the cooled melt with hot hydrochloric acid. The measure-
ments were restricted to the rod shaped crystals which will now be de-
scribed.

The rods formed a parallelopiped with the long axis along the c-
direction. The cross section is square in shape. Typically the side
of this square was $\frac{1}{2}$ mm while the rod length was 2 to 3 mm.

After selection on the basis of freedom from visible flaws, the
ends of the rod were ground flat on silicon carbide paper taking care
not to damage the longitudinal faces. Following cleaning with aqua
regia, organic solvents and distilled water, they had a nominal resis-

tance of 10^{12} ohms at room temperature.

The two types of ceramic samples were prepared by H. E. Matthews[40] by a pressing and firing procedure described in his M.S. Thesis.

The dense ceramic specimens were doped with 0.7% ZnO in a base of reagent grade SnO_2. After pressing to 10,000 psi and firing at 1460°C for 4 hours their density was 6.4 gm/cm^3 which is roughly 90% of crystal density (7.0 gm/cm^3). The grain size resulting from this sintering process is around 5 microns. The resultant ceramic pellets were very hard and strong with a white color.

The porous or pure ceramic specimens were pressed from reagent grade SnO_2 and fired at 1245°C for 16 hours. They had a density of 4.4 gm/cm^3 and were somewhat weaker as they chipped easily. Their grain size was around 2 microns. Again the samples were white in color.

As fired the samples were disks 1/2 inch in diameter and 1/8 inch thick. Samples approximately 4 mm x 2 mm x 2 mm were cut from these disks with a carborundum saw. After cleaning in the same manner as the single crystals, they were very resistive (around 10^{13} ohms) at room temperature.

Experimental Requirements

The size and resistance of the samples, as well as the desired range of measurements, impose severe restrictions upon the design and construction of the sample holder. Electrically the sample holder must have a very high leakage resistance ($\sim 10^{14}$ Ω). In addition the construction materials must be capable of withstanding high temperatures at high and low pressures. There must be provisions for making electrical contact to the sample and temperature measurement at the points

of contact.

In addition the sample needs to be enclosed in a vacuum tight chamber in which the pressure and constitution of the atmosphere may be varied. As stannic oxide is a photoconductor, the sample must be shielded at all times from extraneous light sources.

The temperature of the sample needs to be variable, and a furnace or heater is necessary for this purpose. The conductivity measurements should be taken with no temperature gradient across the sample; whereas the thermoelectric power measurement requires a temperature difference of approximately 10°C across the sample. This requires either a moveable furnace or a furnace constructed with two or more separately con-trolled heating elements.

Due to the difficulty of meeting these requirements it was decided to measure the sample resistance with the two-probe method instead of the more desireable four-probe method. The resulting design consists of a sample holder which can be inserted into a 1 1/4" diameter ceramic tube. The electrical leads are all led out through the vacuum flange on which the sample holder is mounted. The ceramic tube which houses the sample, is connected to an atmosphere control system and is sur-rounded by a moveable tube furnace.

Atmosphere Control System and Sample Chamber

Figure 4 is a block diagram of the sample chamber and atmosphere control system. By manipulating the gas inlet valves and the valve to the diffusion pump any pressure down to 10^{-7} torr could be maintained at lower temperatures. At high temperatures (~ 1200 °C) the low pressure limit was only 10^{-5} torr due to outgassing and/or diffusion through the
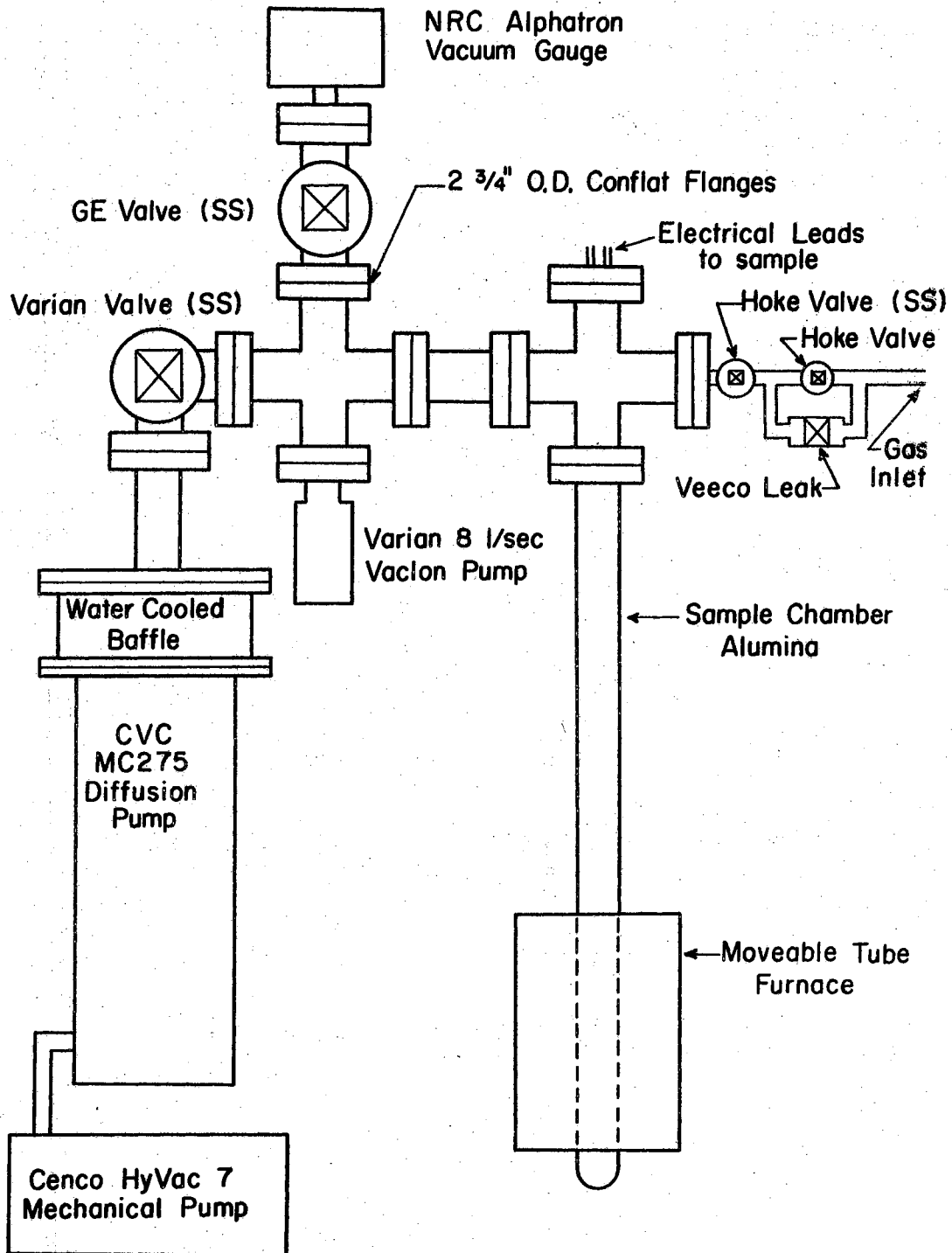
Figure 4. Ambient Control System

chamber walls.

Pressure readings from 10^{-4} torr to 760 torr were obtained with the Alphatron vacuum gauge, while lower pressures were obtained from the built-in pressure indicator associated with the Vacion pump. The diffusion pump was added after the system was designed due to the large gas load at high temperatures.

All vacuum seals in the main chamber are Con-Flat 2 3/4" O.D. flanges except for the ceramic-to-metal seal which connects the alumina sample chamber to the remainder of the system. For this seal a Con-Flat flange was machined to accept the ceramic tube, which was then glued into place with Varian Torr Seal vacuum epoxy. As this joint must be maintained at a temperature below 100°C, it was necessary to place the sample and the heater some distance away.

Prior to installation of the ceramic chamber the system could be evacuated to the 10^{-9} torr range as indicated by the Vacion pump control unit. To reach this pressure it is necessary to valve off the Alphatron gauge head and the diffusion pump as well as heat the chamber thoroughly for outgassing purposes.

Sample Holders

Two different two-probe sample holders were constructed; one of quartz and the other of high purity alumina ceramic. As both were similar, only the ceramic sample holder will be described.

Figure 5 is a detail sketch of the platinum and ceramic components of this holder. The platinum contact plates are held to the ends of the two-hole alumina capillary by the lead wires. The upper alumina capillary is spring loaded and presses the contact plates against the
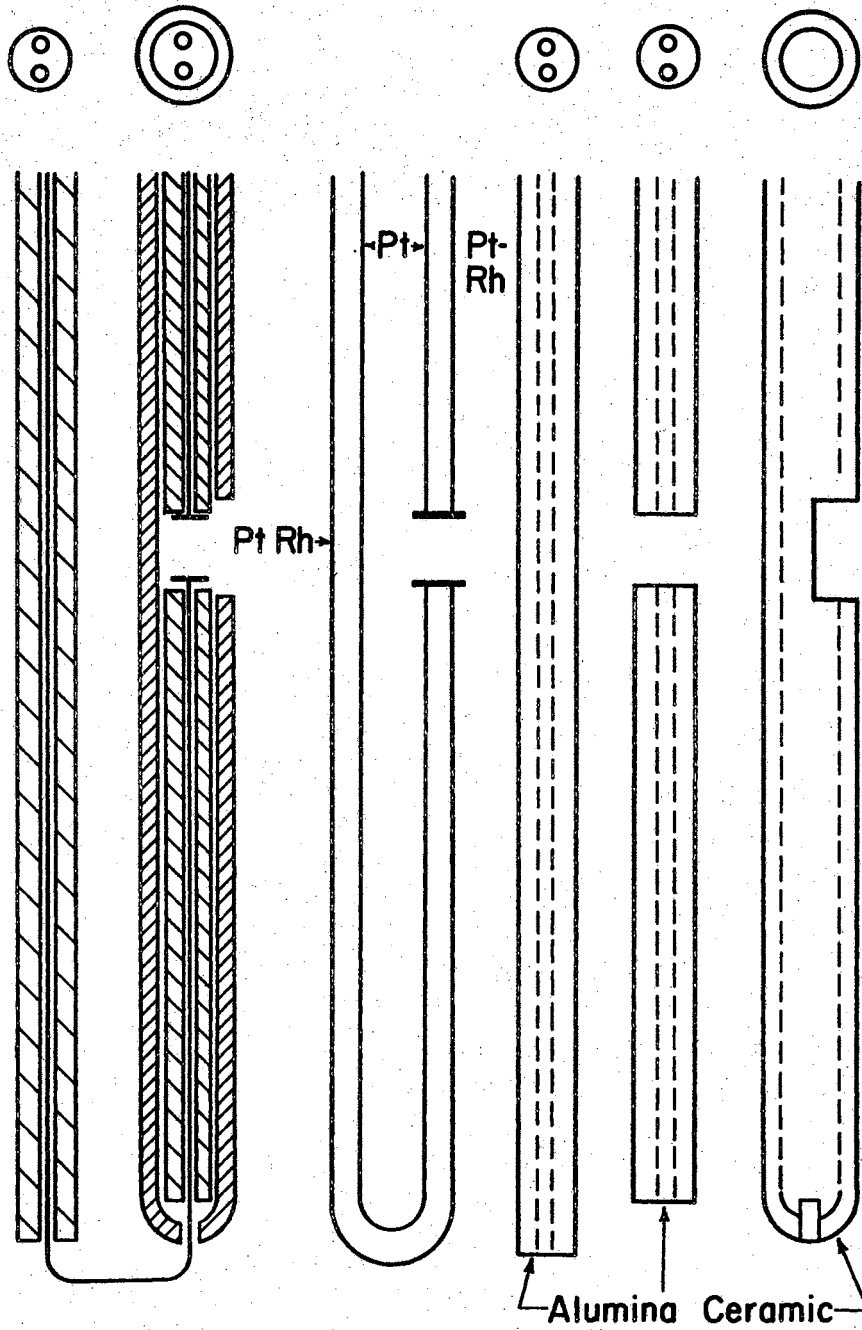
Figure 5. Two Probe Sample Holder

sample. The larger alumina tube serves to hold the two capillaries in alignment while the long capillary to the side serves to support the leads to the bottom of the sample.

The method of supporting the ceramic components is shown in figure 6. Where necessary the brass is glued to the ceramic with Torr Seal epoxy. The vacuum seal is accomplished by gluing the ceramic capillary into the stainless steel flange. The lead wires are sealed to the ceramic with Torr Seal epoxy in such a manner that the only electrical leakage path is through alumina.

During the course of the study current transients were noticed. Consequently it was felt that four-probe measurements were necessary to determine whether the resistance changes were due to the contacts or were truly a bulk effect. Because of small size of the single crystals it was decided to restrict the four-probe measurements to the larger ceramic specimens. The resulting four-probe sample holder is depicted in figures 7 and 8. It is designed for conductivity measurements on samples approximately 1/2 inch long and 1/8 inch on the side and is constructed of alumina ceramic and platinum. The vacuum seal is again accomplished with Torr Seal epoxy.

Electrical Circuitry

Earlier it was noted that four leads were attached to the sample. On either end were one platinum and one platinum-10% rhodium lead attached to a common platinum contact. By attaching a reference junction and a Sargent model SR recorder to either pair the temperature of that end of the specimen could be determined. By attaching an electrometer and a battery in series with the sample via the platinum leads the cur-
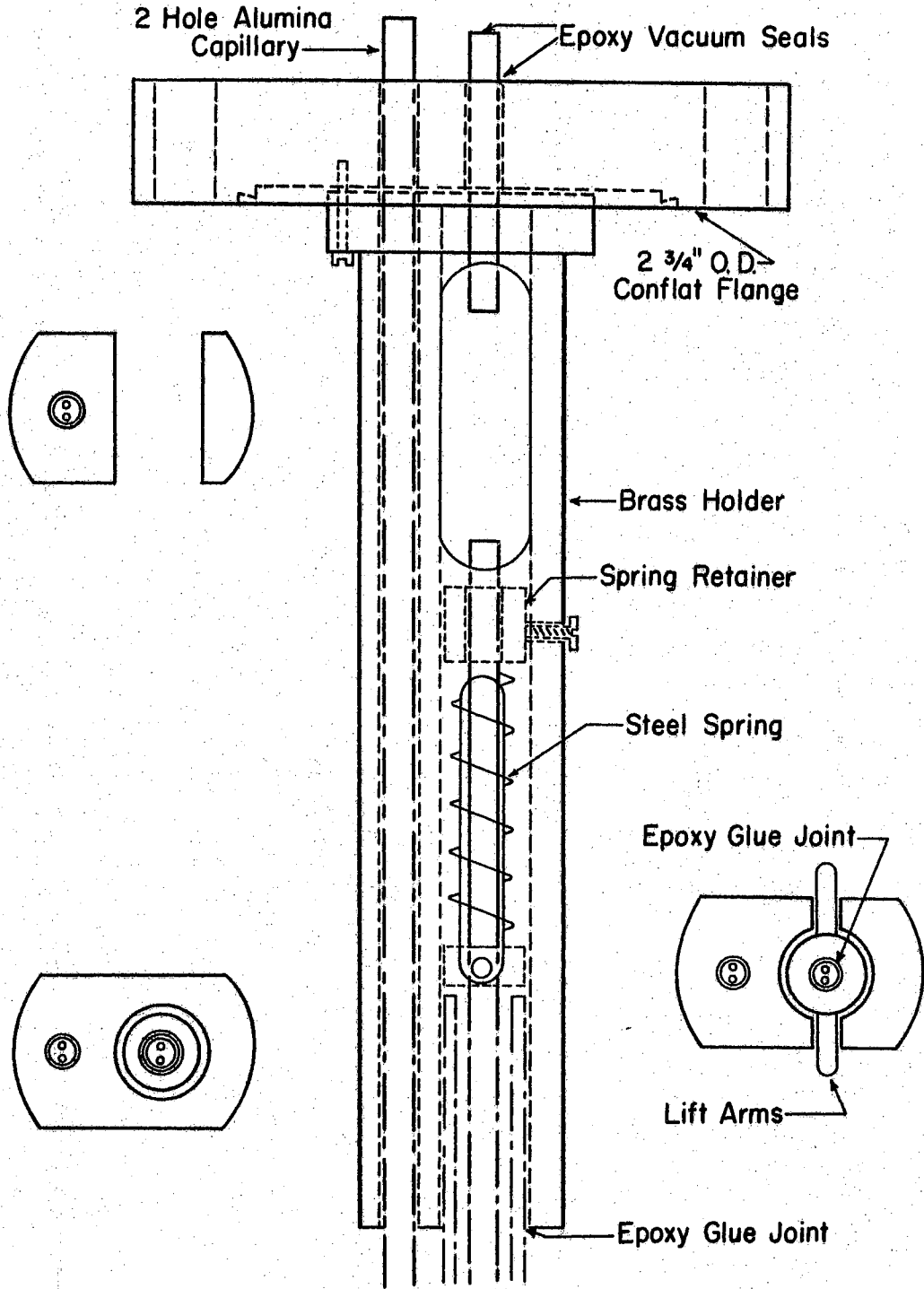
Figure 6. Support and Pressure Mechanism
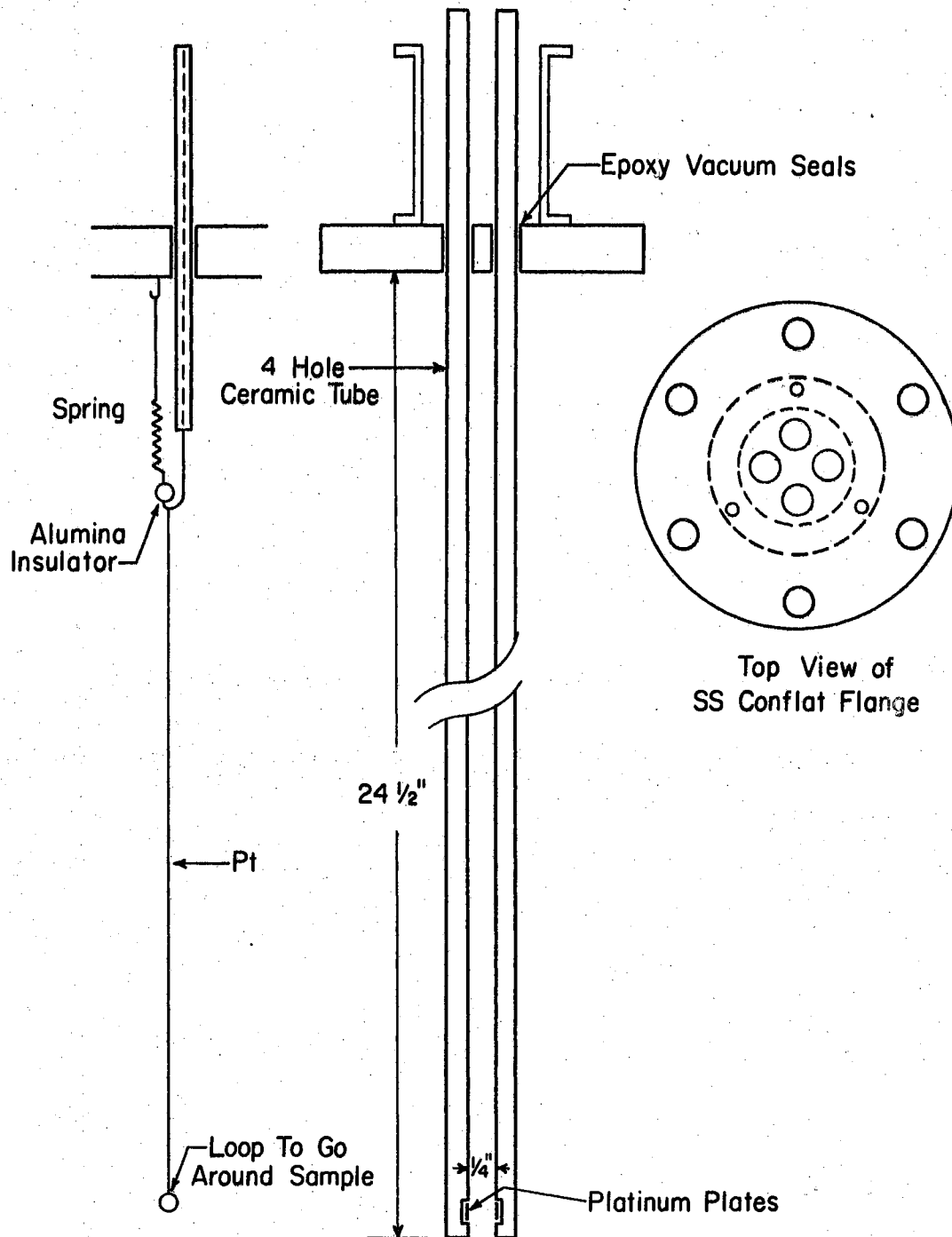for Two Probe Sample Holder

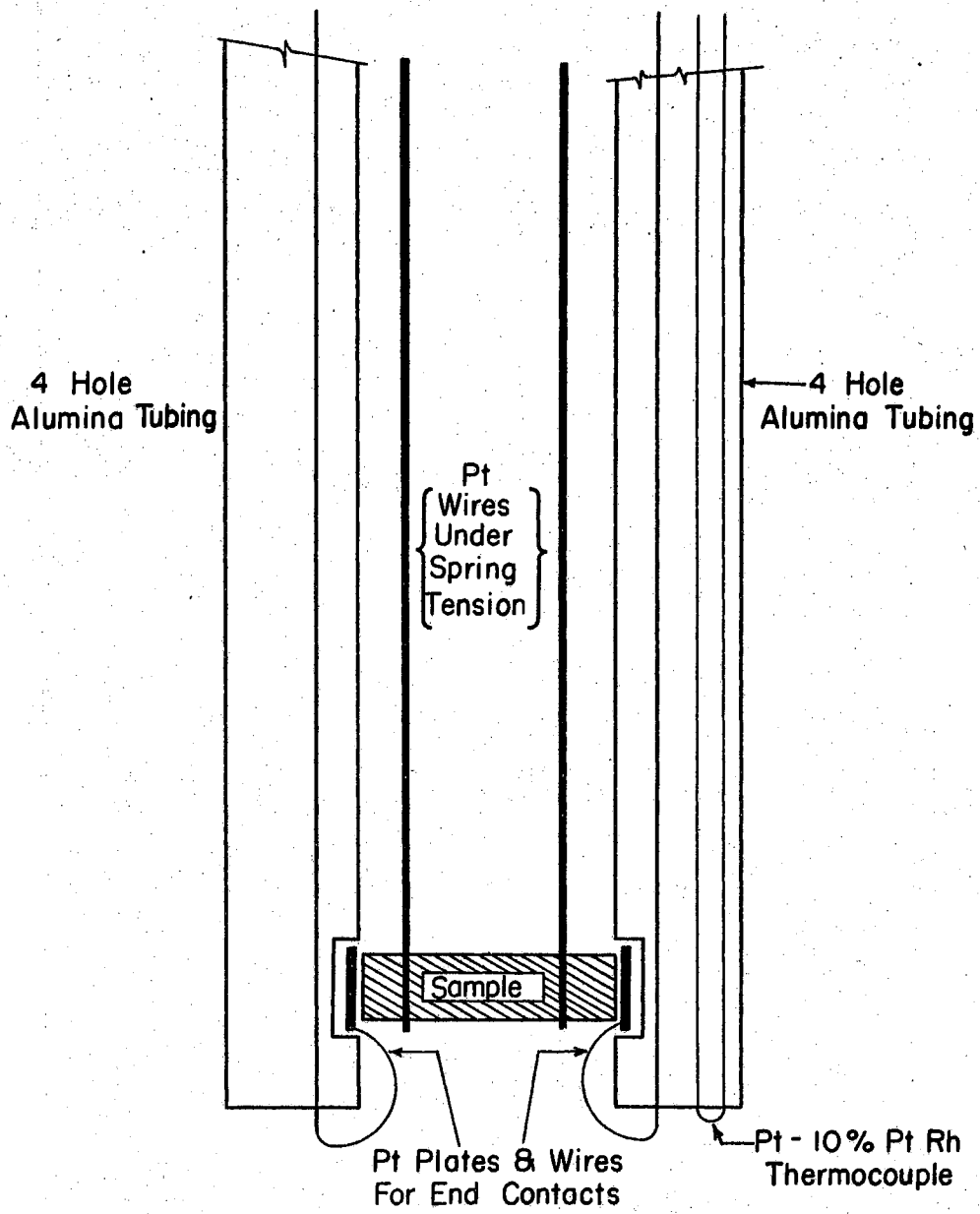Figure 7. Overall View of Four Probe Sample Holder

Figure 8. Detail of Sample End of Four Probe Sample Holder

rent could be measured thus giving the resistance. Upon removal of the

battery and switching the electrometer to the voltage range the electro-

meter could read the thermoelectric voltage across the samples. Thus

all the necessary parameters could be readily measured.

The circuit diagram, figure 9, indicates the switching network

used to connect the desired wires to the measuring apparatus. The

switches used in this circuit are Shallcross Series 4 which have an in-

sulation resistance greater than 10^{12} Ω and a contact resistance less

than 2×10^{-3} Ω. The thermocouple connections were made with Leeds and

Northrup quick disconnect thermocouple connectors. All other connec-

tions used Amphenol series 82 connectors. Though not shown in the

drawing this circuit is completely shielded.

Table 1 indicates the functions of the five switches involved in

this circuit. It must be noted that in addition to correct settings of

these switches the Keithley 610 B electrometer must be in the correct

range and mode (i.e., current or voltage). The purpose of the circuit

composed of R_1, R_2, S_3, S_4, and S_5 is to improve the accuracy of measur-

ing ΔT needed for the thermoelectric power measurements. It is used to

electrically subtract a portion of the thermocouple voltage so that the

two temperatures may be read on the most sensitive (1.25 MV) scale of

the Sargent recorder. This circuit is not calibrated so the difference

voltage was read directly and converted to a temperature difference by

means of thermocouple tables. This differential temperature should be

accurate to within 1°C.

As is apparent, the sample may be grounded to the case or through

the thermocouple lead. The provision for removing the thermocouple

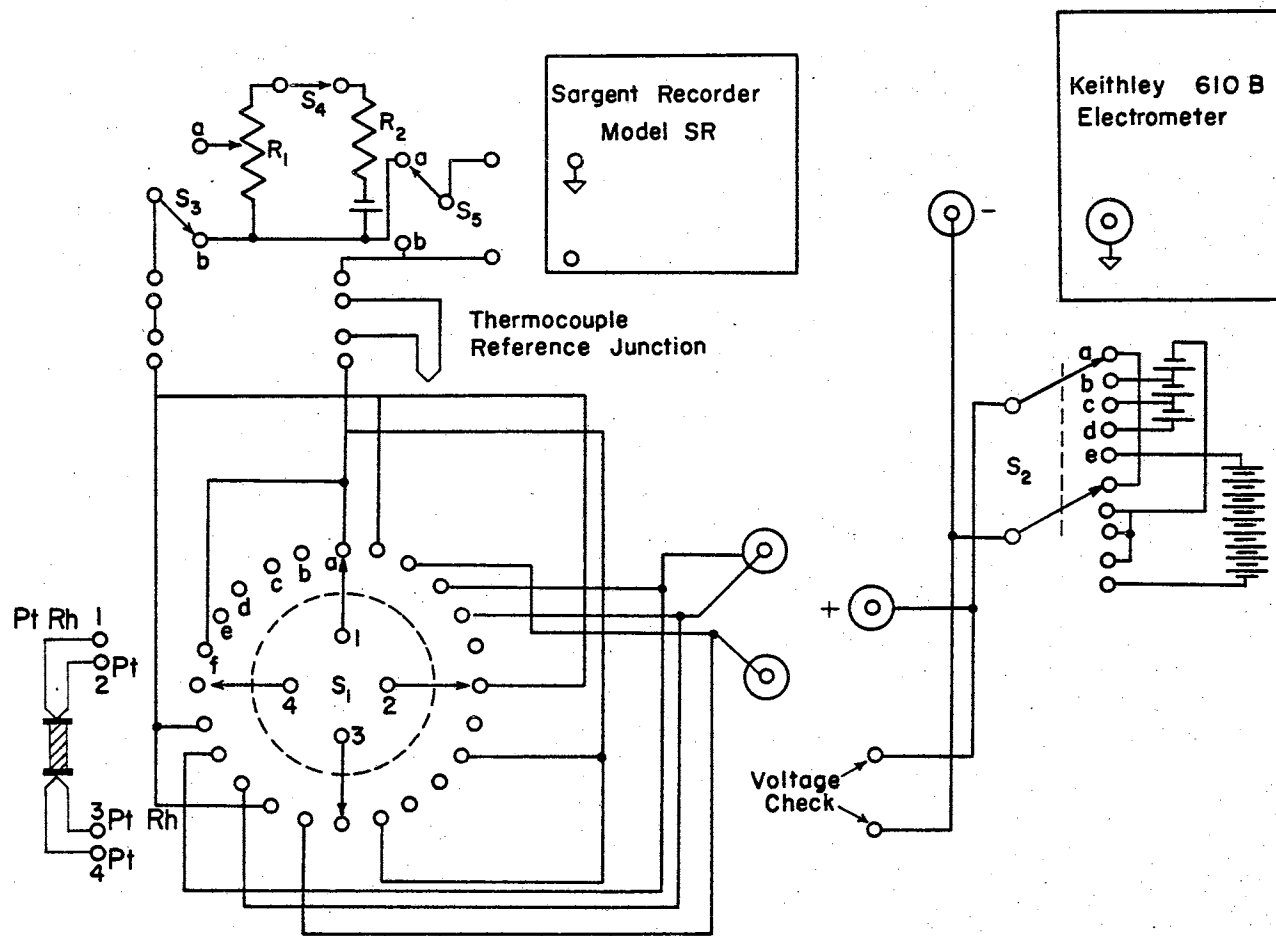while measuring currents is due to the IR voltage drop in the thermo-

Figure 9. Schematic Diagram of Electrical
Circuitry for Two Probe Sample
Holder

Switch Number	Function	Settings
1	Sample Selector	6 Position
2	Battery Voltage	5 Position
3	Bucking Voltage	on - off
4	Bucking Power	on - off
5	Recorder Shorting	TC - short

Stepwise Readout for Conductivity and Thermopower

Reading Number	Reading	Switch Number and Position				
		1	2	3	4	5
1	Top Temp.	a	Na	b	Na	a
2	Top Temp. w Bucking	a	Na	a	c	a
3	Bottom Temp.	b	Na	b	Na	a
4	Bottom Temp. w Bucking	b	Na	a	c	a
5	Fwd. Thermal Voltage	c	a	Na	Na	b
6	Reverse Thermal Voltage	d	a	Na	Na	b
7	Reverse Current	d	b,c,d,e	Na	Na	b
8	Fwd. Current	c	b,c,d,e	Na	Na	b

(Readout Order 1,2,4,5,6,7,8)

Continuous Monitor of Current and Temperature

Reading Number	Reading	1	2	3	4	5
9	Fwd. Current Bottom Temp.	e	b,c,d,e	b	Na	a
10	Reverse Current Top Temp.	f	b,c,d,e	b	Na	a

Table I.   Switch Information for High Temperature
Conductivity and Thermopower Apparatus

couple lead which introduces an error in the thermocouple voltage when "large" currents ($> 10^{-6}$ amps) are flowing.

The lead resistance must be taken into account when the sample resistance is low. Consequently, the sample contacts were pressed together and the lead resistance measured as a function of temperature in order that this correction could be made. At this same time measurement of temperature as indicated by both thermocouples was made in order to evaluate the possibility of error due to different couples. This difference voltage corresponded to less than 0.2 degrees in all temperature ranges.

Due to slightly different wiring of the quartz sample holder it was used for making some low frequency (10 and 100 cps) A.C. conductivity measurements in accordance with the schematic figure 10. For this measurement the Keithley 610B electrometer was used as a unity gain amplifier. The electrometer amplifier has a frequency response from 0 to 200 cps but the circuit is effectively limited to measurements of sample resistance less than 10^4 Ω due to RC time effects.

In order to reduce the sample voltage for some measurements, the sample holder and electrometer were connected according to figure 11. In this mode of operation the sample resistance (R_x) is given by:

$$R_x = \frac{V_k}{V - V_k} R_s - R_L \tag{65}$$

where R_L is the lead resistance, V_k the voltage read on the electrometer, V the applied voltage, and R_s the series current limiting resistor. Measurements taken in this manner were limited to higher temperatures. Normally the sample voltage was less than 0.1 volts when this circuit was used.
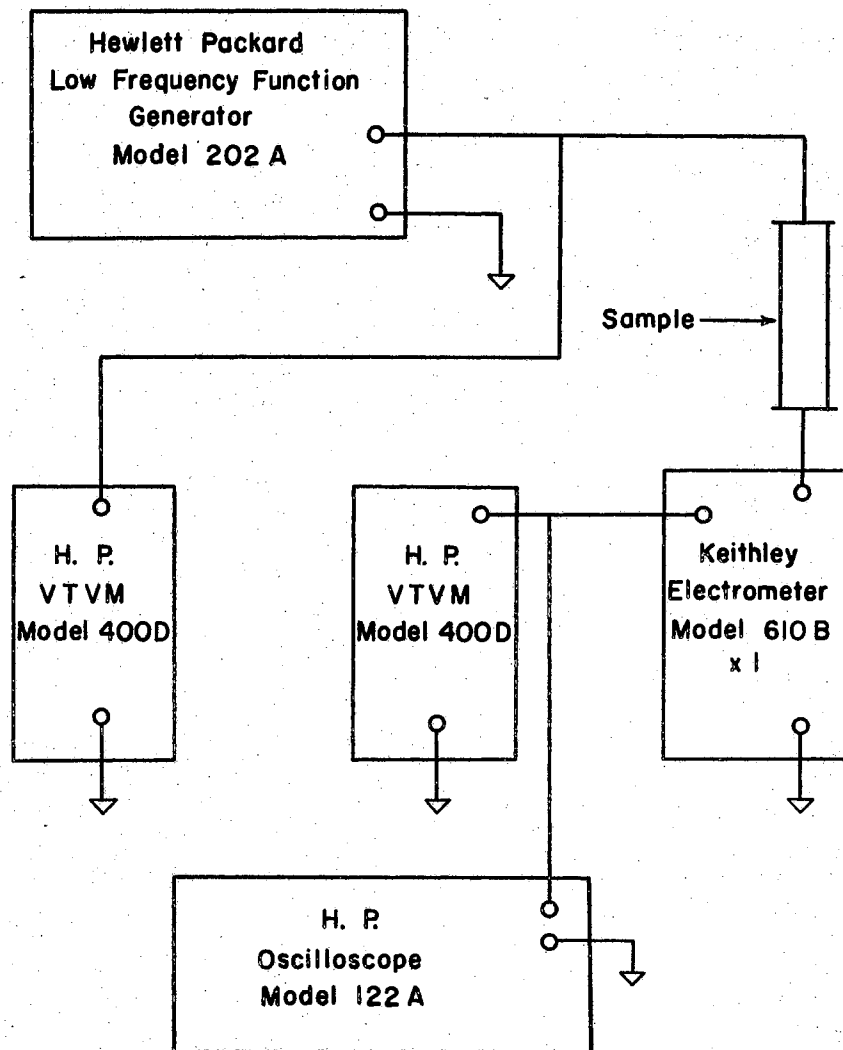
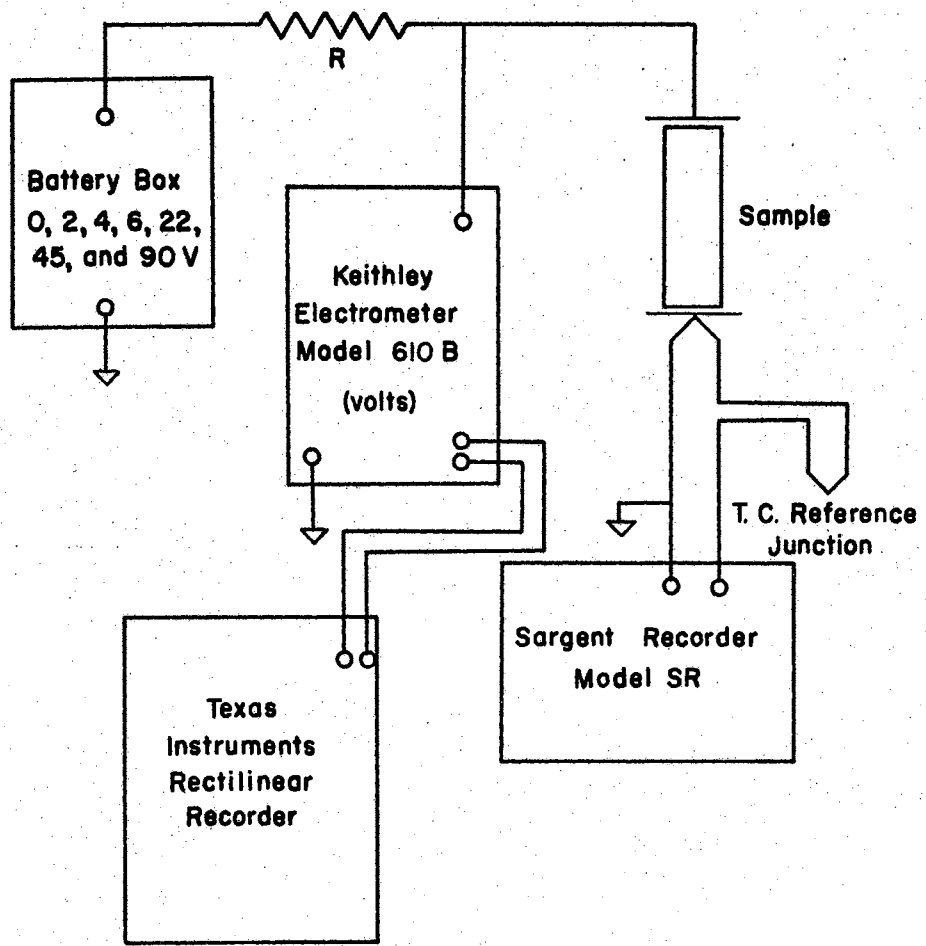Figure 10. Schematic Diagram for Low Frequency
A-C Conductivity

Figure 11. Schematic Diagram of Circuit for Measuring
Conductivity with Low Applied Fields

The four-probe measurement required a somewhat different measuring technique. As the observations of transients was desired, a four channel recorder was used to simultaneously plot the current, the thermocouple voltage and the two probe voltages. The block diagram of this circuit is shown in figure 12.

In the absence of bulk resistance changes, the difference in the probe voltages divided by the current reading should be constant. By feeding the two probe voltages into the differential input of the Moseley X-Y recorder on the Y axis and the applied current into the X axis as indicated in figure 13, one obtains a straight line passing through the origin if the bulk resistance is constant.

General Experimental Procedures

As the samples upon which the measurements were made are very resistive at low temperatures, it was necessary to insure that no surface contaminants were affecting the measurements.

In general the samples were cleaned of cutting oils, fingerprints and other contaminants by the following procedure:

a) 3 washes in acetone in ultrasonic cleaner

b) 2 washes in methanol in ultrasonic cleaner

c) 2 washes in distilled water in ultrasonic cleaner

d) Boiling for 15 minutes in aqua regia

e) 1 rinse in distilled water

f) Boiling for 15 minutes in hydrochloric acid

g) 4 rinses in distilled water in ultrasonic cleaner

h) 2 rinses in methanol in ultrasonic cleaner

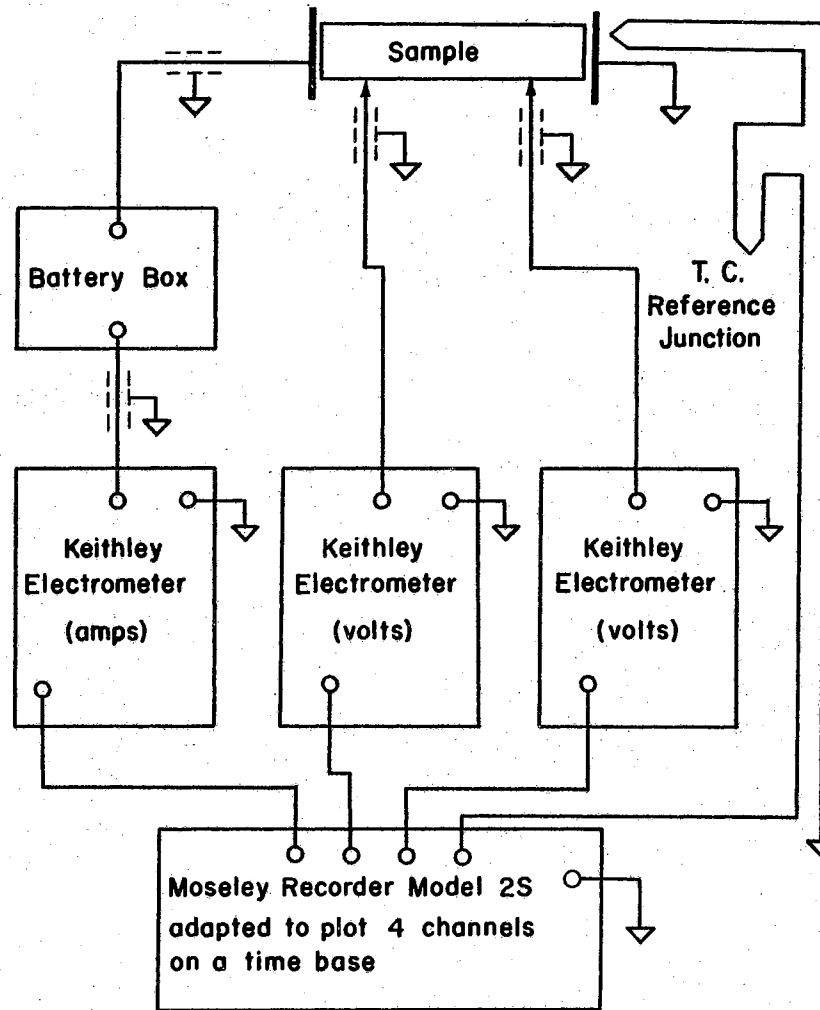After this cleaning procedure special care was taken to prevent further

Figure 12. Schematic Diagram of Electrical Circuitry
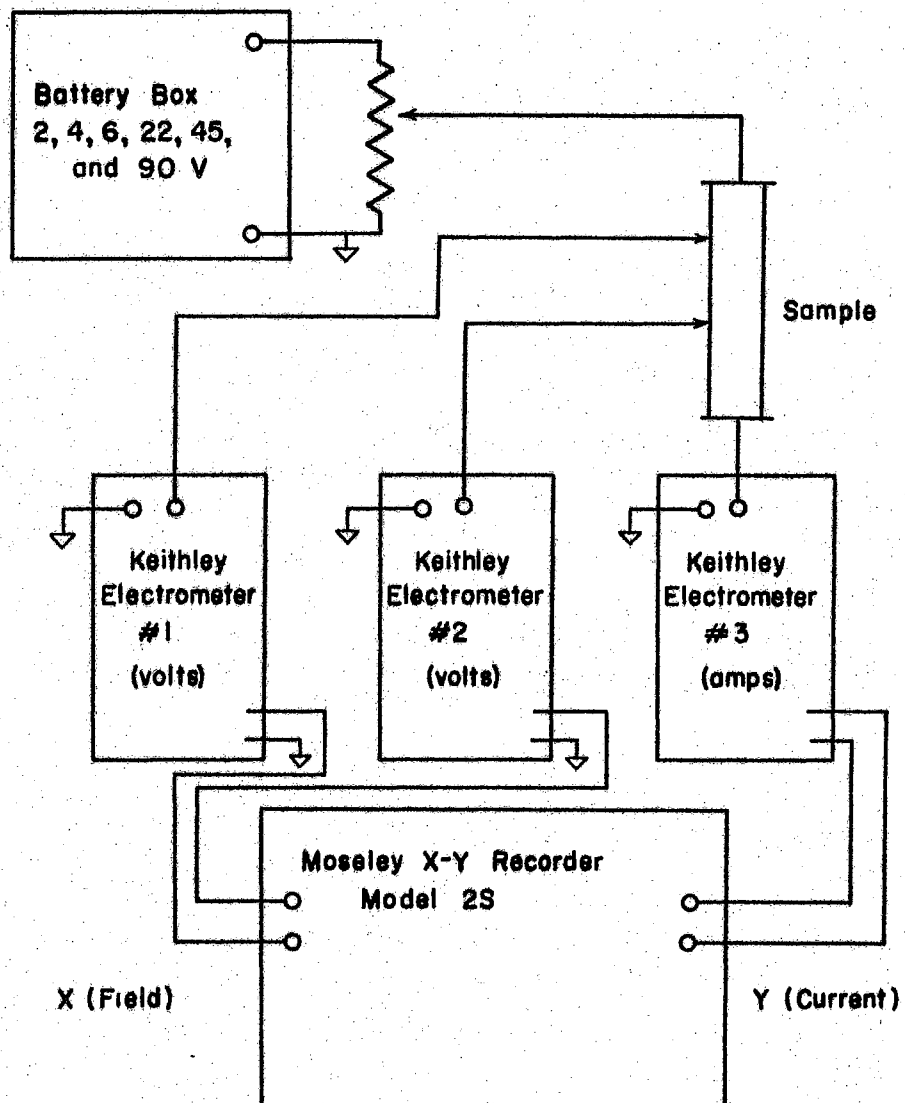Used with Four Probe Sample Holder

Figure 13. Schematic Diagram for Observing Field
Dependence with Four Probe Sample
Holder

contamination of the samples until they were installed in the sample holder.

It is to be expected that water remains upon the surfaces after this cleaning. As a consequence the samples were heated to around 400° C in a vacuum of 2 microns or less for a period of two to four hours. In order to obtain reproducible starting conditions the samples were then heated to 1000°C in dry air which leaves the samples in a highly resistive state.

In an attempt to improve contact to the sample, end portions were plated with platinum bright; however, no significant differences from simple pressed contacts were observed.

For measurement of electrical conductivity and thermopower the sample temperature was allowed to change slowly. Several checks were made by reversing or reducing the rate of change of temperature to determine if the samples were near equilibrium.

The conductivity and thermopower were normally taken on subsequent days in order that the conductivity could be measured without a temperature gradient across the sample. Occasionally the conductivity was measured with a temperature gradient and no significant difference was noted for larger measuring fields.

In measuring the conductivity of the porous ceramic as a function of pressure the sample was maintained overnight at the desired temperature. Depending upon the temperature a thirty minute to four hour period was allowed for the sample to reach equilibrium after a pressure change.

At the lower temperatures (less than 500°C) the fixing treatment is quite important and this data will be supplied with the results.

CHAPTER IV

EXPERIMENTAL RESULTS

Introduction to Experimental Results

The experimental results will be presented in three major sections which are distinguished only by experimental details. In the first section are presented data taken at temperatures from 500°C to 1100°C. In this region both electrical conductivity and thermoelectric power were evaluated. In the second section the data presented were taken at lower temperatures (20°C to 500°C). In the final section are presented data associated with current transients following application of an electric field and with variation of resistance with the applied field strength.

In the analysis it will be assumed that the effective mass of the free electrons is 0.2 m_O and that they may be characterized by a lattice scattering mobility (μ_n) which is 100 cm^2/volt-sec at room temperature. These parameters have been evaluated by several authors but weight has been given to the results of Marley and Dockerty[19].

In addition it will be assumed that the conduction band is not degenerate and that the density of states is derived from the standard parabolic energy relation as described earlier.

High Temperature Results

The majority of the electrical conductivity data was taken by a

51

two probe technique with the apparatus described earlier. At temperatures above 700°C this data was taken with an applied potential of 100 MV or less due to the appearance of field induced transients at higher applied potential values. Below 700°C, in air, the sample resistance was large enough to require the use of larger fields which did on occasion result in transient values of the current. In these cases it was attempted to evaluate the current prior to the onset of the field induced changes.

The sample heater was positioned to reduce the temperature differential across the sample to a minimum. By following this procedure the conductivities measured in both directions agreed in value, which was not always the case with higher fields at the high temperatures.

Figures 14 and 15 exhibit the temperature dependence of the electrical conductivity of single crystal G-25 (0.65 mm x 0.65 mm x 1.5 mm) in an air atmosphere of 140 torr. The conductivity σ is obtained from the experimentally determined resistance, R, through the relation $\sigma = L/(AR)$, where L and A are the geometrical length and cross-sectional area of the sample. This slightly reduced pressure was maintained by allowing dry air flow into the system and pumping at slow rates.

Figure 16 presents thermoelectric power data taken the following day under indentical conditions except that a temperature gradient of 10 to 20°C was developed across the sample by moving the heater to an off-center position. The Seebeck coefficient Q is the ratio of the thermal voltage to the temperature differential across which it is developed. Here use is made of the conventional sign convention[20].

In both cases the specimen was maintained over-night at the high temperature, and the measurements taken as the temperature slowly de-
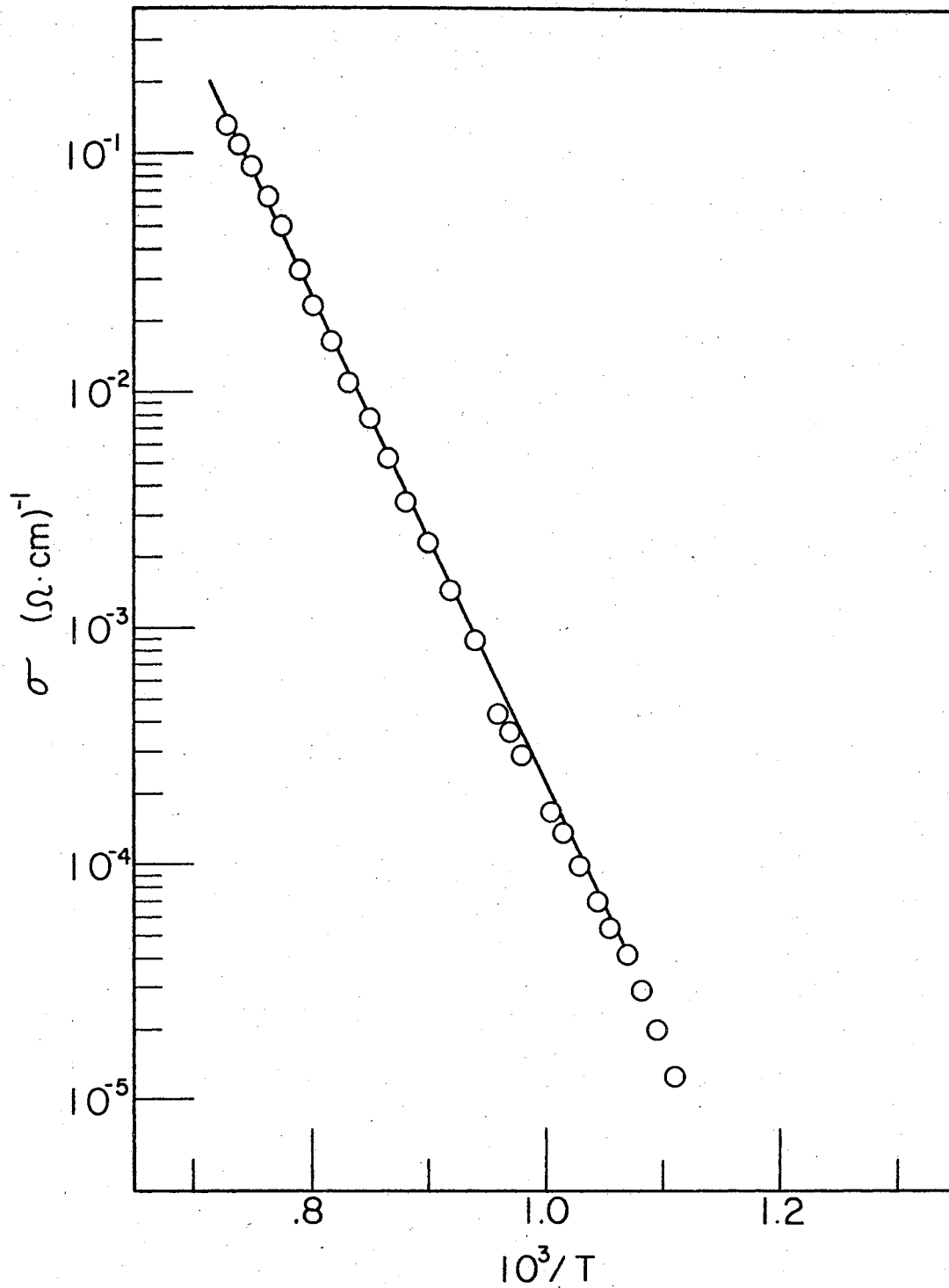
Figure 14. Conductivity of Single Crystal at
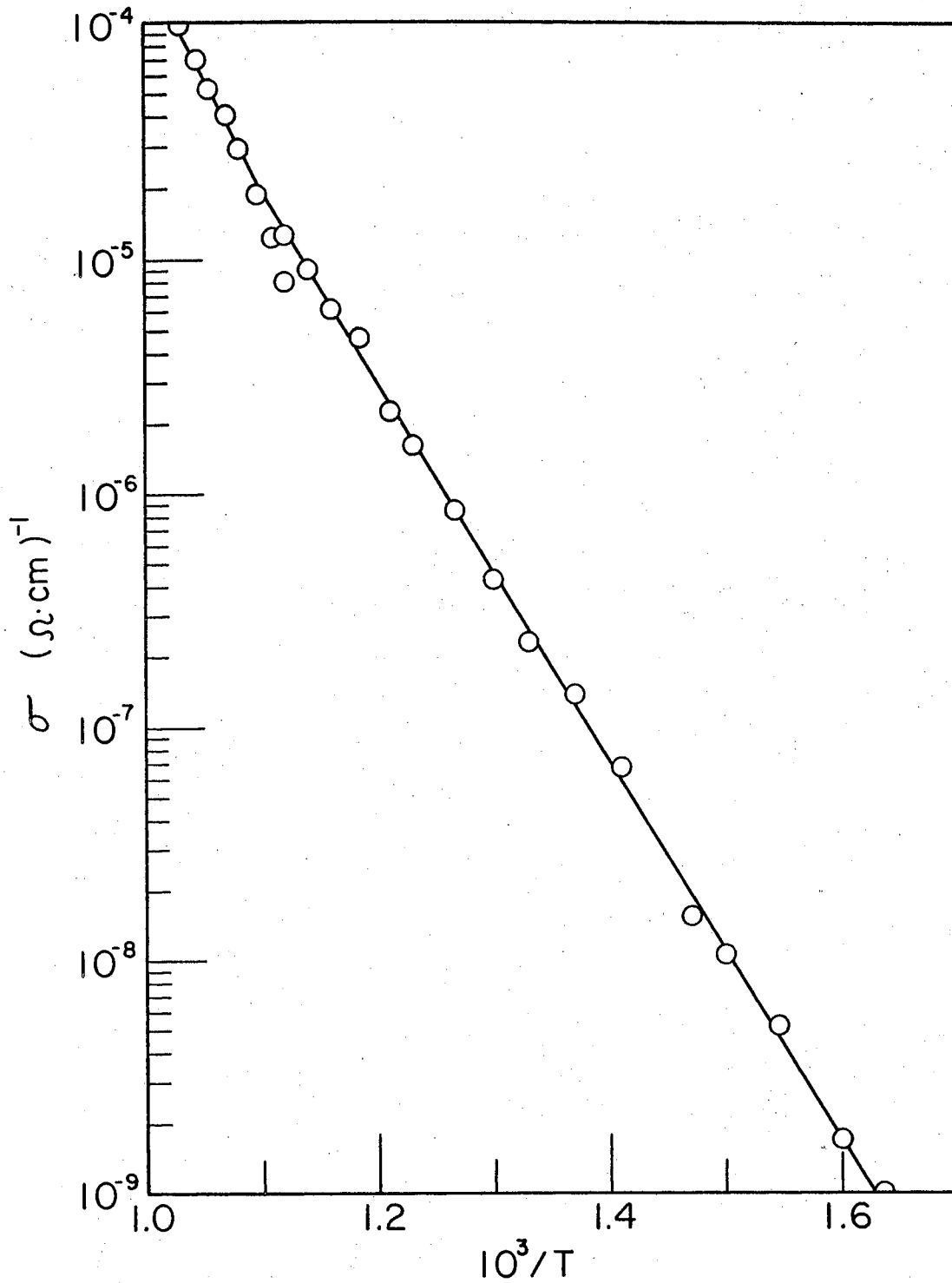140 Torr at High Temperatures

Figure 15. Conductivity of Single Crystal at 140 Torr at
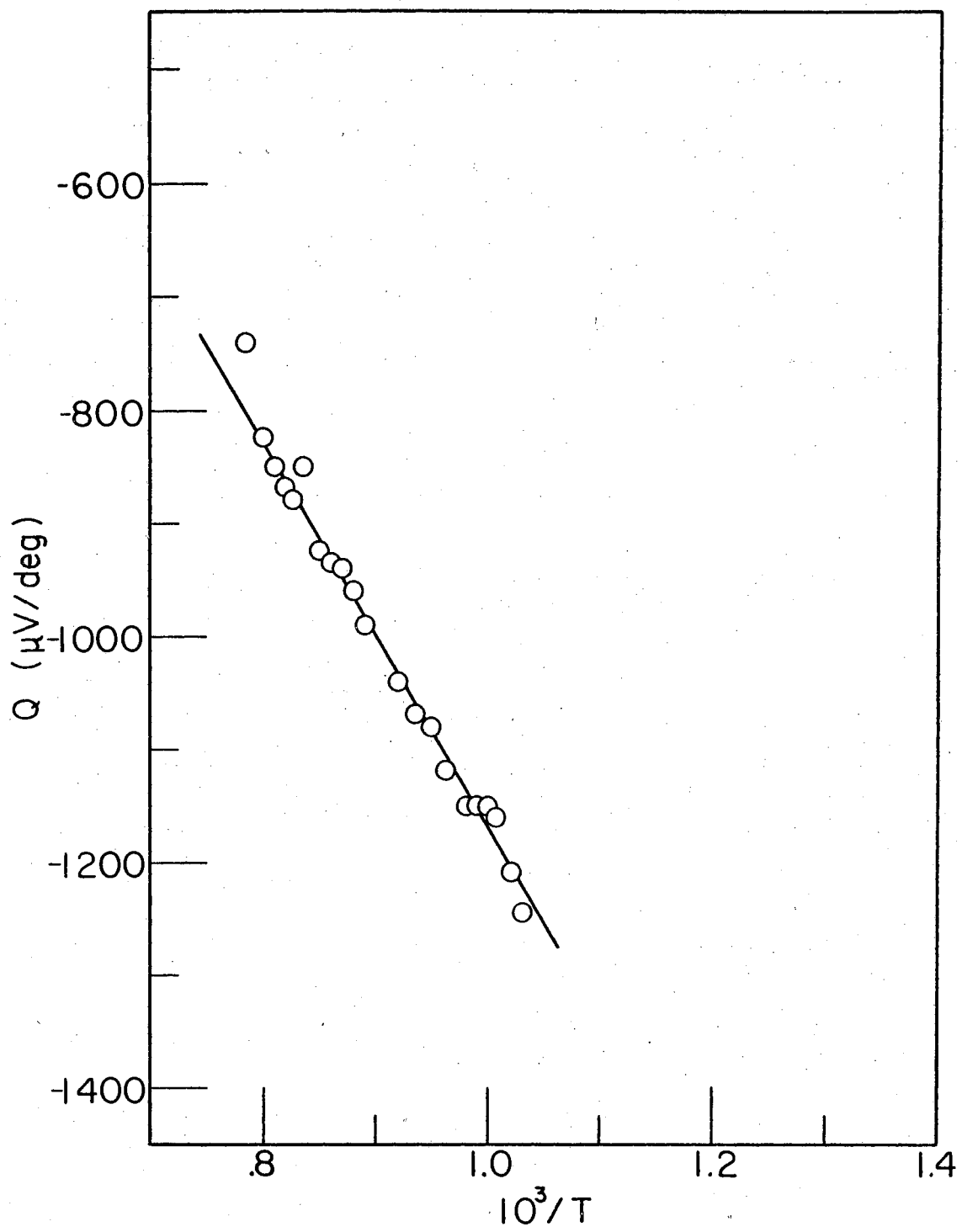Intermediate Temperatures

Figure 16. Thermoelectric Power of Single Crystal at 140 Torr

creased after reducing the heater power. This rate was from 60 to 100°
C/hr. The effect of making the measurements during a temperature change
was periodically checked by increasing the heater power and attempting
to observe an hysteresis effect. In the high temperature region no
effects of this nature were observed.

In the following three figures (figures 17, 18 and 19) are plotted
similar data on G-25 taken at a reduced pressure; again these data were
taken with a dynamic gas flow.

Figure 20 presents conductivity data on the same sample taken by
means of a low frequency A.C. technique at atmospheric pressure. The
deviation of the 10 cps and the 100 cps data is believed to lie in cal-
ibration of the meters used in making the measurement. At lower temp-
eratures this curve deviates from the D.C. data due to RC time constants
but the high temperature region agrees quite well with the equivalent
D.C. measurements.

Figures 21, 22 and 23 give the dependence of the electrical con-
ductivity and thermoelectric power of a dense (doped 0.7% AnO) ceramic
specimen S-14 (1.19 mm x 1.90 mm x 3.95 mm). In this case the data are
taken at atmospheric pressure in static air.

Similar data for a pure ceramic S-15 (1.99 mm x 2.50 mm x 3.01 mm)
under dynamic air flow at 180 torr are presented in figures 24, 25 and
26.

The concluding conductivity curve of this section is presented in
figures 27 and 28. The measurement technique used in this case was the
four-probe technique with a potential of 10 to 100 MV across the po-
tential probes. This sample was a dense ceramic specimen 4P2 and the
data taken under a dynamic air flow at 480 torr.

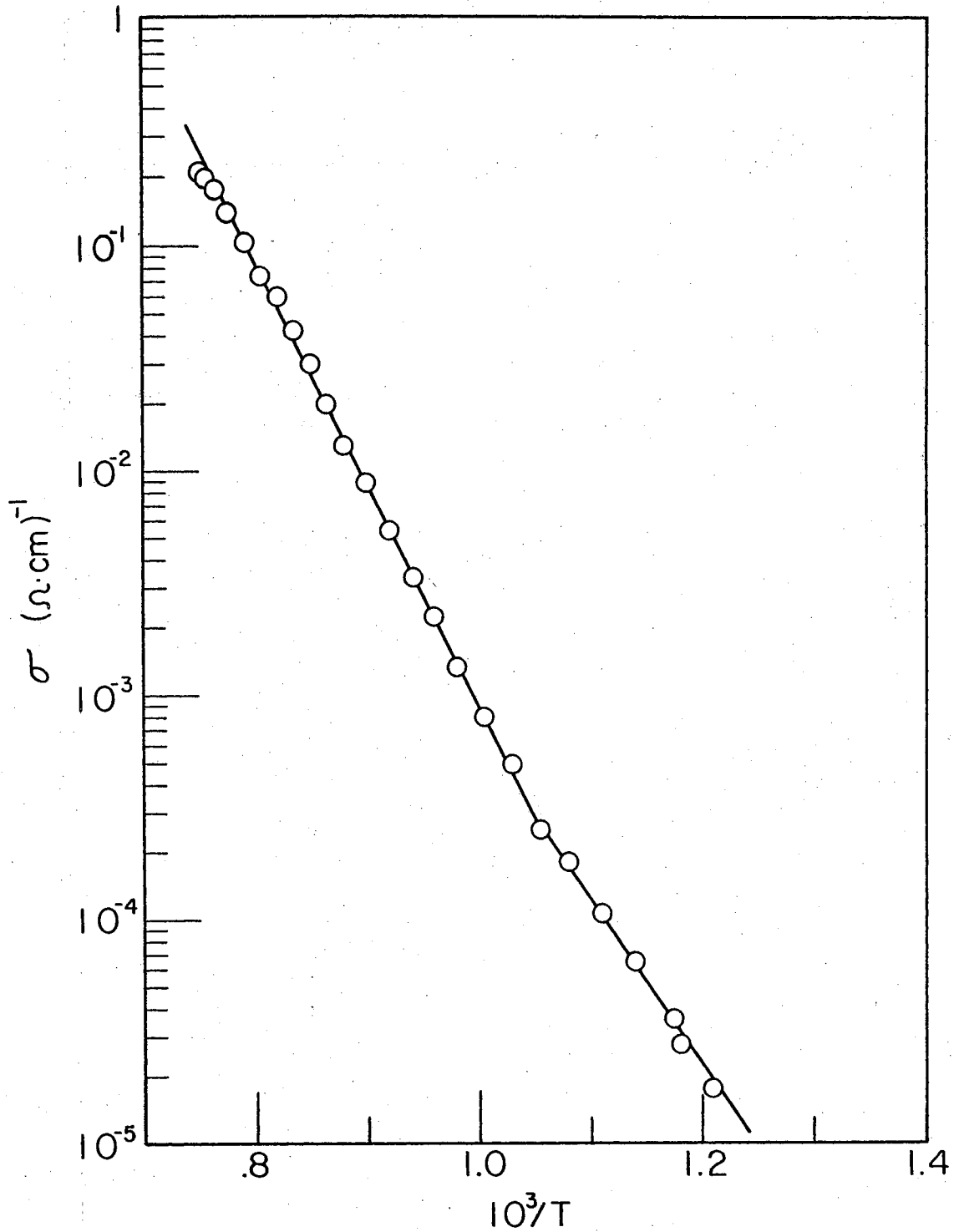The data at higher temperatures were analyzed on the basis of an

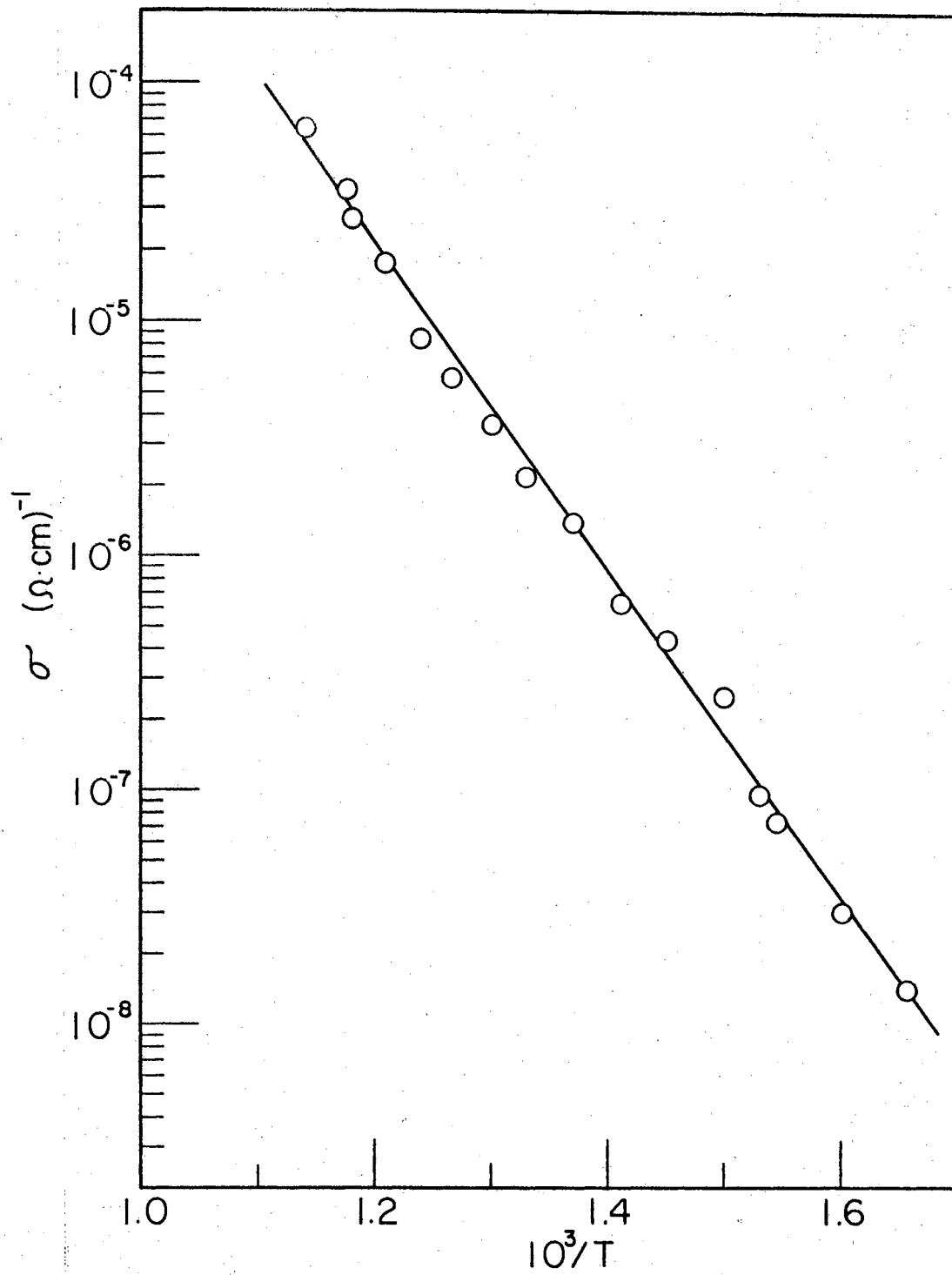Figure 17. Conductivity of Single Crystal
at 100μ at High Temperatures

Figure 18. Conductivity of Single Crystal at 100μ at Intermediate Temperatures
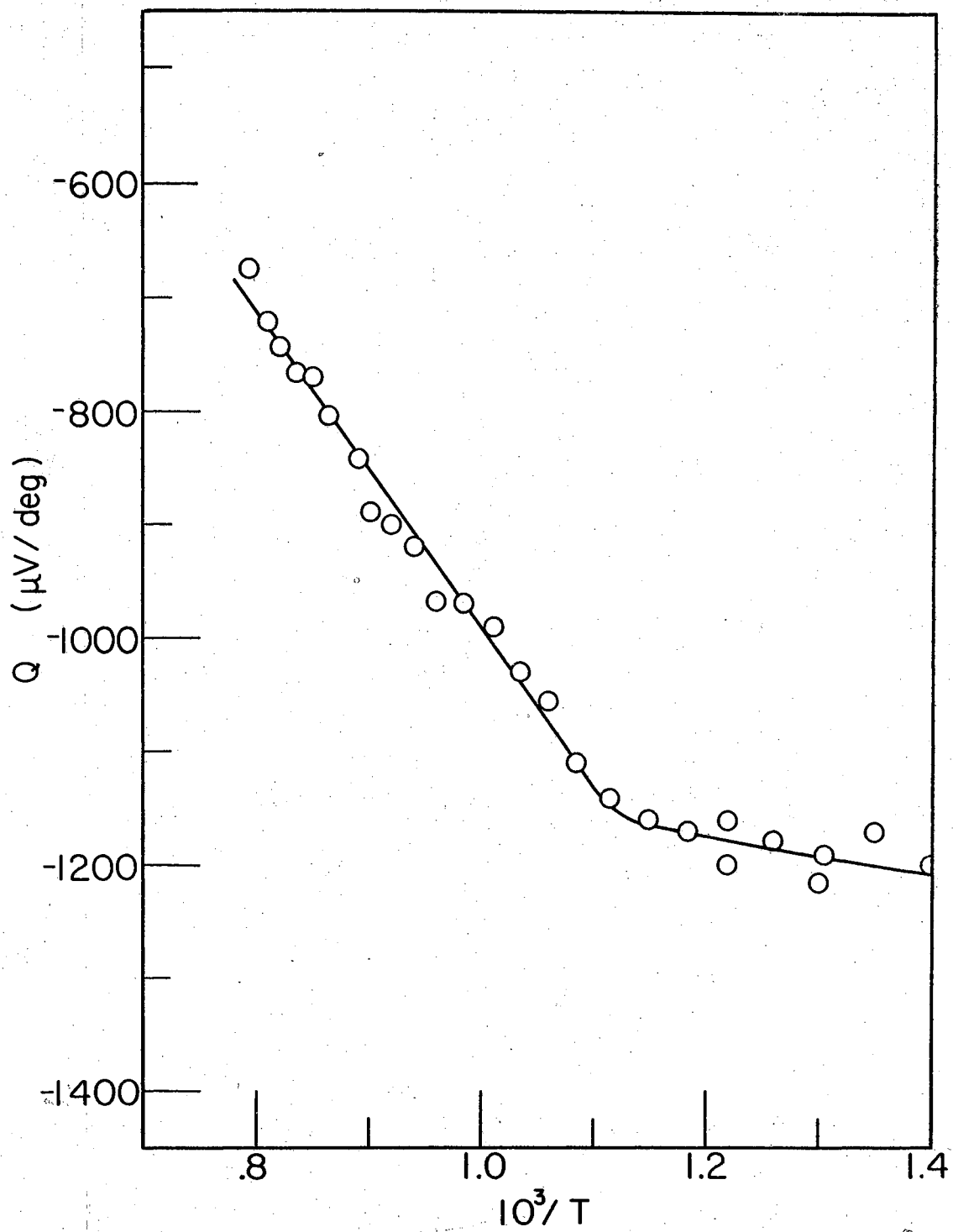
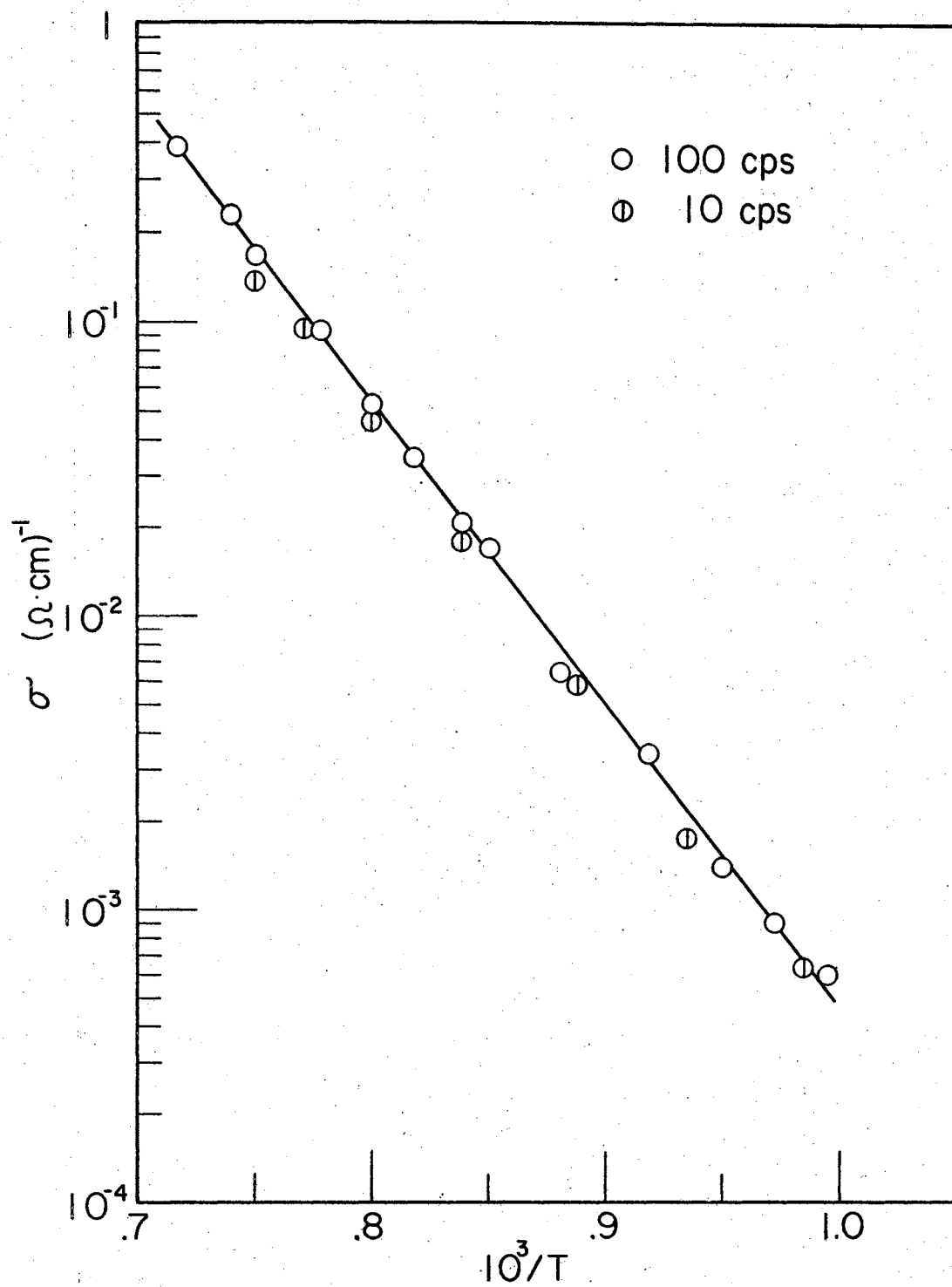Figure 19. Thermoelectric Power of Single Crystal at 100μ

Figure 20. A.C. Conductivity of Single Crystal
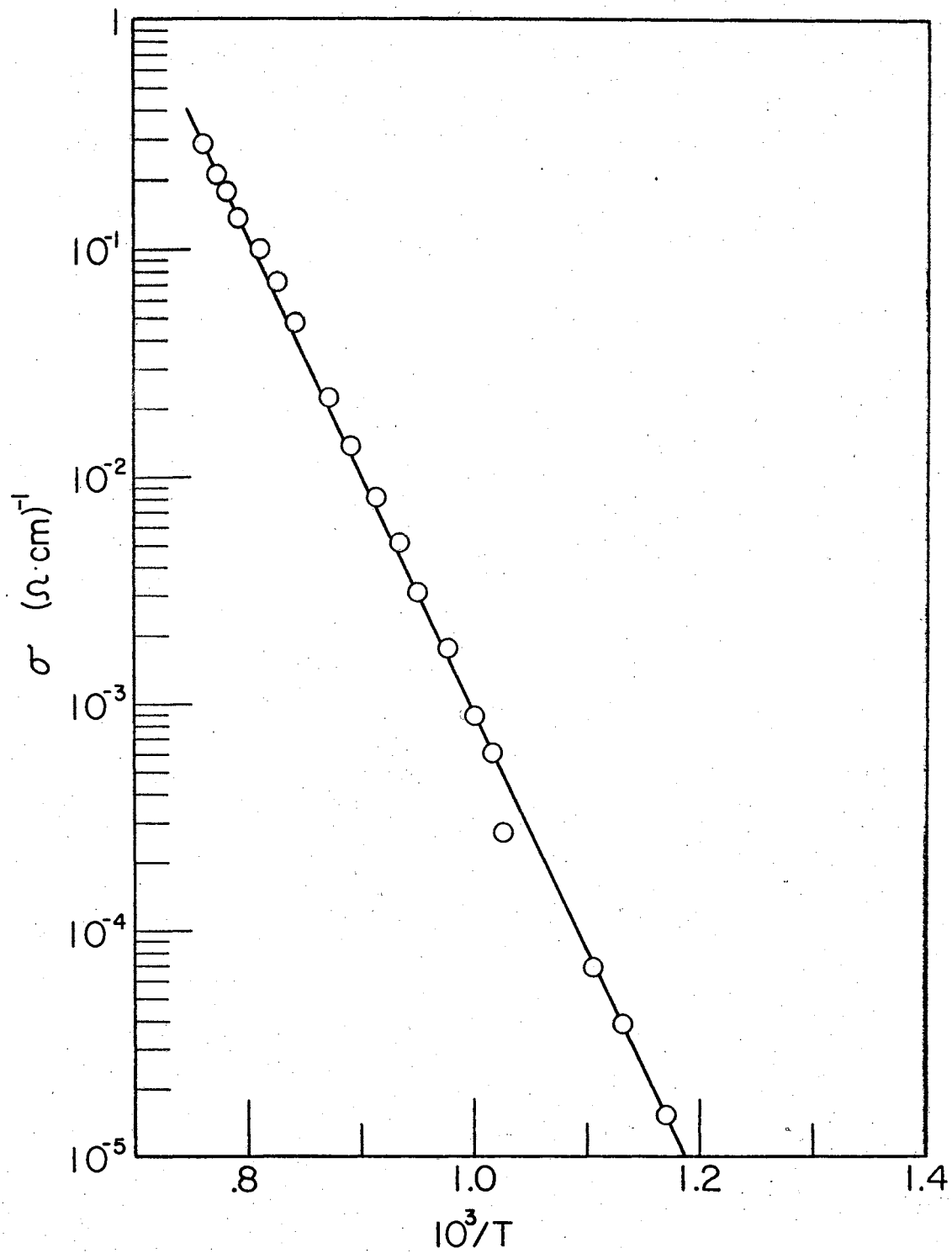at High Temperatures in Dry Air

Figure 21. High Temperature Conductivity
of Dense Ceramic in Dry Air
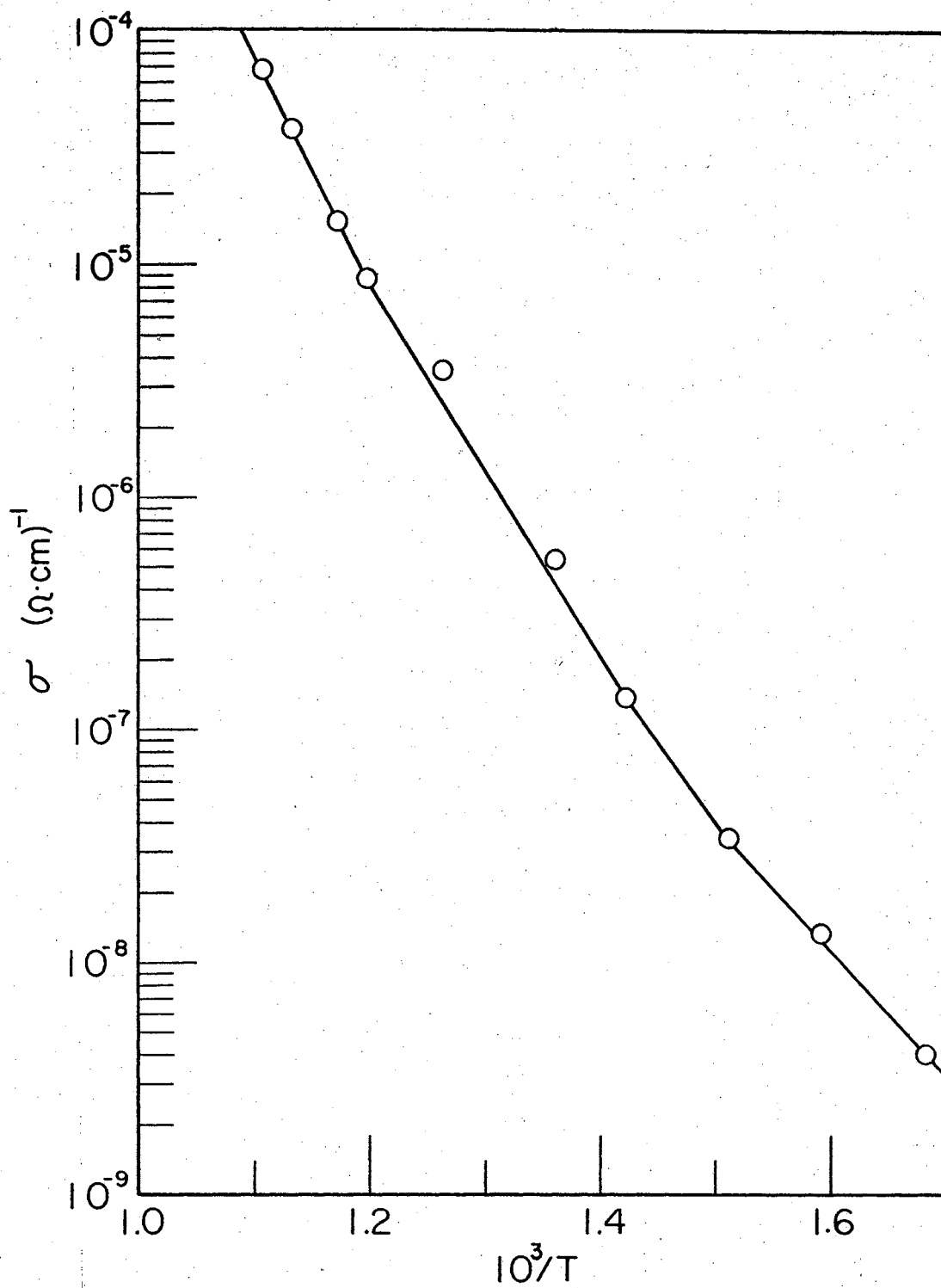
Figure 22. Intermediate Temperature Conductivity
of Dense Ceramic in Dry Air
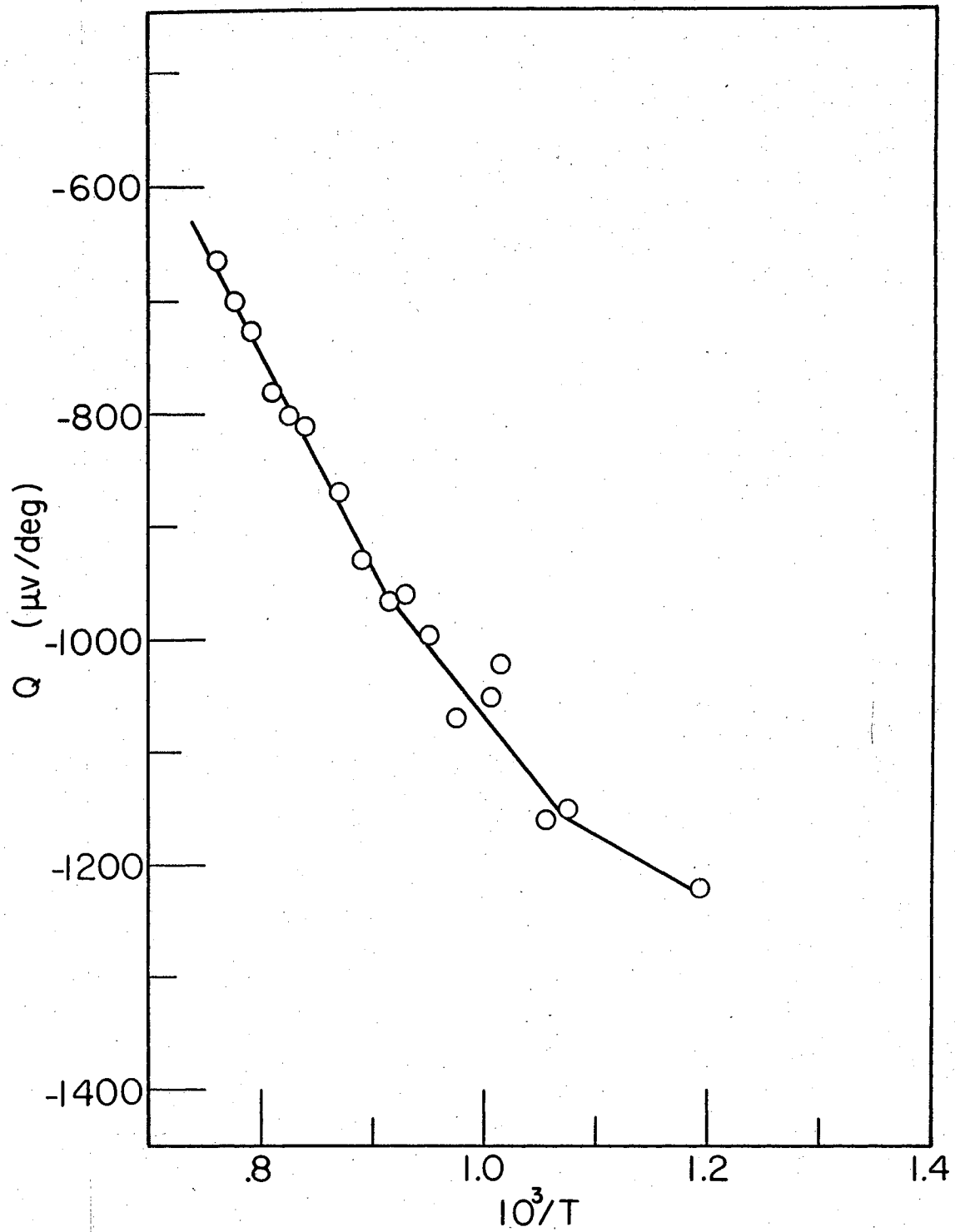
Figure 23. Thermoelectric Power of Dense Ceramic in Dry Air

Figure 24. High Temperature Conductivity
of Porous Ceramic at 180 Torr

Figure 25. Intermediate Temperature Conductivity
of Porous Ceramic at 180 Torr

Figure 26. Thermoelectric Power of Porous
Ceramic at 180 Torr

Figure 27. High Temperature Conductivity of Dense Ceramic
in Four Probe Sample Holder at 480 Torr

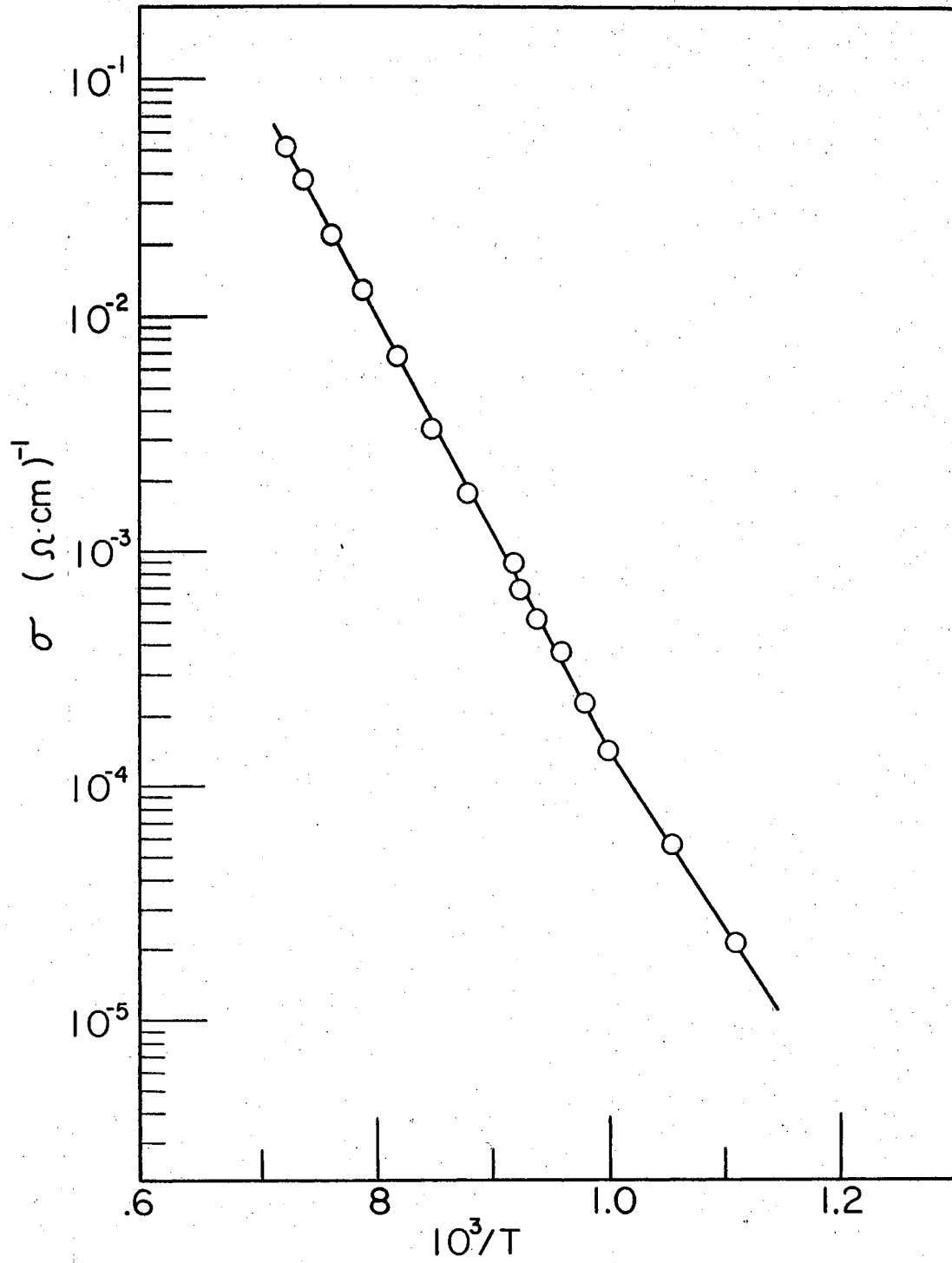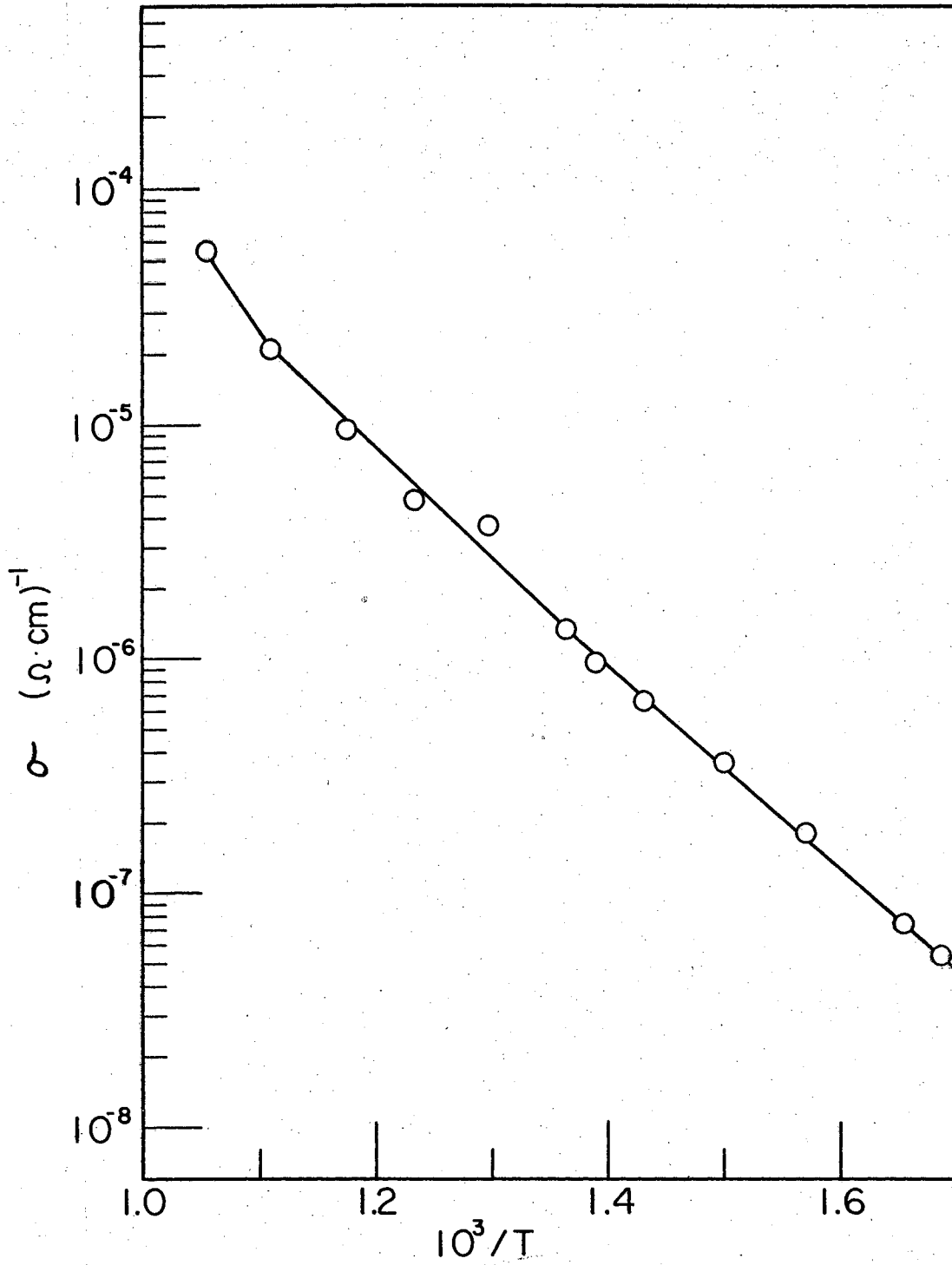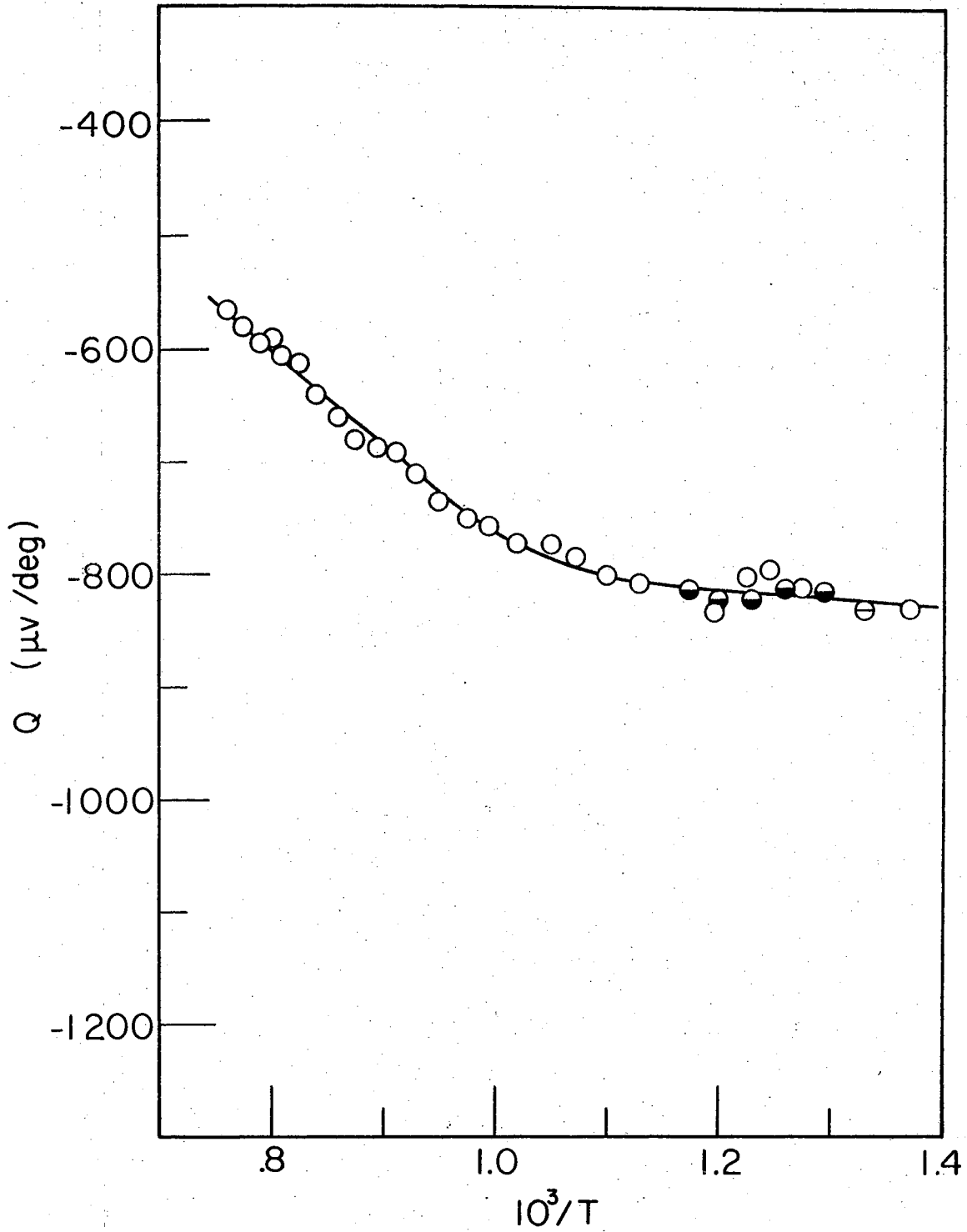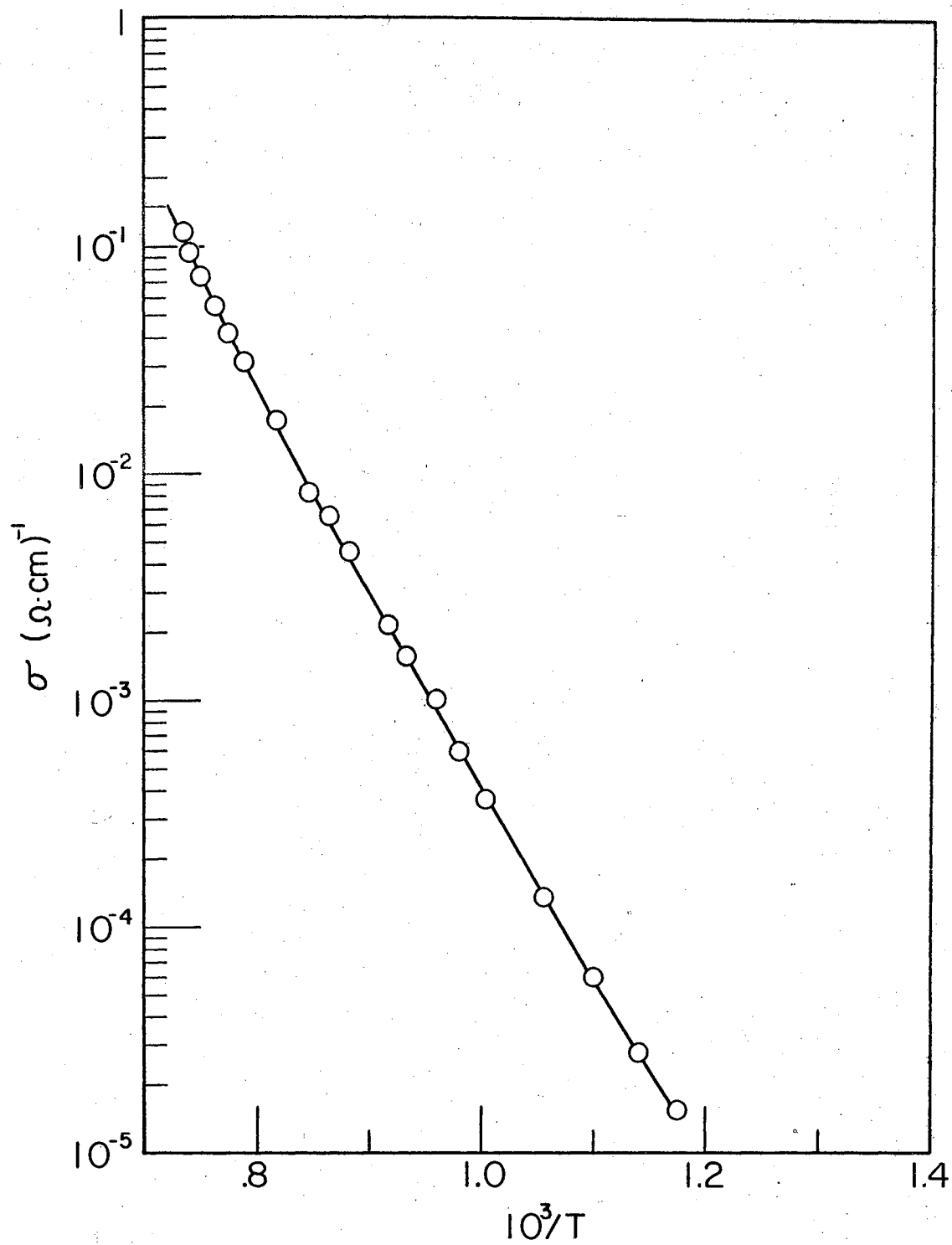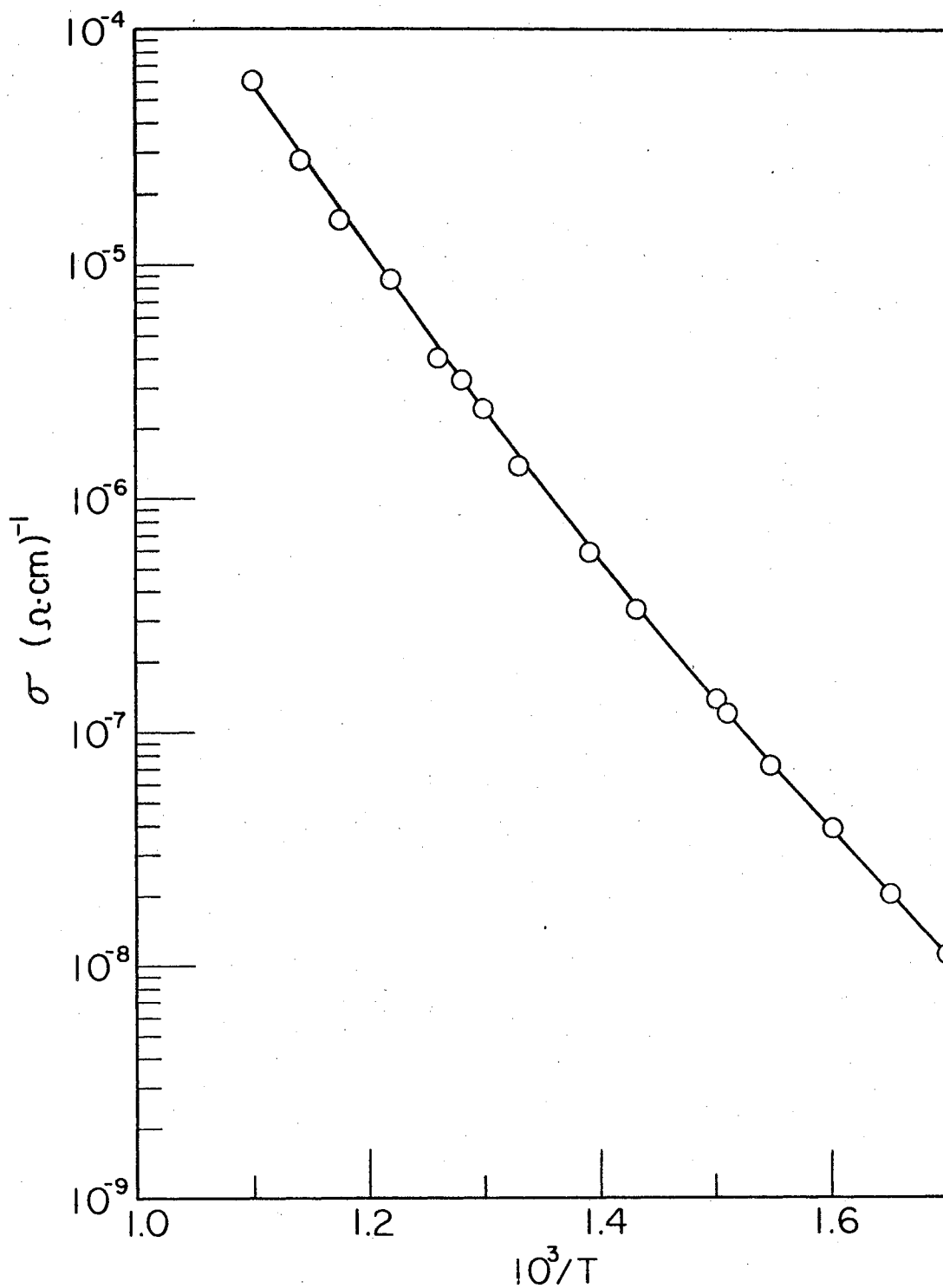Figure 28. Intermediate Temperature Conductivity of Dense Ceramic in Four Probe Sample Holder at 480 Torr

intrinsic model with μ_n and m_n given by:

$$\mu_n = 100 \ (300/T)^{3/2} \ (cm^2/volt\text{-}sec) \tag{66}$$

$$m_n = 0.2 \ m_o. \tag{67}$$

In addition it was assumed that the temperature dependence of the energy gap is given by

$$E_g = E_{go} - \alpha T, \tag{68}$$

where α and E_{go} are constants.

These data are tabulated in Table II. In addition this table lists results on two other single cyrstals, G-9 and G-21.

In calculating the values for this table the effective energy gap at $T = 0$ (E_{go}) was calculated from

$$E_{go} = -2 \ \frac{\partial ln\sigma}{\partial 1/kT} \tag{69}$$

which is readily obtained from equations 5 and 23.

Then the mobility ratio ($\mu_n/\mu_p = c$) was calculated from

$$-2 \ \frac{\partial eQ}{\partial 1/T} = \frac{(c - 1)}{(c + 1)} \ E_{go} \tag{70}$$

which is obtained by differentiating equation 24 using the relation given in equation 5 for E_g.

Since the conduction is taken to be intrinsic, one can estimate α utilizing equations 5 and 23:

$$\sigma_i = e\mu_n \ (1 + \mu_p/\mu_n) \ (N_c N_v)^{\frac{1}{2}} \ exp \ (-E_{go} + \alpha T)/2kT \tag{71}$$

	σ	Q	log σ	Q	$\frac{-\partial\ln\sigma}{\partial 1/kT}$	$\frac{-\partial eQ}{\partial 1/T}$	E_{go}	$\frac{\mu_n}{\mu_p}$	α	$\frac{m_p}{m_n}$	E_g	Figure
	1250°K $(\Omega.\text{cm})^{-1}$	1250°K (μV/deg)	$10^3/T = 0$	$10^3/T = 0$ (μV/deg)			(eV)		(eV/deg)		300°K (eV)	
G-25 c 140 Torr	2.5×10^{-2}	-825	6.60	555	2.05	1.73	4.10	11.8	15.7×10^{-4}	1.65	3.63	14,15,16
G-25 c 10^{-9} Torr	8.0×10^{-2}	-710	6.90	410	1.93	1.40	3.86	6.3	17.0×10^{-4}	0.28	3.35	17,18,19
G-25 c AC	5.0×10^{-2}				2.03		4.06					20
G-21 c 760 Torr	1.0×10^{-1}	-700	6.95	460	2.00	1.57	4.00	7.0	17.2×10^{-4}	0.41	3.48	
G-9 c 200 Torr	2.4×10^{-2}	-	6.70		2.00	1.53	4.00		16.2×10^{-4}		3.51	
G-9 c 260 Torr	3.2×10^{-2}	-685	7.16	575	2.10	1.57	4.20	6.9	18.0×10^{-4}	1.57	3.66	
G-9 c 13 x 10^{-3} Torr	3.6×10^{-2}	-690	7.26	250	2.10	1.37	4.20	4.8	18.4×10^{-4}	0.02	3.65	
Crystal mean	4.96×10^{-2}	-722	6.93*	450*	2.03*	1.53*	4.06	7.3	17.1×10^{-4}	0.79	3.55	
Calculated from crystal mean values with*							4.06	7.5	17.0×10^{-4}	0.30	3.55	
S-15 180 Torr	1.0×10^{-2}	-600	5.60	100	1.87	0.80	3.74	2.5	11.8×10^{-4}	3.65	3.39	24,25,26
S-14 760 Torr	1.1×10^{-2}	-750	7.48	800	2.00	1.60	4.00	9.0	19.3×10^{-4}	9.78	3.42	21,22,23
4P2	2.5×10^{-2}		6.48		2.00		4.00		15.4×10^{-4}		3.54	27,28

Single Crystals G-9, G-21 and G-25
Pure Ceramic (porous) S-15
Doped Ceramic (dense)   S-14 and 4P2

Table II. Summary of High Temperature Results and Intrinsic Analysis

Taking $\mu_n = 100 \ (300/T)^{3/2}$ and $m_n m_p = 1$ obtains from equation 71:

$$\ln \sigma_i \ (10^3/T = 0) = \ln \ [1.6 \times 10^{-19} \ 100 \ (300/T)^{3/2} \ 4.82 \times 10^{15}]$$

(72)

$$+ \ 3/4 \ \ln m_n^* m_p^* + \ln \ (1 + \mu_p/\mu_n) + \alpha/2k.$$

The assumption that $m_n^* m_p^* = 1$ introduces but little error in the calculated value of α for reasonable values of this product.

The ratio m_p/m_n can now be calculated from the $10^3/T$ intercept of the thermoelectric power with the relation (from equations 5 and 24):

$$Q = -k/e \ \frac{\mu_n - \mu_p}{\mu_n + \mu_p} \ \{ \ \frac{\alpha}{2k} + 2 \ \} + 3/4 \ \ln m_p/m_n.$$

(73)

Other methods which use the magnitudes of σ and Q at a finite temperature result in values quite comparable to those obtained in this more direct manner.

For the single crystals the derivation from sample to sample is small for the measurements and the calculated values of E_{go} and α.

There is a somewhat larger deviation in the relative mobilities, but these values are very sensitive to small inaccuracies in the thermoelectric power measurements. The obtained values for the effective mass ratio center around unity and may be interpreted to signify that there is no great disparity between the two masses. This calculated parameter is again highly dependent upon the magnitude and slope of the thermoelectric power.

It might be pointed out at this time that the dense ceramics behave quite similarly to the crystals although there are significant deviations in the case of the porous ceramic.

The values obtained from this analysis are in reasonable agreement with previously reported values. A more direct comparison will be presented in the concluding chapter.

Other mechanisms due to defect formation have been considered but the lack of an oxygen pressure dependence in the single crystals and dense ceramics does not appear to be consistent with this possibility. The stoichiometric thermal defect model[26] is not considered likely since the intrinsic model yields a good explanation for the experimental results.

Between 500 and 700°C the conductivity curves break slowly into a shallower slope as other conductivity mechanisms come into play. The existence of the negative thermoelectric power indicates conduction by electrons, but their sources have not been uniquely identified. Because of the experimental difficulty in obtaining thermoelectric power values for the region where it is assured that hole conduction is completely negligible, no accurate check of the values of m_n and μ_n has been possible. However, the results indicate plausible consistency with the values given earlier.

As mentioned earlier, a variation of conductivity with ambient pressure may be readily explained by a thermal defect mechanism in which stoichiometry is not maintained. Since the conductivity of the samples below 700°C varied with treatment, it was originally felt that the high temperature conductivity might be controlled by a thermal defect mechanism instead of intrinsic behavior, and, as a consequence, a direct evaluation of this phenomenon was attempted.

At temperatures above 1000°C the conductivity of all samples did show a slight variable behavior. However, the single crystals and the

doped ceramics after reaching a steady state condition yielded no consistent pressure dependence. The dense ceramic specimen used in the four-probe sample holder showed essentially no change in conductivity at 1050°C over a pressure range of five orders of magnitude. Consequently, it is felt that the changes noted at high temperatures are not due to an oxygen vacancy mechanism even though, after various pressure treatments at high temperatures, differences show up readily at lower temperatures, tending to higher conductivity with reduced pressure. The small changes noted at high temperatures may be associated with the contacts.

The porous ceramic specimen S-15 differed from the others in that from the conductivity slope the activation energy measured in the high temperature region was somewhat smaller. In addition it showed a definite dependence of conductivity upon ambient oxygen pressure (figure 29). This effect appeared in air and oxygen but was greatly diminished in nitrogen. Between 700°C and 1100°C the conductivity appeared to be related to the oxygen pressure by:

$$\sigma \propto P^{-1/n} \qquad 4.9 < n < 5.5 \qquad\qquad (74)$$

where P is the oxygen pressure and n a constant which varies with temperature. Conductivity isobars from this same data are presented in figure 30. This figure indicates a change in conductivity magnitude but no change in activation energy with a change in pressure. The activation energy from this plot $\left(\dfrac{\partial \ln\sigma}{\partial \frac{1}{kT}} \right)$ is 2.1 eV which agrees well with other data but is somewhat higher than that measured on this sample at a constant pressure of 180 torr.

When an analysis based on an oxygen vacancy mechanism was tried,
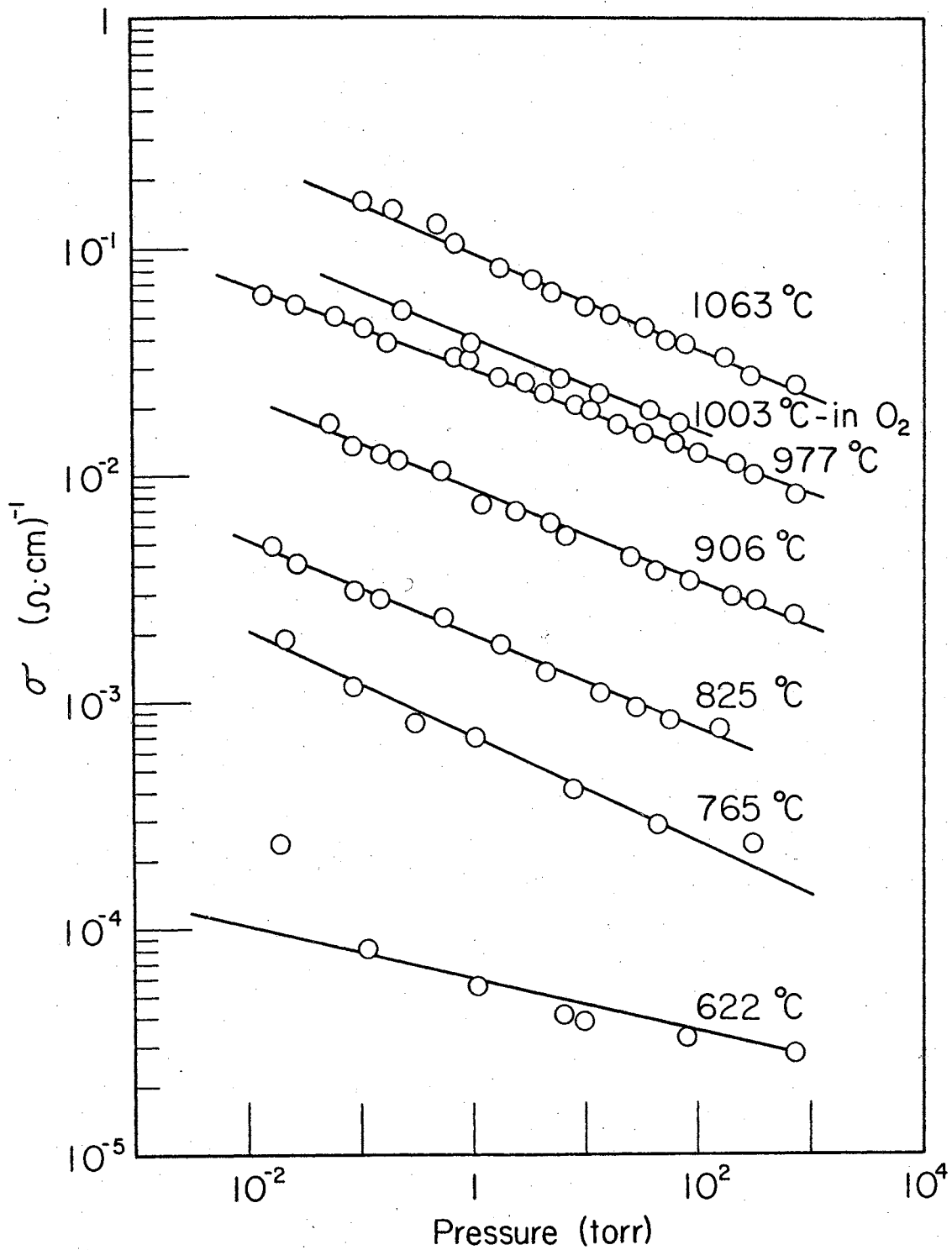
Figure 29. Pressure Dependence of Conductivity of Porous
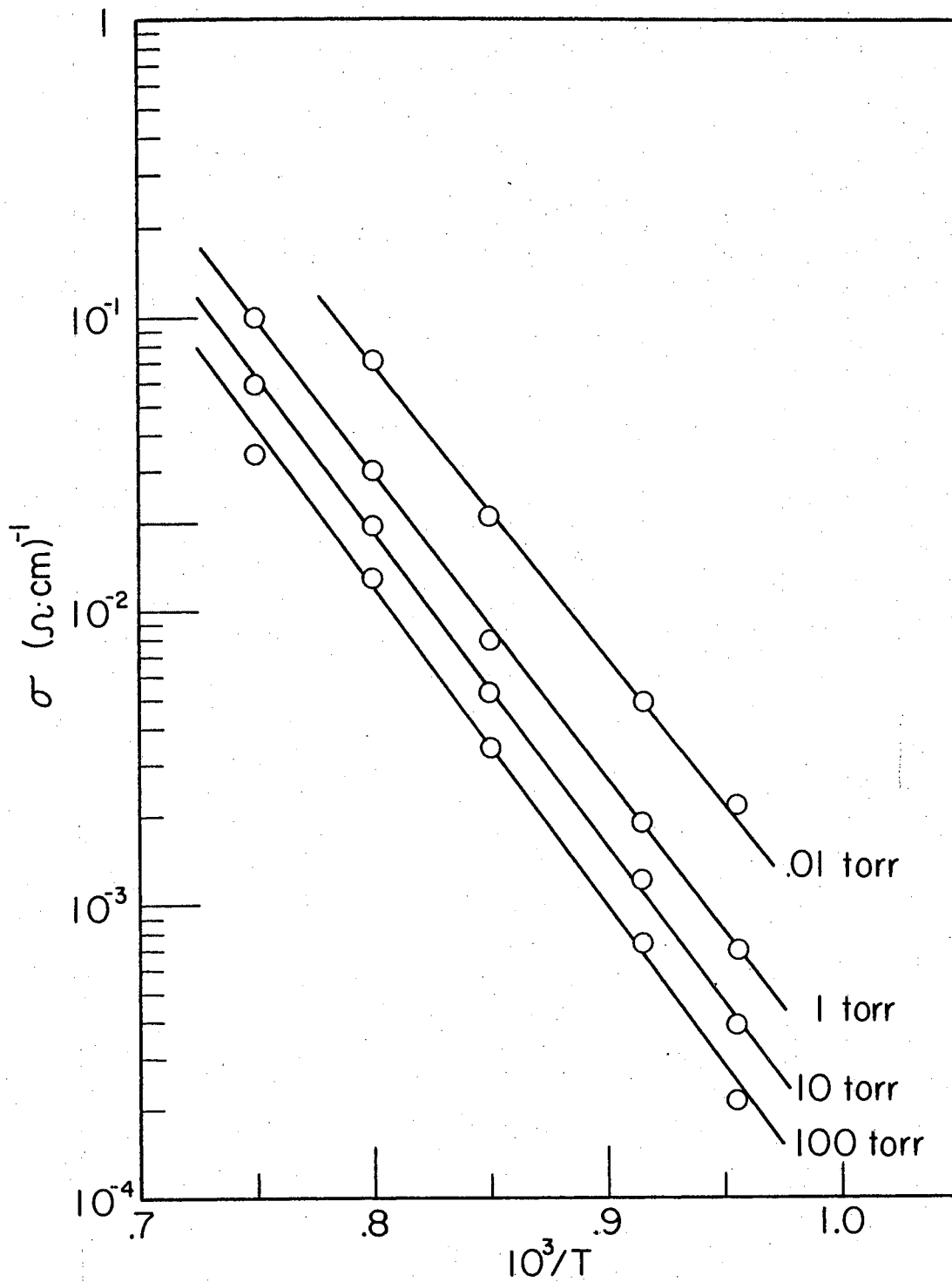Ceramic at Several Temperatures

Figure 30. Conductivity of Porous Ceramic
at Several Pressures

it yielded values of 8 eV for the energy required to form a doubly ion-
ized vacancy, and 5.5 eV for the energy of formation of a singly ionized
vacancy. These values seem to be much too large if this mechanism is
to predominate over intrinsic conductivity.

The calculation described requires the elimination of $[V_A]$, $[V_A^\circ]$
and $[V_A^{\circ\cdot}]$ from equations 55 through 58, resulting in:

$$n^3 \, P^{\frac{1}{2}} - (K_2/K_3)n - 2K_2 = 0 \qquad (75)$$

which is linear in (K_2/K_3) and K_2. Inserting experimental values of n
and P allows ready calculation of (K_2/K_3) and K_2 from any pair of points
at each temperature. Averaging over several pairs resulted in the best
values for these constants. Since both K_2 and K_3 are of the form C exp
-E/kT (equations 59 and 60), Arrhenius plots of K_2 and (K_2/K_3) give the
approximate value of the associated energies.

Because the effect was not noted in the remaining samples, the ana-
lysis was not pursued. The sample in question is quite porous and the
effect could well be related to this fact. For example, if the total
conduction is affected by pore conduction, it should increase with a
cleaner surface (i.e., lower pressure). Due to the nature of the two-
probe experimental method, the possibility that the changes noted with
this sample are due to contacts has also not been eliminated.

Even though intrinsic conductivity appears to be dominant at the
higher temperatures, it should be emphasized once again that thermal
production of defects does occur as evidenced by the reduction of all
samples at high temperatures and reduced pressure. Figures 31 and 32
indicate the difference in behavior of the doped ceramic sample S-14 as
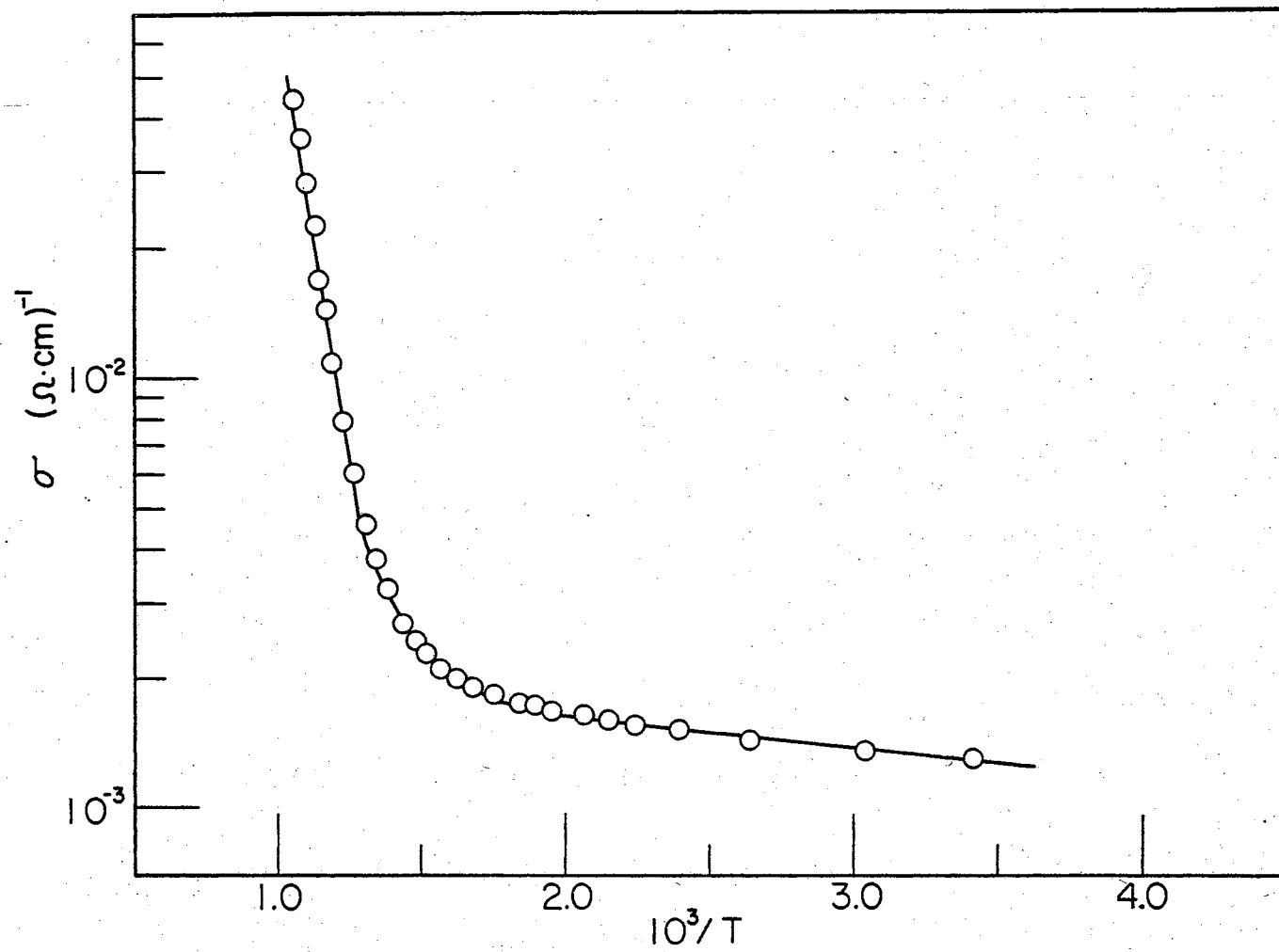treated for one week at 700°C under a pressure of 10^{-3} torr from that

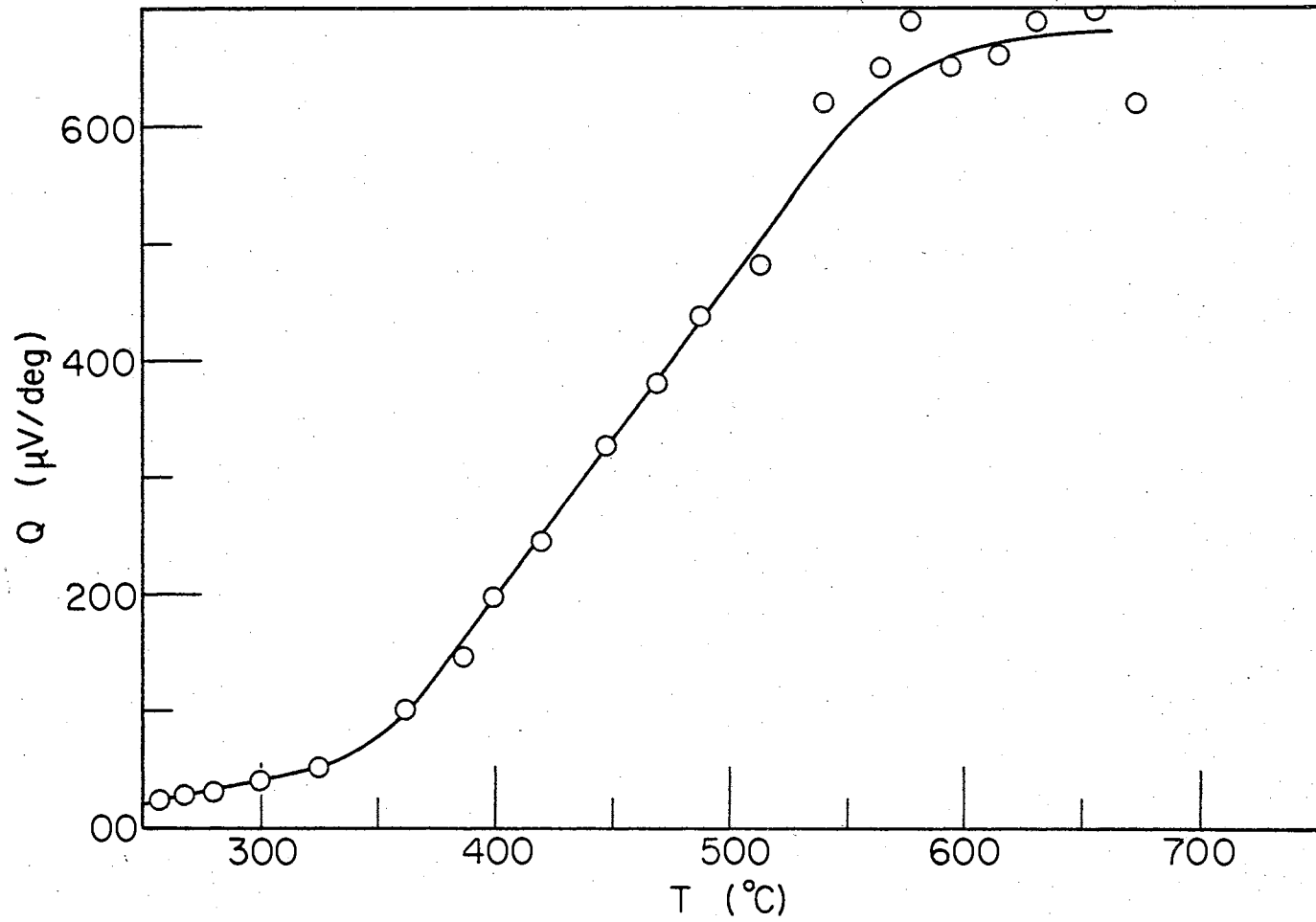Figure 31. Conductivity of Reduced Dense Ceramic

Figure 32. Thermoelectric Power of Reduced Dense Ceramic

observed with atmospheric pressure measurements (vide figures 22 and 23). In this case, as in the others, the room temperature conductivity is increased by several orders of magnitude. This phenomenon is accompanied by the appearance of gray color throughout the ceramic specimens. The samples regain their initial properties after being heated to 1000°C in air at atmospheric pressure for a few hours.

Low Temperature Measurements

Between room temperature and 500°C measurements of thermoelectric power were not possible on non-reduced samples due to their high resistance. The single crystal conductivity data in this region are, of course, primarily dependent upon the previous high temperature treatment. Of particular interest for this section is the variation in the properties of the non-reduced ceramics following low temperature-pressure treatments. There seemed to be both a slow mechanism and a fast mechanism changing the conductivity between 200 and 500°C. These were exhibited in conductivity overshoots and undershoots as the temperature was increased or decreased. This phenomenon is believed to be related to the long times associated with reaching a chemisorption equilibrium following a change in external parameters.

Figure 33 is typical of the behavior just noted. In this case a dense ceramic specimen was held at about 440°C overnight in air and the current measured with a two volt potential drop across the sample while the temperature was allowed to decrease. After tracing the conductivity upon cooling the heater power was then increased to return the sample to its original temperature. The resulting curve shows a hysteresis effect near the high temperature fixing point. The phenomenon is re-
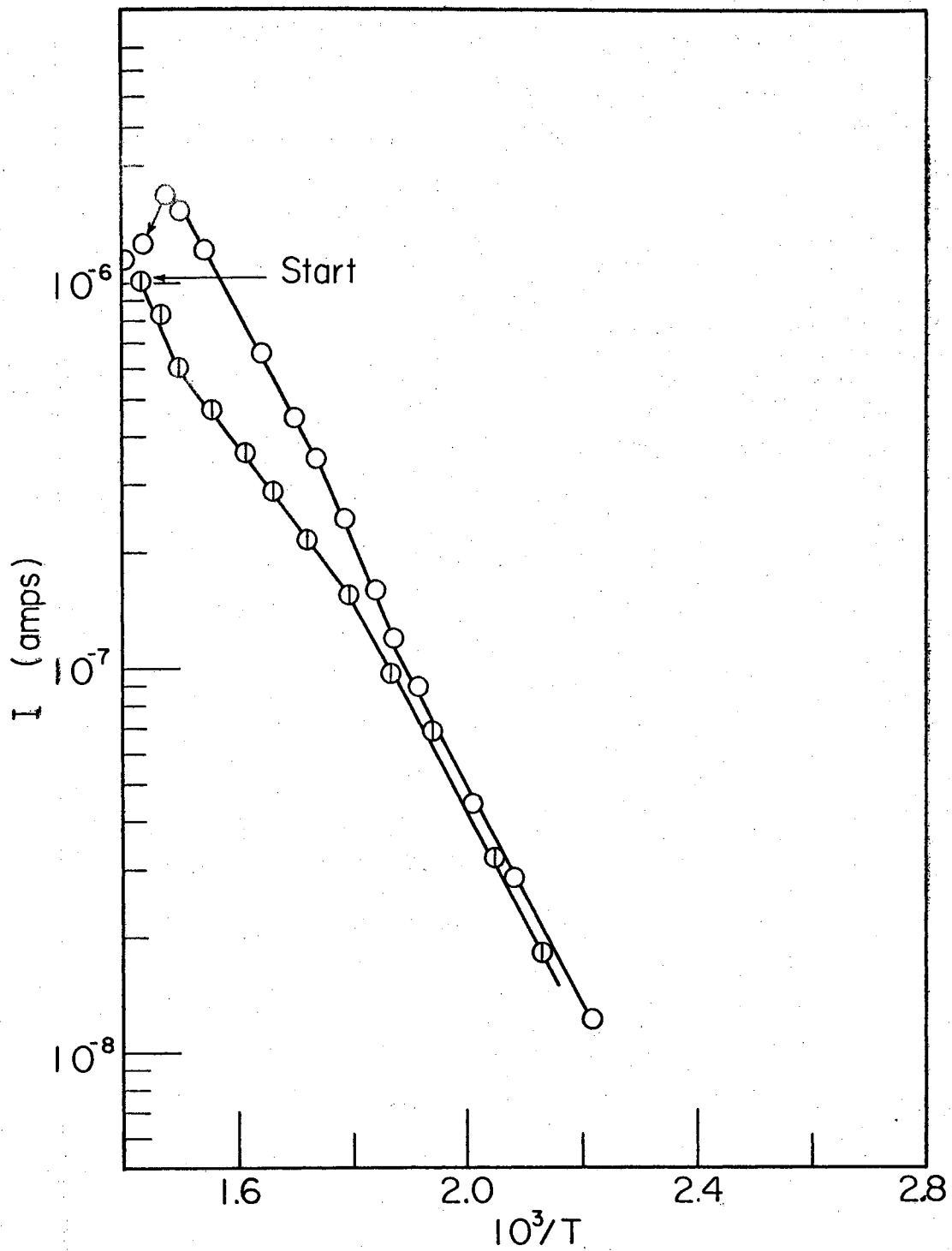
Figure 33. Evidence of Non-Reproducible Behavior
near Fixing Temperature

producible in a qualitative manner but seems to vary with fixing time, temperature, and rate of temperature change. It was also noted that by keeping somewhat below the original fixing temperature the conductivity is reproducible upon heating and cooling.

Figure 34 relates the variability of the conductivity following the low temperature treatment. In this case the treatments were in a vacuum (10^{-7} torr) following a high temperature air treatment. The sample was successively fixed for short periods at higher and higher temperatures. At fixing temperatures above 300°C the system seemed to stabilize with reproducible conductivity slopes and values until drastic reduction (see figure 31) occurred at 700°C.

On a compensated model (equation 29) the curve fixed at 114°C indicates a donor level at 0.4 eV. The 227°C curve indicates a donor level around 0.2 eV. The higher temperature curves indicate even shallower donor levels coming into play.

These changes upon low temperature treatments implied a surface mechanism, in which the conductivity of a closely compensated semiconductor may be changed quite drastically by a slight change in surface acceptor density.

If this is true and the surface acceptor states are associated with chemisorbed oxygen, then the conductivity should also change following a change of ambient from vacuum to air. This proves to be the case but the high temperature design did not allow accurate measurements at room temperature. Some difficulty was also experienced at higher temperatures since the specimen temperature fluctuated upon change of ambient in this region.

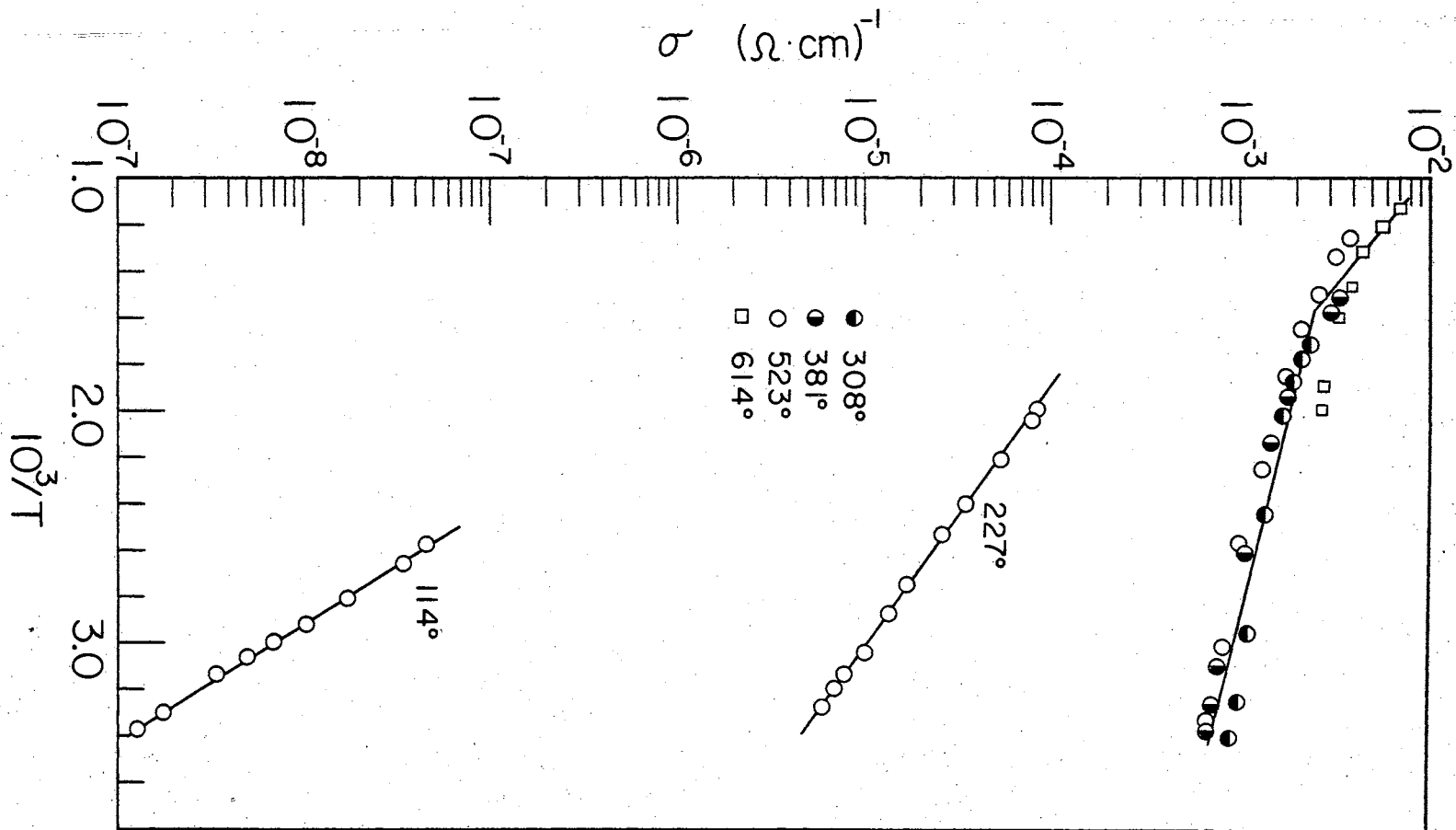Figure 35 gives the room temperature change of conductivity of a

Figure 34. Conductivity of Dense Ceramic Following Vacuum
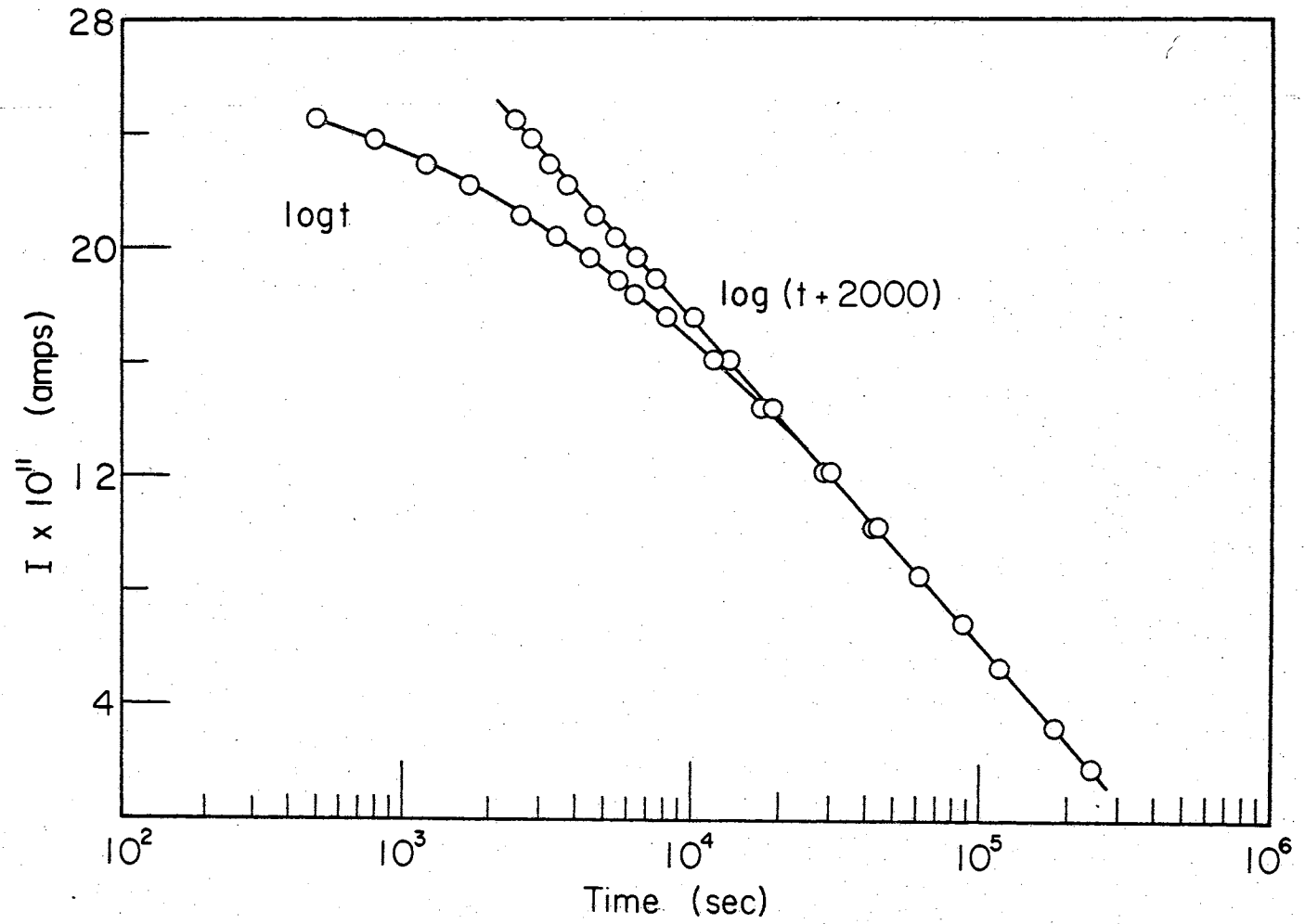Treatment at Different Temperatures

Figure 35. Transient in Dense Ceramic Following Admission
of Air at 20°C. (Obtained by H. E. Matthews)

dense ceramic as taken by another member* of this research group in an-
other apparatus. In this case the curve agrees with the theory for a
closely compensated semiconductor given in Chapter II in that i vs ln
(t + t') gives a straight line dependence.

Figure 36 shows both the current and inverse current of a dense
ceramic at 219°C as a function of log t. In neither case does a well-
defined linear dependence occur, perhaps since in this case there was
some temperature change associated with the pressure change.

In the following curve (figure 37) taken at 396°C the inverse cur-
rent appears linear with ln(t + t') as predicted by the previously de-
scribed theory for a less highly compensated semiconductor. Again the
temperature change hinders an accurate analysis of the data.

In order to insure that the phenomenon is not associated with the
contacts a dense ceramic specimen was used for this measurement at 380°
C in the four-probe sample holder (figure 38). In this case the inverse
dependence seemed to hold for short times and then a break occurred
followed by a region in which the direct dependence occurred. This is
the expected order if the material is becoming more highly compensated
with time.

In conclusion, this section indicates that surface controlled be-
havior via a chemisorption mechanism is affecting the conductivity. The
measurements here are only preliminary and no quantitative analysis has
been attempted. Some experimental difficulties have been noted and a
following section will include designs for reducing these problems.
While the data indicates that the theory presented earlier may be cor-
rect, it is by no means conclusive. A more detailed study of this be-
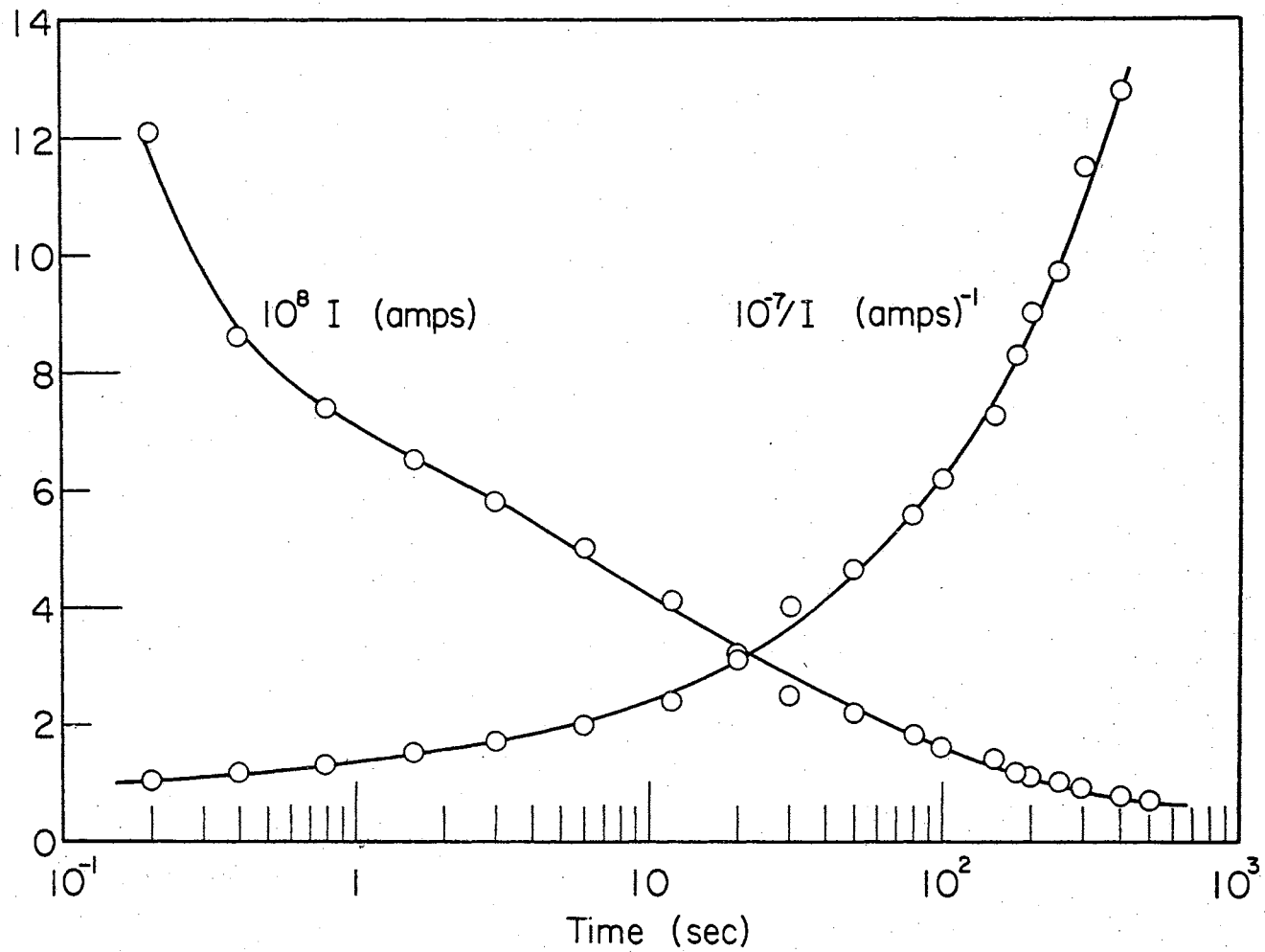
---

*H. E. Matthews

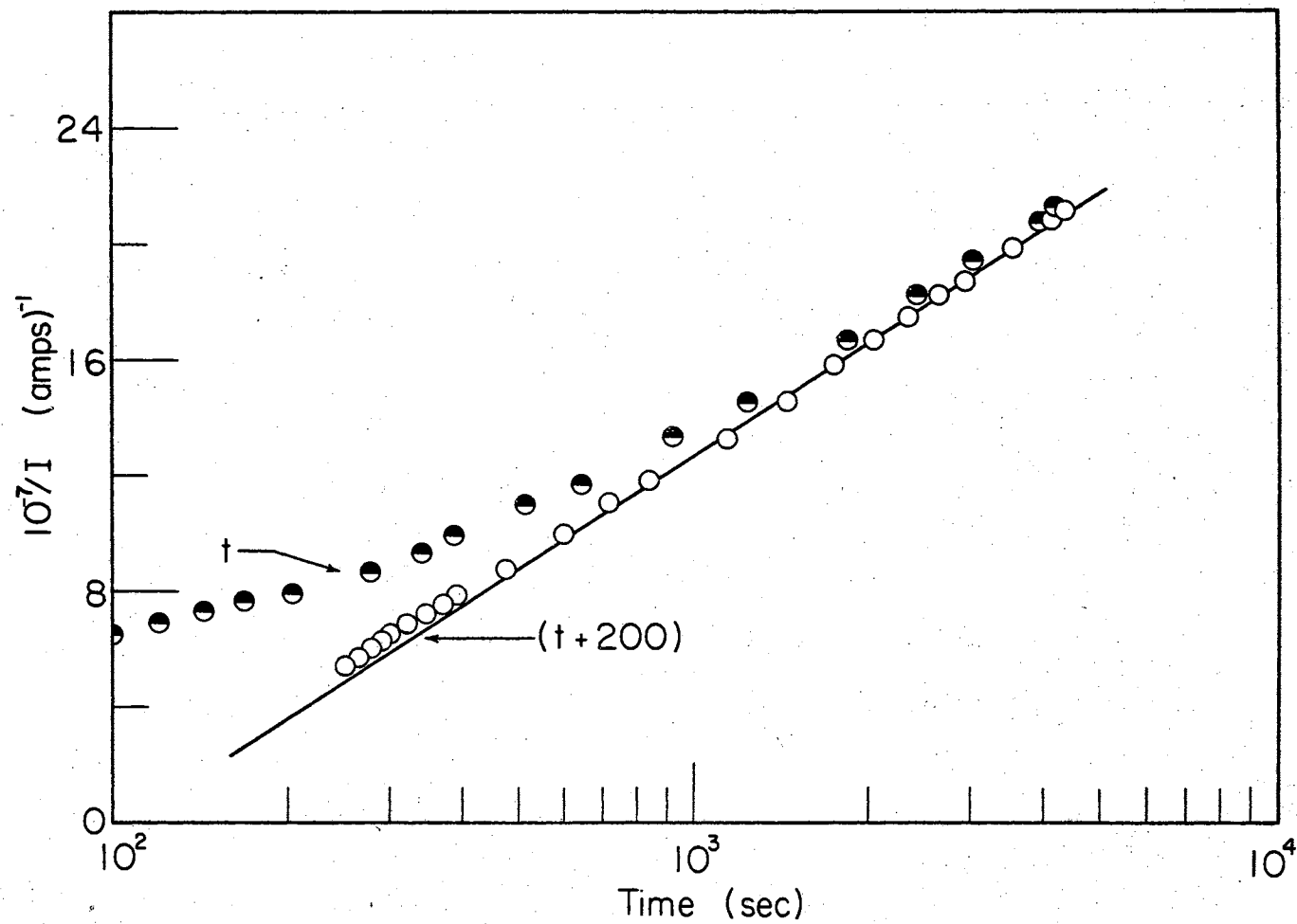Figure 36. Transient in Dense Ceramic Following Admission of Air at 220°C

Figure 37. Transient in Dense Ceramic Following
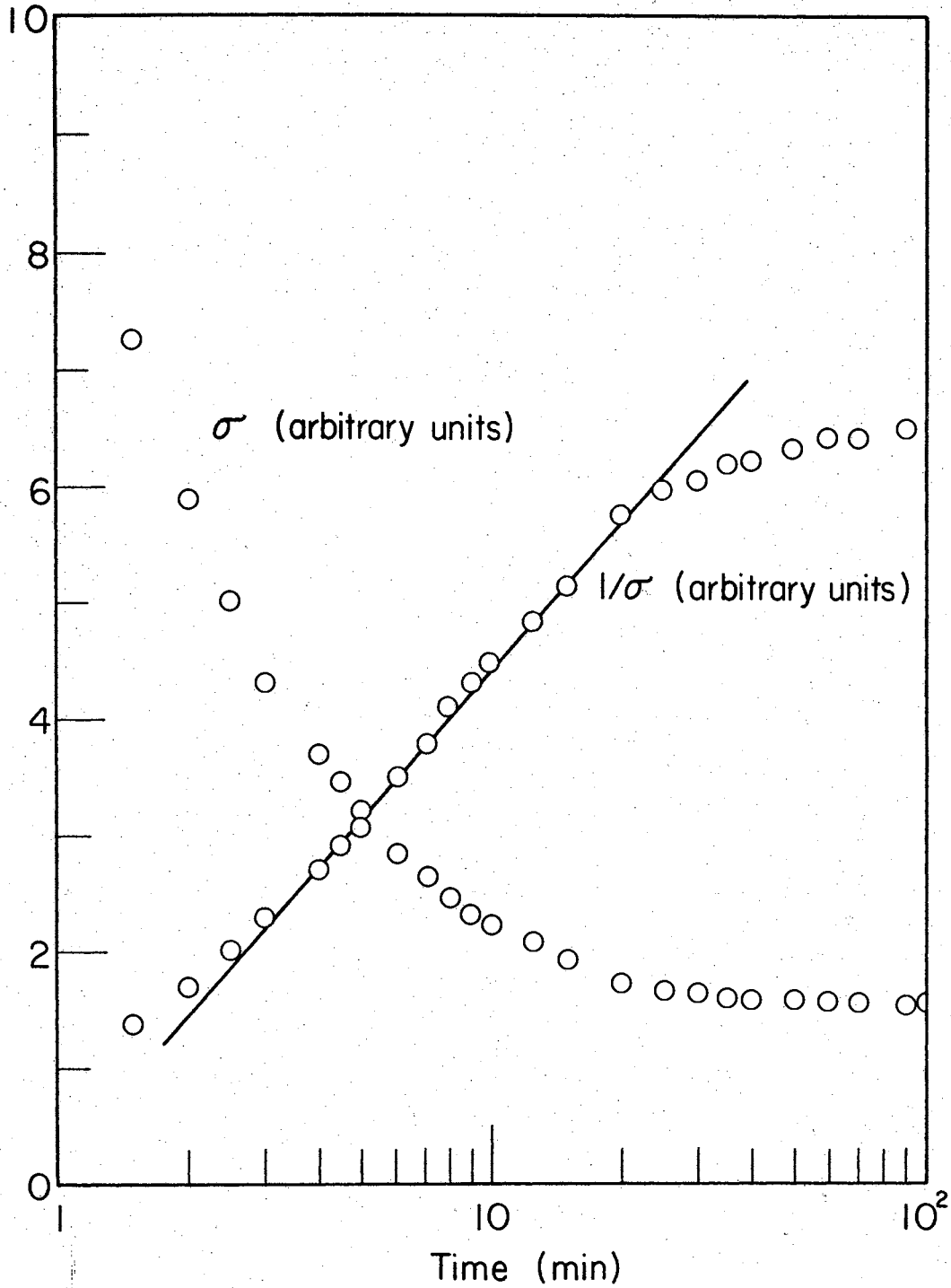Admission of Air at 396°C

Figure 38. Transient in Dense Ceramic Following Admission
of Air 380°C in Four Probe Sample Holder

havior is being given the attention of other members of this group.

Time and Field Dependence of Conductivity

This concluding portion of the presentation of experimental results is devoted to current transients following the application of the external field and to the dependence of sample current on field strength.

Figure 39 shows the current voltage relationship on a porous ceramic specimen at 438°C in dry air in a two probe sample holder. In this case platinum paint electrodes were fired onto the ends of the sample.

Figure 40 is a tracing of the time-base recorder plot of temperature, current and probe potentials from ground in a four-probe sample holder of a dense ceramic specimen. This data was taken at 416°C with a 90 volt potential applied to the sample.

Figure 41 gives the apparent resistance as a function of time in the four-probe sample holder following the application of a 90 volt potential at 416°C to a dense ceramic sample. It is to be noted that the center (~ 1/3 sample length) resistance remains constant while the end-to-end resistance changes significantly.

Figure 42 gives the apparent resistance is a function of applied potential on the same sample. Again the change in center resistance is much less than the change in end-to-end resistance.

Figure 43 is a direct plot from the recorder of the temperature, current for a 90 volt potential, and the two probe voltages all as a function of time for the same sample at 720°C. It is to be noted that there is a rapid change in end-to-end current while the probe voltages remain reasonably constant. In addition only about 15 volts appears
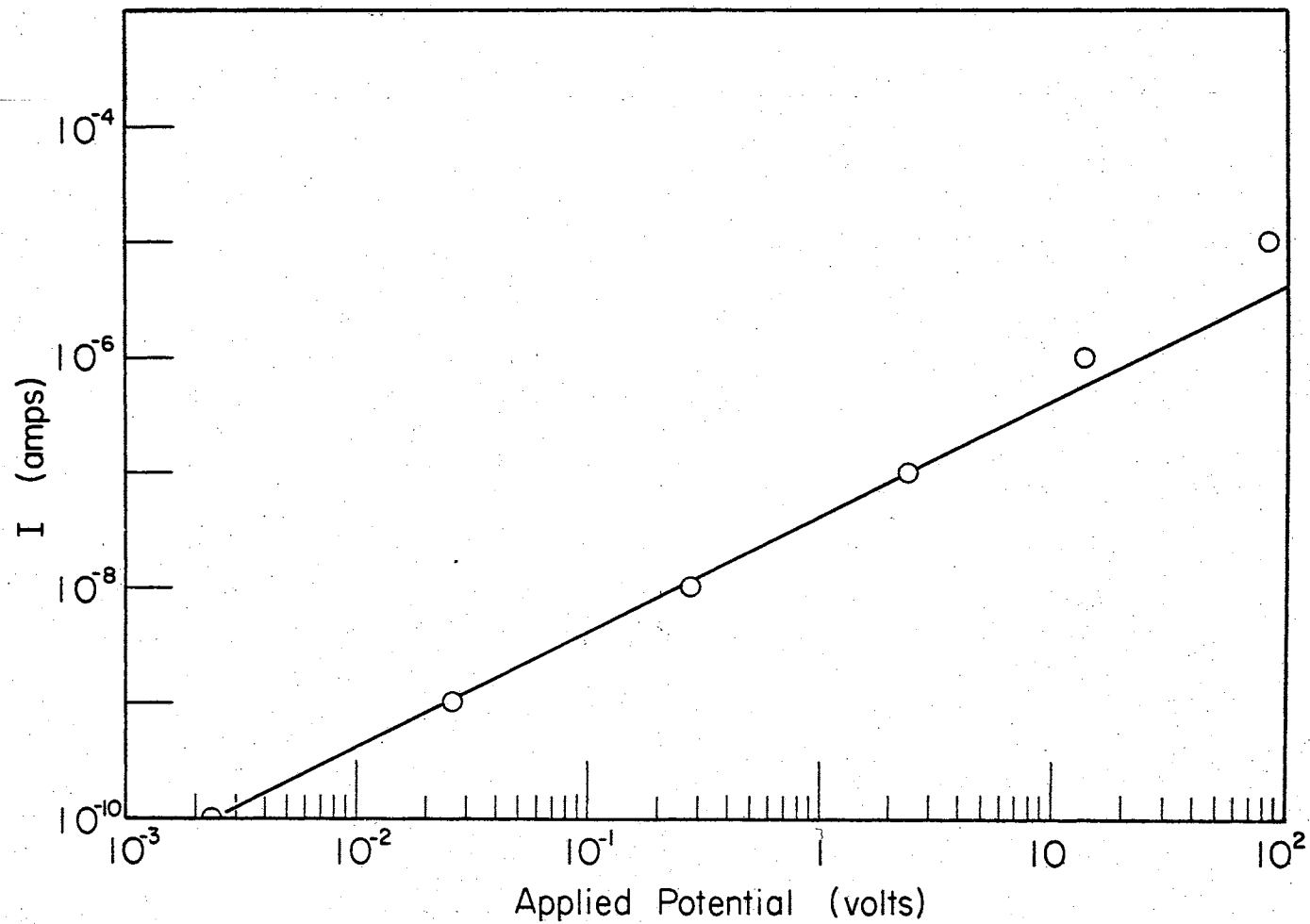
Figure 39. Current as a Function of Applied Potential
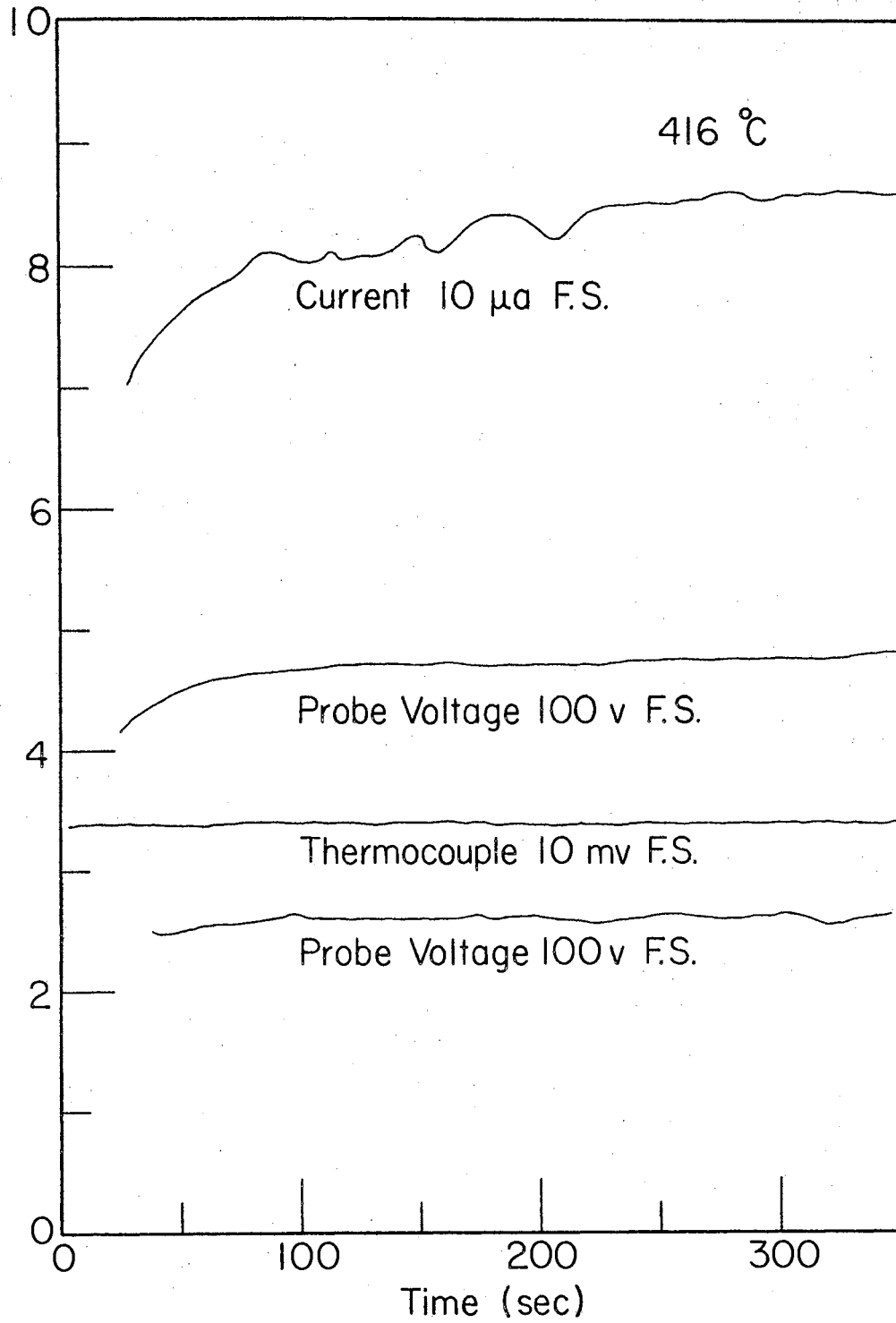of Porous Ceramic at 438°C

Figure 40. Recorder Plot of Transient in Dense Ceramic with
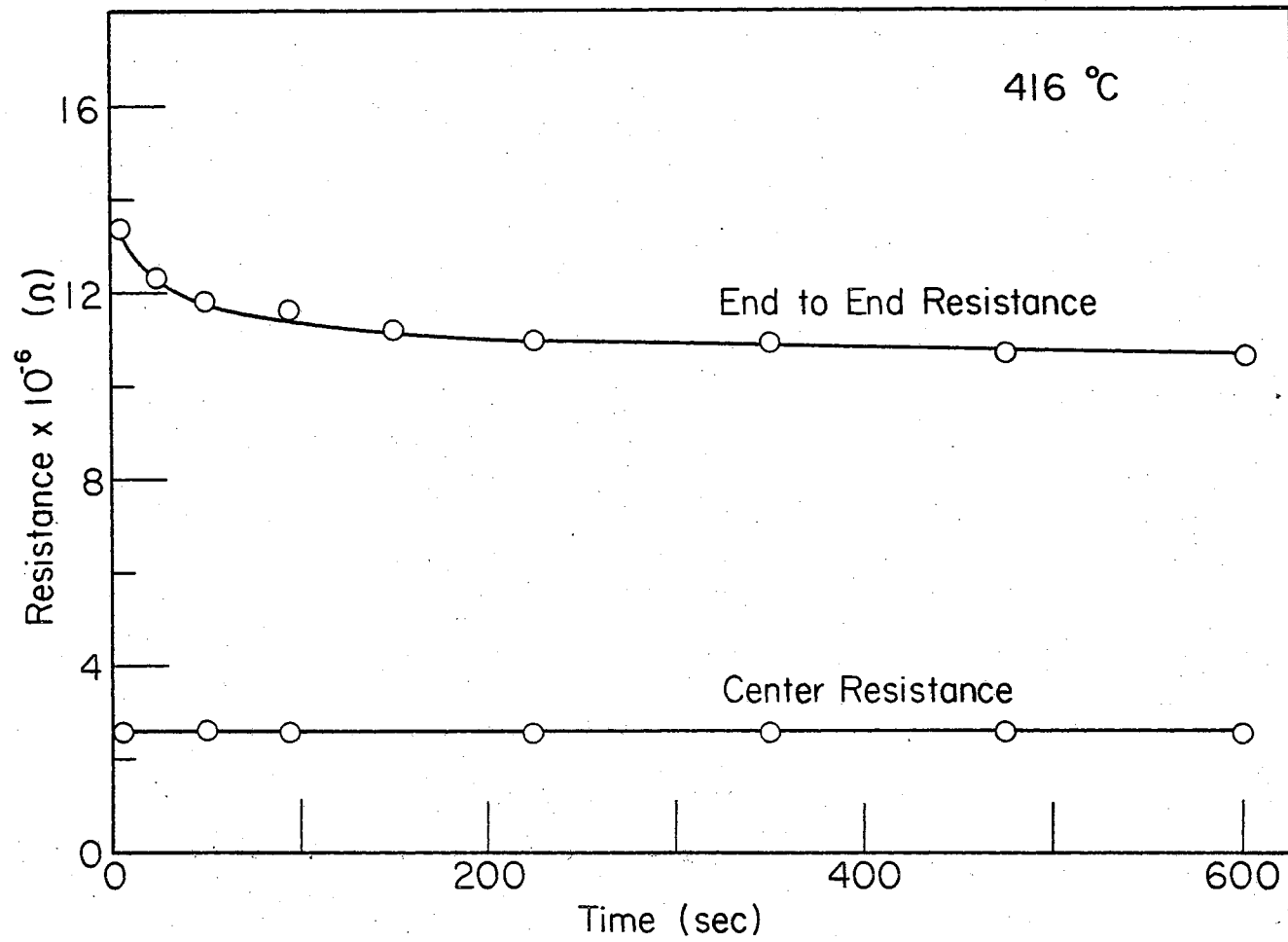Four Probe Sample Holder in Dry Air at 416°C

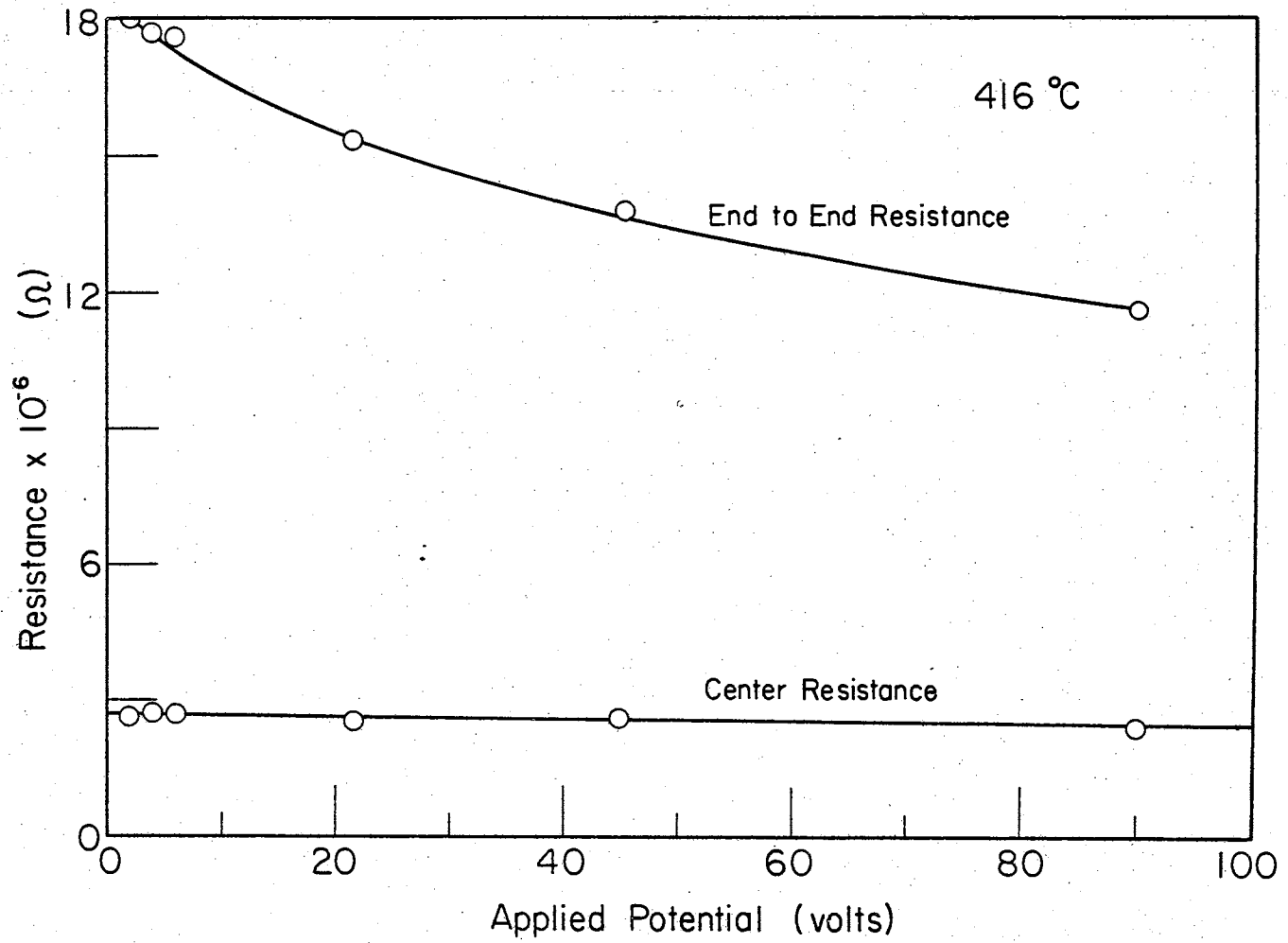Figure 41. Resistance Transients Obtained From Figure 40.

Figure 42. End to End Resistance and Center Resistance as a Function of
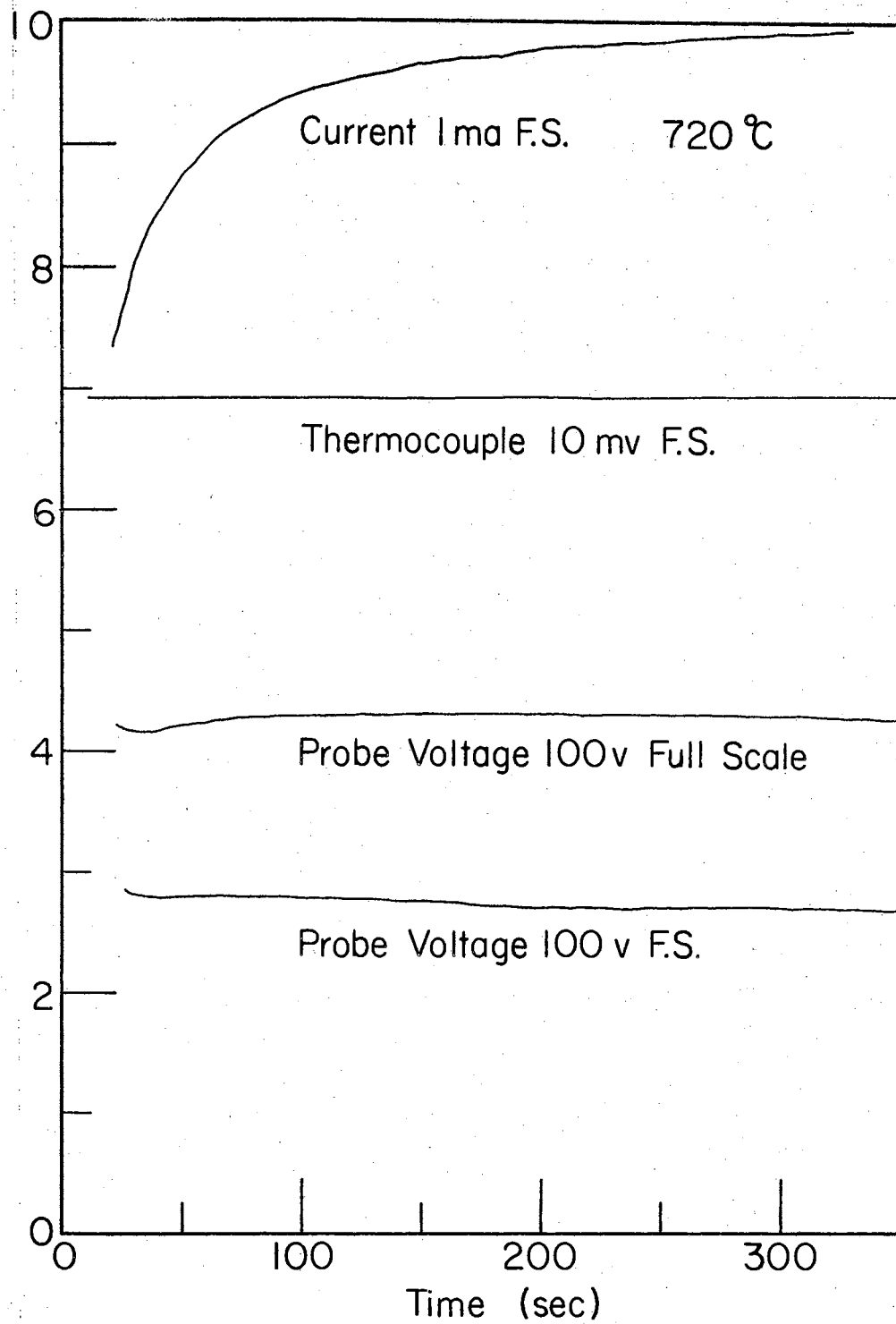Applied Potential, Dense Ceramic at 416°C

Figure 43.   Transient in Dense Ceramic at 720°C

across the center probes while the geometrical relationship of the probe placement predicts around 30 volts.

Figure 44 shows the resistances calculated from figure 43 as a function of time. Again the majority of the resistance change occurs at the ends of the sample.

The end-to-end and center resistances of this sample at 720°C as a function of applied potential are given in figure 45. A slight variation of center resistance is apparent but is much smaller than the variation of end-to-end resistance.

The next series of figures (figure 46 through figure 51) indicates the current as a function of time for a porous sample with platinum paint electrodes at various temperatures with different applied potentials. For each temperature a separate figure appears with curves at each of several applied potentials. The complexity of the transients increases with both the temperature and applied potential. The lower voltages do not produce transients until higher temperatures are reached.

The four-probe data suggests that the origin of the transients is connected with the electrodes. The increasing (with time) nature of the transients is not fitted by ionic conduction with blocking electrodes[38]. The origin is believed to lie in imperfect contacts making necessary high current densities at a few points on the contact surface region and/or in electrolysis reactions at the electrodes. The small changes in center resistivity in the four-probe sample holder indicate that field-induced defect production occurs primarily at the electrodes. No long term data was taken to ascertain whether this damage can eventually penetrate to the center of the specimen.

Similar transients occurred in all specimens, and, as a consequence,
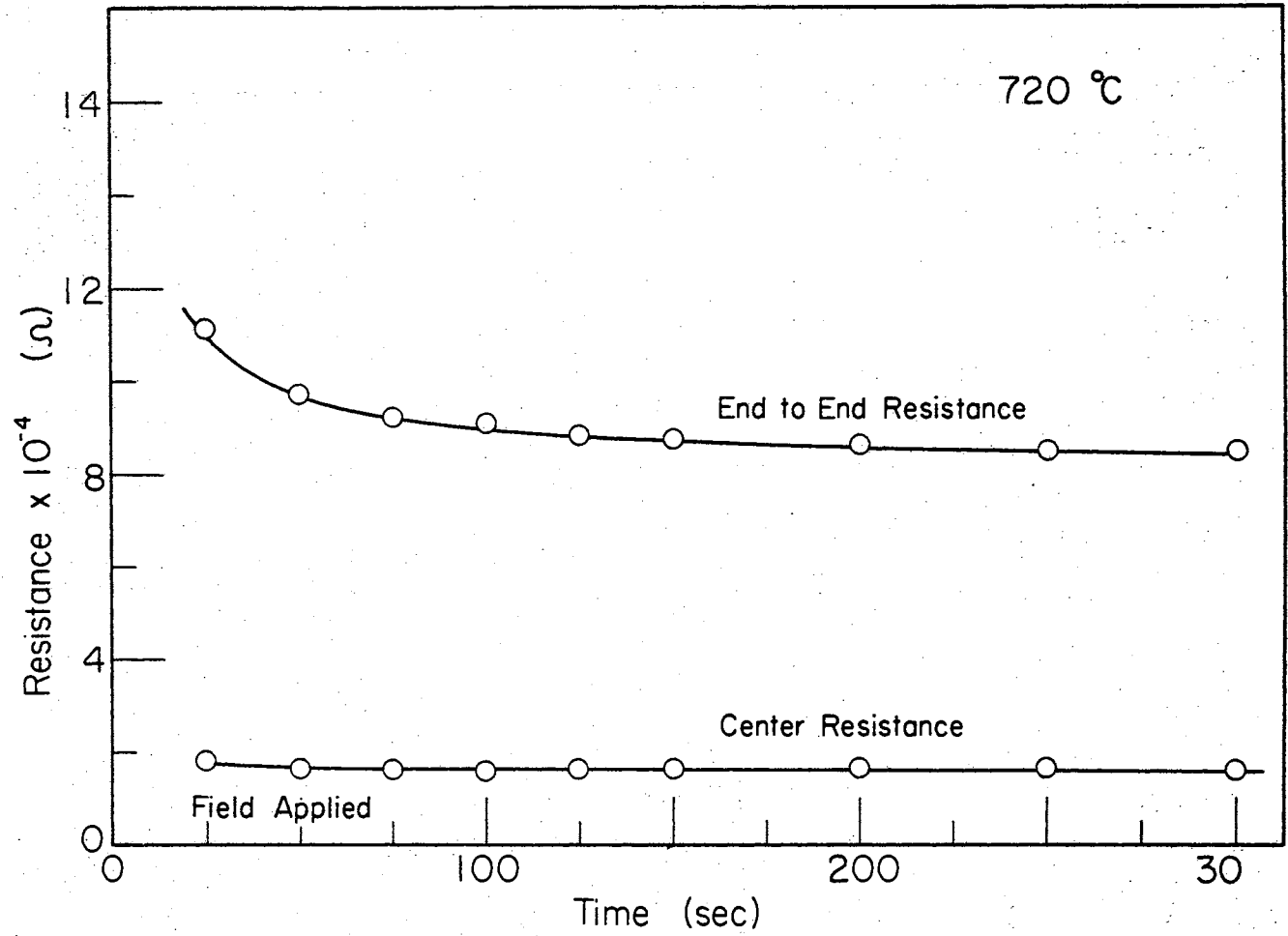
Figure 44. Resistance Transients in Dense Ceramic at 720°C
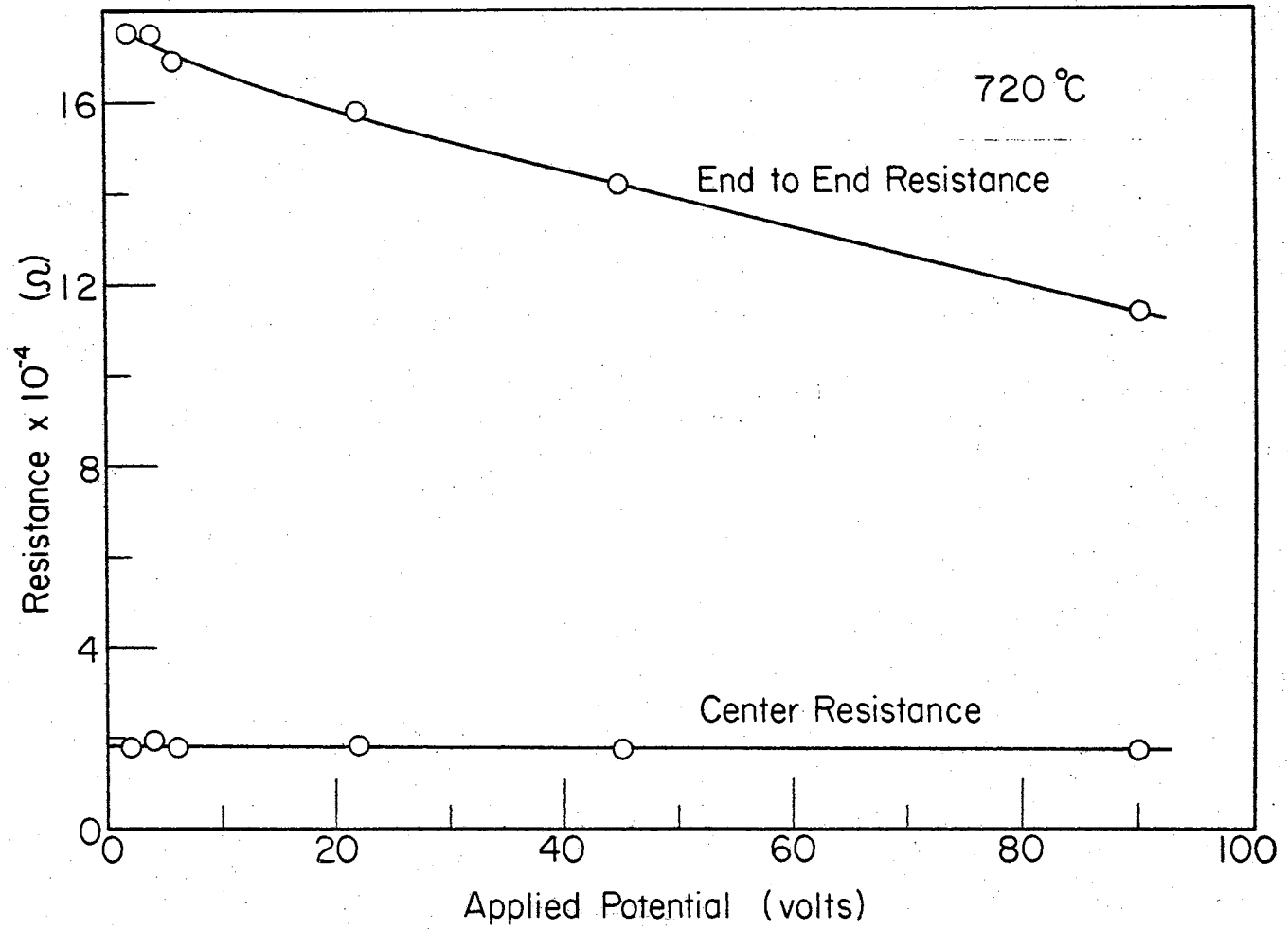
Figure 45. Resistance of Dense Ceramic as a
Function of Potential at 720°C
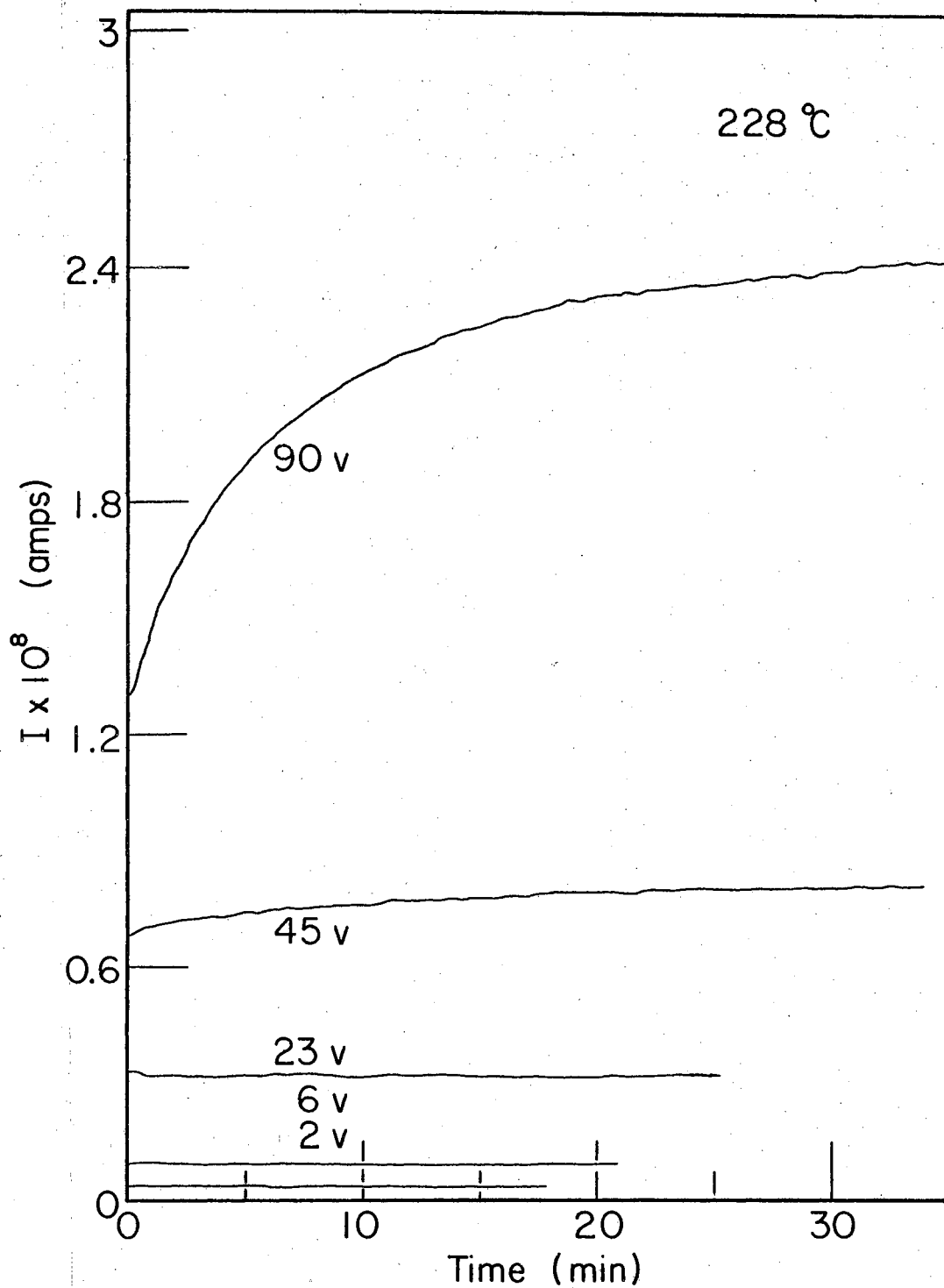
Figure 46. Current Transients with Different Applied Potentials of Porous Ceramic at 228°C

Figure 47. Current Transients with Different Applied
Potentials of Porous Ceramic at 430°C

Figure 48. Current Transients with Different Applied
Potentials of Porous Ceramic at 522°C

Figure 49. Current Transients with Different Applied
Potentials of Porous Ceramic at 638°C

Figure 50. Current Transients with Different Applied
Potentials of Porous Ceramic at 788°C
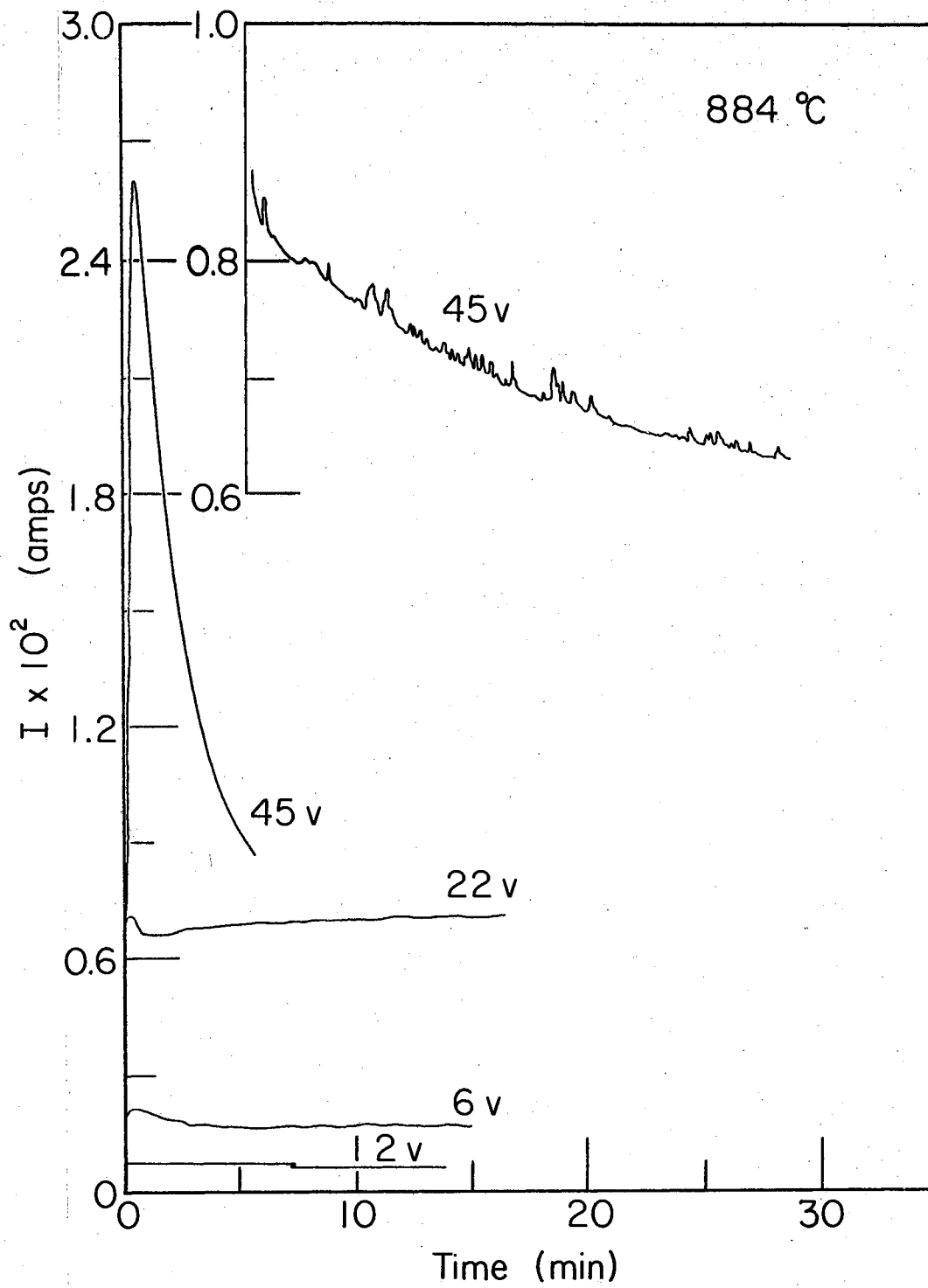
Figure 51.   Current Transients with Different Applied
Potentials of Porous Ceramic at 884°C

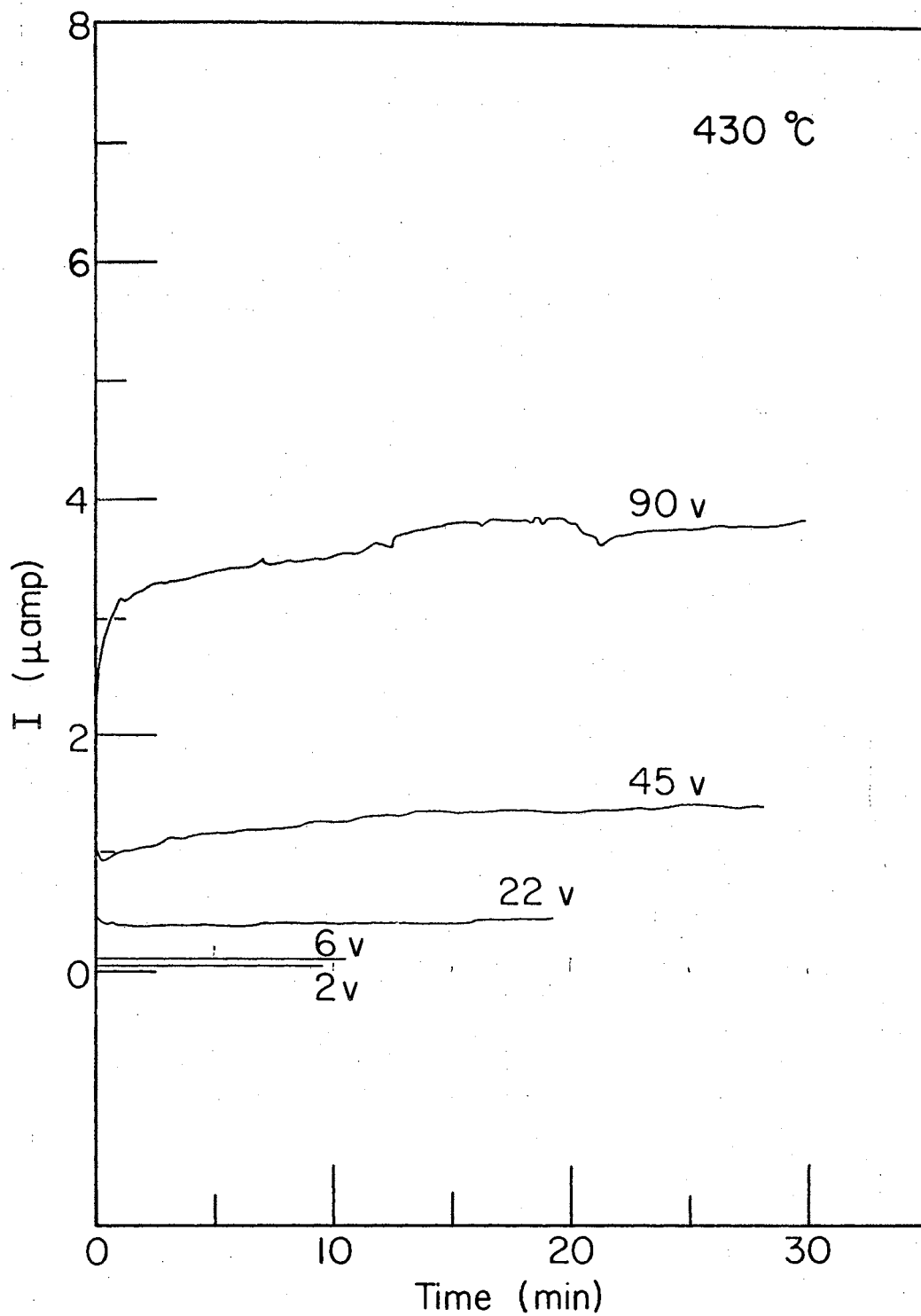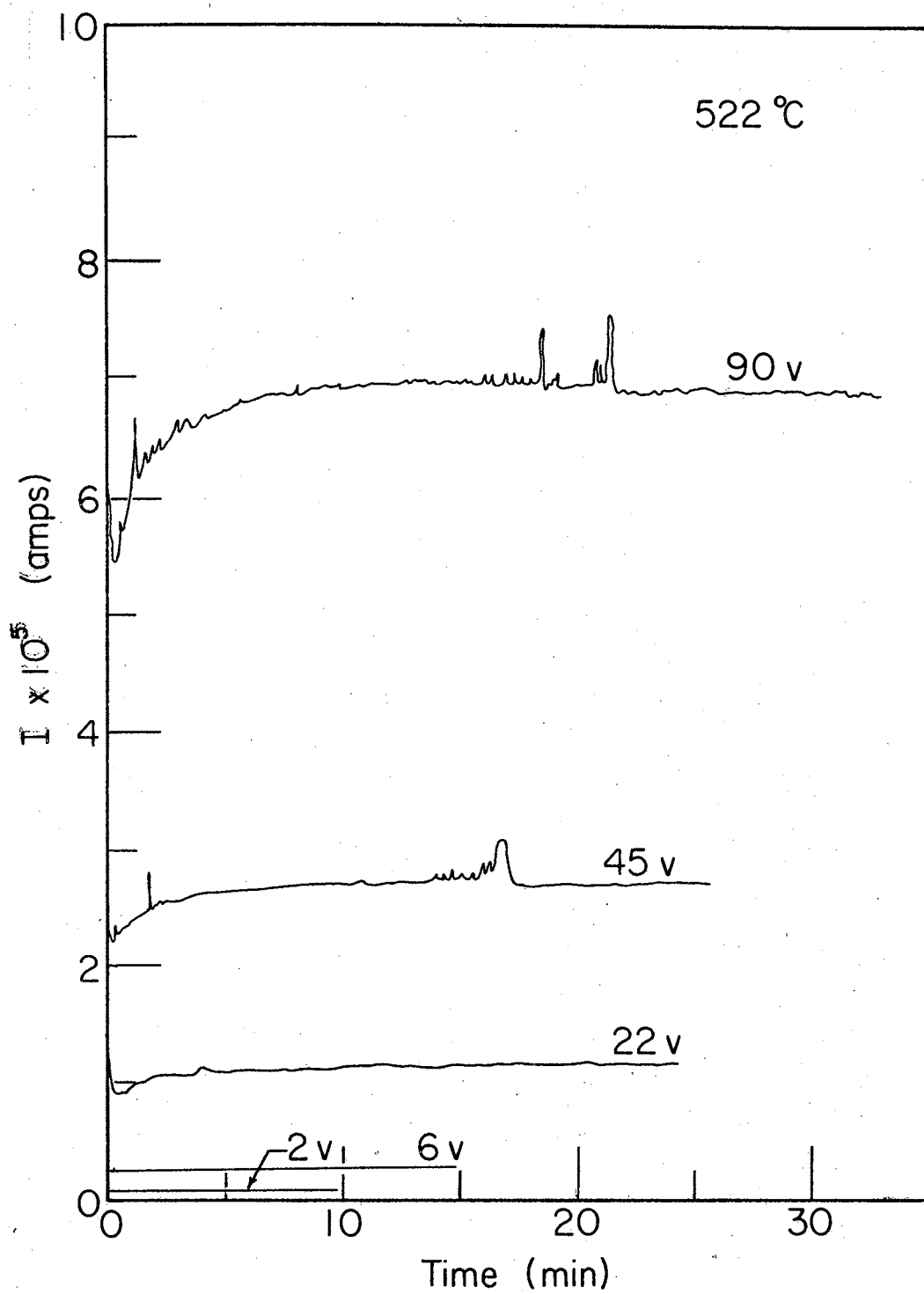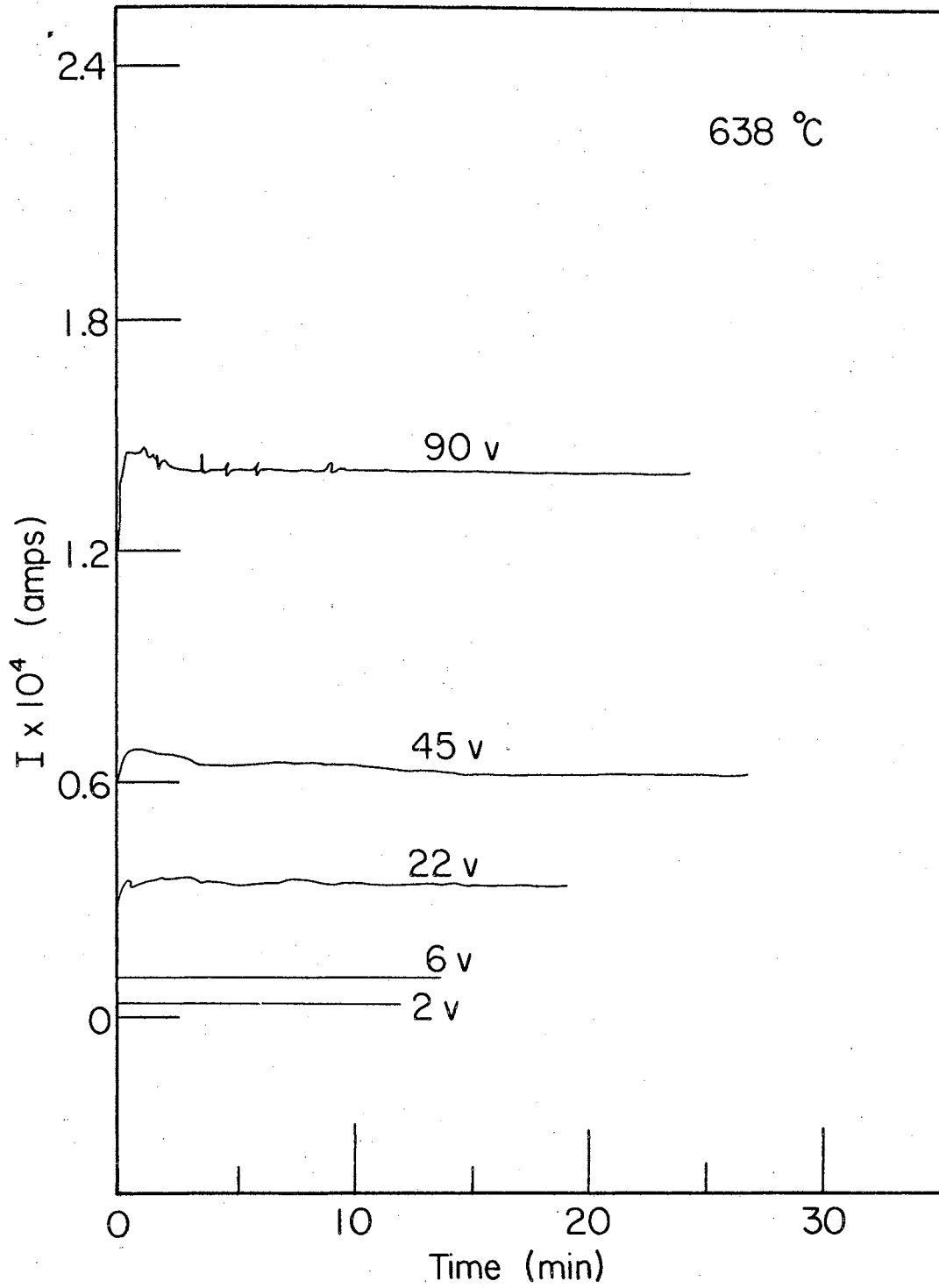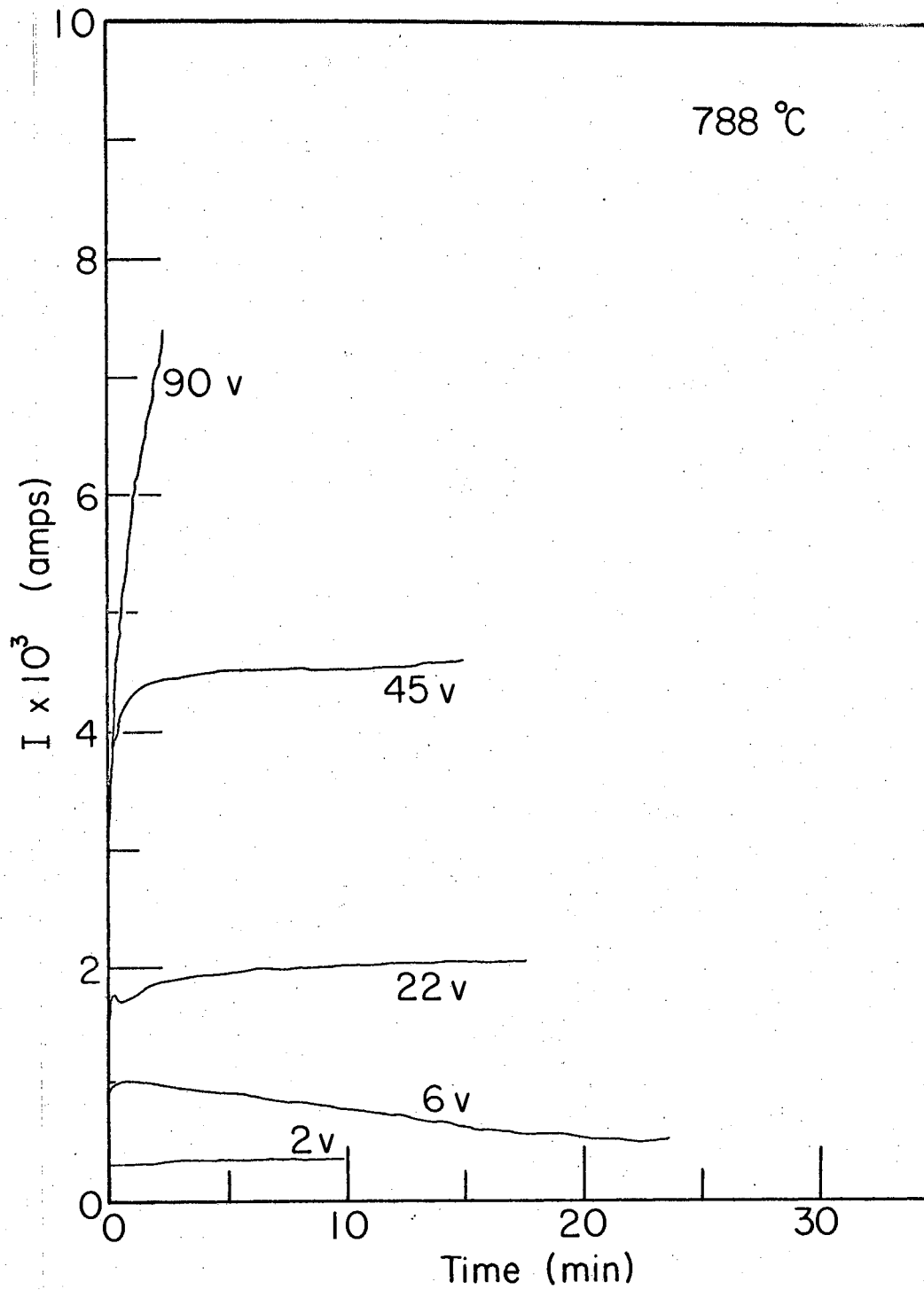all conductivity measurements at high temperatures were taken with low fields (10 to 100 MV). This made it necessary to take great care to eliminate thermal voltages which are of similar magnitude. This was accomplished by adjusting the heater so that no temperature different-ial appeared across the sample. In addition the meters were zeroed while in contact with the sample but with no external applied field.

This procedure eliminates all transient effects due to contacts which are apparent at the higher fields. The relatively good agreement of the conductivity data taken in the four-probe sample holder indicates that the values of conductivity reported in this study are not greatly in error even though a small amount of spreading resistance due to non-uniform contacts may still be present.

Summary of Results

At high temperatures the activation energy as determined by an Arrhenius plot of conductivity is in the order of 2 eV. Below 700°C the slope of the conductivity plots slowly changes to a smaller value which corresponds to less than 1 eV at room temperature. The nature of this lower portion is highly fixing pressure dependent tending to lower values of energy as the pressure is decreased.

On the porous ceramic sample above 700°C a direct dependence of electrical conductivity upon amibient pressure was noted.

Prolonged heat treatment in a vacuum of 10^{-3} torr or less at tem-peratures greater than 700°C tended to reduce the samples, leaving them in a high conductivity state at room temperature. In the ceramic materials this effect is accompanied by a change in color from white to grey. The change in conductivity level is reflected in a reduction in

the magnitude of the thermoelectric power which always indicates that electrons are the main current carriers.

At temperatures below 500°C there is a conductivity change in the polycrystalline specimens following a change in pressure. This appears to be associated with chemisorbed oxygen. At the higher end of this range, reciprocal of the current shows a proportionality to $\log(t + t')$ while at room temperature the currently is proportional to $\log(t + t')$.

At all temperatures above 200°C it was possible to observe current transients following the application of an electric field. The magnitude and complexity of these transients increased both with temperature and field strength. The application of platinum paint to the contacts did not significantly alter the nature of these transients. At the highest temperatures (1100°C) reached in this study, a potential of 2 volts was sufficient to induce this transient behavior, and as a consequence, measurements of electrical conductivity were taken with applied fields varying from 10 to 100 MV. With these fields no transients were noted. Observation of the transients with a four-probe technique on a doped ceramic indicated that most of the end-to-end resistance change occurred at the ends of the sample and not in the bulk.

CHAPTER V

CONCLUSIONS AND SUGGESTIONS FOR FURTHER STUDY

Conclusions

In the temperature region studied the electrical behavior was controlled by several different mechanisms. The measurements and calculations may be logically divided into three groups dependent upon the information they yielded. The first group was utilized to identify the mechanism and to determine which experimental parameters were important. Once the mechanism had been identified, measurements were taken to verify that the measurement process had no derogatory effect. And finally specific experimental data were employed to evaluate parameters associated with each mechanism.

Single crystals, porous ceramics and dense ceramics were used in this study for comparison purposes and for study of different mechanisms which were dependent upon sample structure.

From 1000 to 1400°K the experimental data for the dense ceramics and single crystals may be fitted to the intrinsic model with the following average parameters:

$$m_n = 0.2 \ m_o, \tag{76}$$

$$\mu_n = 100 \ (300/T)^{3/2} \ (cm^2/volt\text{-}sec), \tag{77}$$

and

$$E_g = 4.05 - 16.5 \times 10^{-4} \ T \ (eV).$$

According to this model the electron-to-hole mobility ratio is found to be of the order of 7. In addition the effective mass ratio was estimated to be near unity. As no direct correlation between oxygen pressure and electrical conductivity could be ascertained at these temperatures and pressures from 10^{-3} torr to atmospheric, it is felt that any pressure dependent defect mechanism produces only a small portion of the observed high temperature behavior. Minor deviations in magnitude of electrical conductivity at this point are believed to be due to imperfect electrical contact with the samples.

Since neither intrinsic behavior nor hole conduction has been previously reported, no direct comparison between the parameters derived on the basis of this model and other electrical studies is possible. However, the optical energy gap near room temperature has been evaluated by other workers. Though the optical gap and the thermal gap are not identical, a degree of correlation should exist between thermally observed gaps and those due to indirect optical transitions. Summit, Marley and Borrelli[41] have reported direct optical gaps of 3.57 eV and 3.93 eV for light polarized parallel and perpendicular to the c axis. They also note indirect optical gaps at 3.4 eV and 3.7 eV. Reddaway and Wright[42] indicate the possibility of an indirect transition at 2.55 eV and a direct gap from 3.65 to 4.05 eV. Kohnke[13] has observed on natural crystals short wavelength optical cutoff energy given by 3.7 - 6 x 10^{-4} T (eV) near room temperature. These values are in reasonable agreement with the room temperature thermal gap value of 3.55 eV given here. Note, the expression $E_g = E_{go} - \alpha T$ is in reality a truncated series expansion. Consequently, studies in different temperature regions may well yield different results for both α and E_{go}.

Since no hole mobilities have been previously noted, the mobility ratio ($\mu_n/\mu_p = 7$) has no direct comparison but appears reasonable. In general, one expects the hole mass to be larger than the electron mass. Arai[43] has found this to be the case in thin films by optical means, reporting a hole effective mass of 0.82 m_o. In the present study the calculations were so sensitive to small differences in measured quantities that it was impossible to obtain a unique value for this parameter. However, all indications point to similar effective masses for the holes and the electrons.

The porous ceramic specimen S-15 behaved somewhat differently in the high temperature range, and the nature of its conduction mechanism has not been established. This sample exhibited a pressure dependent conductivity at all temperatures above 600°C.

At temperatures above 700°C a reversible thermal production of defects dependent upon oxygen pressure is noted for all samples. Although this mechanism does not control the conductivity above 700°C, the changes induced by it are readily apparent at lower temperatures where both the activation energy and the magnitude of the electrical conductivity are affected. This mechanism is further supported by reversible weight-loss measurements obtained by another member of this research group.*

Upon extreme reduction the samples appear degenerate at room temperature. This may be related to a donor level at 0.15 eV noted by Marley and Dockerty[19] which merges with the conduction band as its density is increased.

The non-reduced polycrystalline samples at temperatures below 500°

---

*J. Tunheim

appear to be closely compensated with at least a portion of the compensation being associated with oxygen chemisorbed upon the surface. The conductivity level is controlled by the degree of compensation and the Arrhenius slope is related to the activation energy of the principal donor level. In this connection, the model has been expanded to explain the transients in conductivity which occur upon a rapid change of ambient, providing qualitative evidence that the model is applicable.

In addition, transient effects following the application of an external field have been noted and presented. Evidence has been presented that these transients are to be associated with the contacts.

Suggestions for Further Study

Throughout the course of this study effects such as transients and non-reproducibility have been apparent. On the single crystals available it has been impossible to separate bulk effects from contact effects at higher applied fields.

It would seem advisable to investigate the transients more closely and make an attempt to verify their origin. Such a study has been completed by Blumenthal and Pinz[44] in CeO, and similar techniques should be applicable in stannic oxide. Use of multi-probe techniques await the availability of larger crystals, however.

The availability of larger samples would also allow measurements of the Hall effect. The information available from these measurements should make possible the determination of such parameters as mobilities and effective masses with a greater precision than possible at this point.

The pressure dependent thermal defect mechanism needs substantia-

tion--probably through a series of weight loss measurements and four-probe conductivity measurements as a function of ambient pressure.

As ceramic specimens of sufficient size for the above mentioned measurements are available, it may be suggested that these samples be used. It is to be noted that a pure ceramic specimen in this study deviated strongly in several ways from the single crystals. The dense ceramics deviated to a lesser degree but it should be remembered that they are quite heavily doped.

Measurements on ceramic specimens should, of course, be treated with care as these materials may be affected by pore structure, grain boundary conditions, and neck or intergranular problems. In addition stannic oxide is known to be anisotropic, and the effects of polycrystallinity will completely obscure these directional effects. From a practical point of view, ceramic materials are easily fabricated and it is possible that future technology will utilize them more and more frequently for electrical uses thus making a knowledge of their special properties a valuable asset.

As evidenced by data taken on the dense ceramic specimens, the high temperature region is remarkably similar to that of single crystals; however, one cannot be certain a priori that this will be the case. In light of both the similarities and the differences noted between the single cyrstals and the ceramic materials, it would be advisable to continue to study the two types in conjunction.

This study has investigated to a small degree the conductivity changes due to an ambient pressure change at temperatures lower than 400°C. As noted earlier, the high temperature requirements made compromise necessary in the final design. As a consequence, during ambient

changes the sample temperature drifted by several degrees. This effect made impossible a completely satisfactory comparison between theory and experiment, and it is suggested that an apparatus be constructed with only this measurement in mind. At present other researchers in this laboratory are working with such an apparatus. Their high temperature limit is around 150°C which now appears to be too low for a comprehensive set of data.

Figure 52 is a design of a sample holder for this measurement which fits into the present sample chamber. It is designed for guarded circuitry and has the sample mounted flat between two heat sink electrodes. By back filling to around 10^{-1} torr of helium and allowing temperature equilibrium to be reached prior to admission of air, the short term temperature transients should be greatly reduced. The addition of a furnace controller would prevent long term drifts thus allowing the transients to be observed over a period of several days.

This design should be applicable to temperatures up to 500°C as the electrodes in the high temperature region are readily removed for cleaning. The construction of a sample chamber to maintain temperatures below ambient may also be warranted at some time in the future.

The possibility of ionic motion or diffusion in these materials has been noted in this study and in others. Measurement of the dielectric constant as a function of frequency at various temperatures will indicate to some degree whether this exists and at what temperature it occurs. Unfortunately the low frequency behavior associated with ionic motion is quite similar to that associated with grain boundary effects. Thus this measurement to be valid must be restricted to single crystals. The determination of ionic motion by measurement of transport numbers
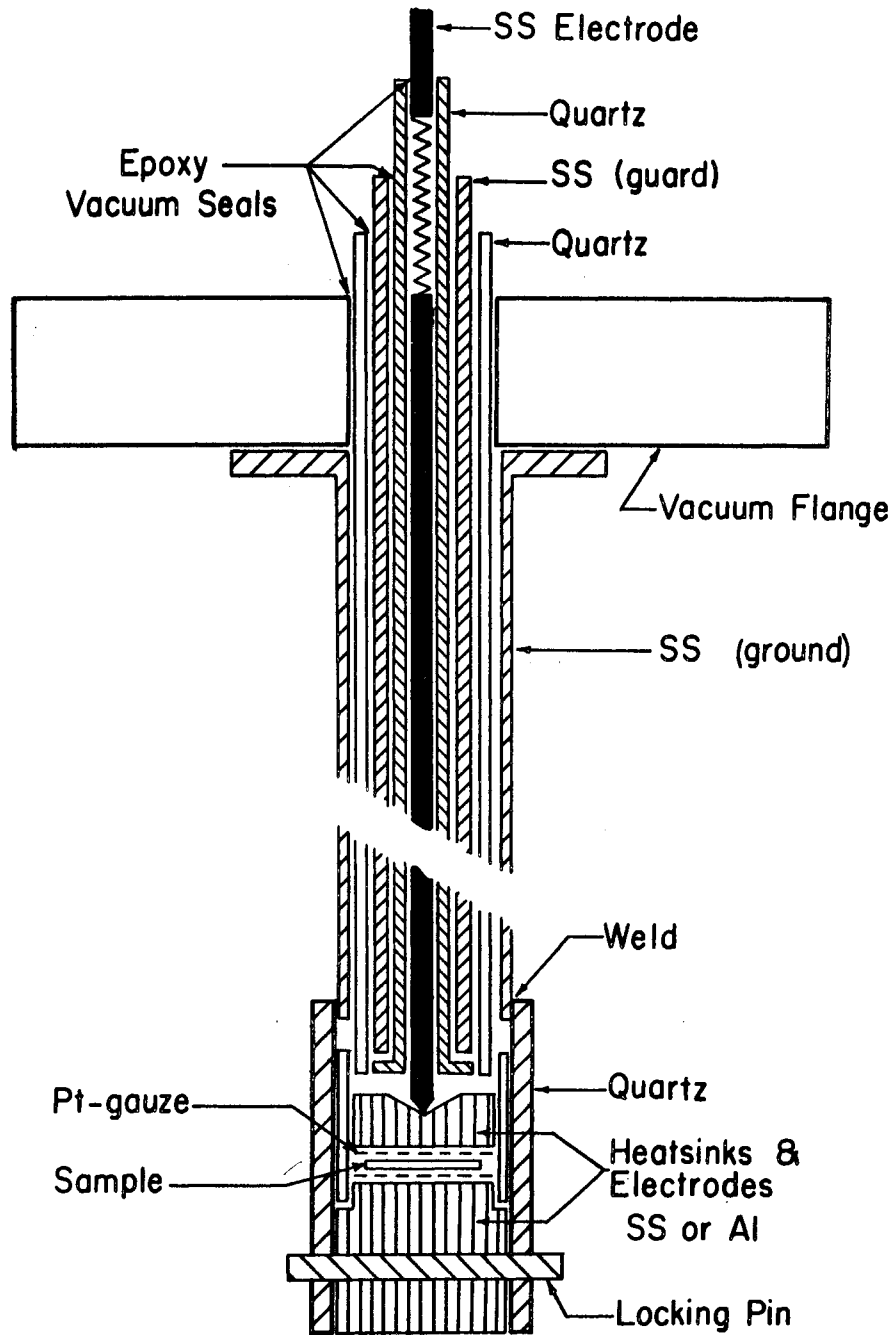
Figure 52. Proposed Sample Holder For Measurement of
Ambient Change Transients

using the galvanic cell method does not seem warranted at present as it is believed that the ionic currents are very small compared to the electronic current.

The origin of the transients has tentatively been assigned to the contact region of the samples and does not appear with low fields. The D.C. measurements described above may be taken with low applied fields with the electrical circuitry depicted in figure 53. With this circuit and careful technique both two-probe and four-probe measurements may be taken with little fear of transient problems.

The circuit is designed for constant current measurements. Use of the correct battery voltage and current limiting resistor will provide currents accurate to within 1%. This method reduces the electrometer requirement from three to one, by proper location of the ground. As given in the schematic, this circuit should be capable of measuring resistances from 1 to 10^9 ohms. Slight modifications of probe positions would allow its use for Hall-effect measurements.
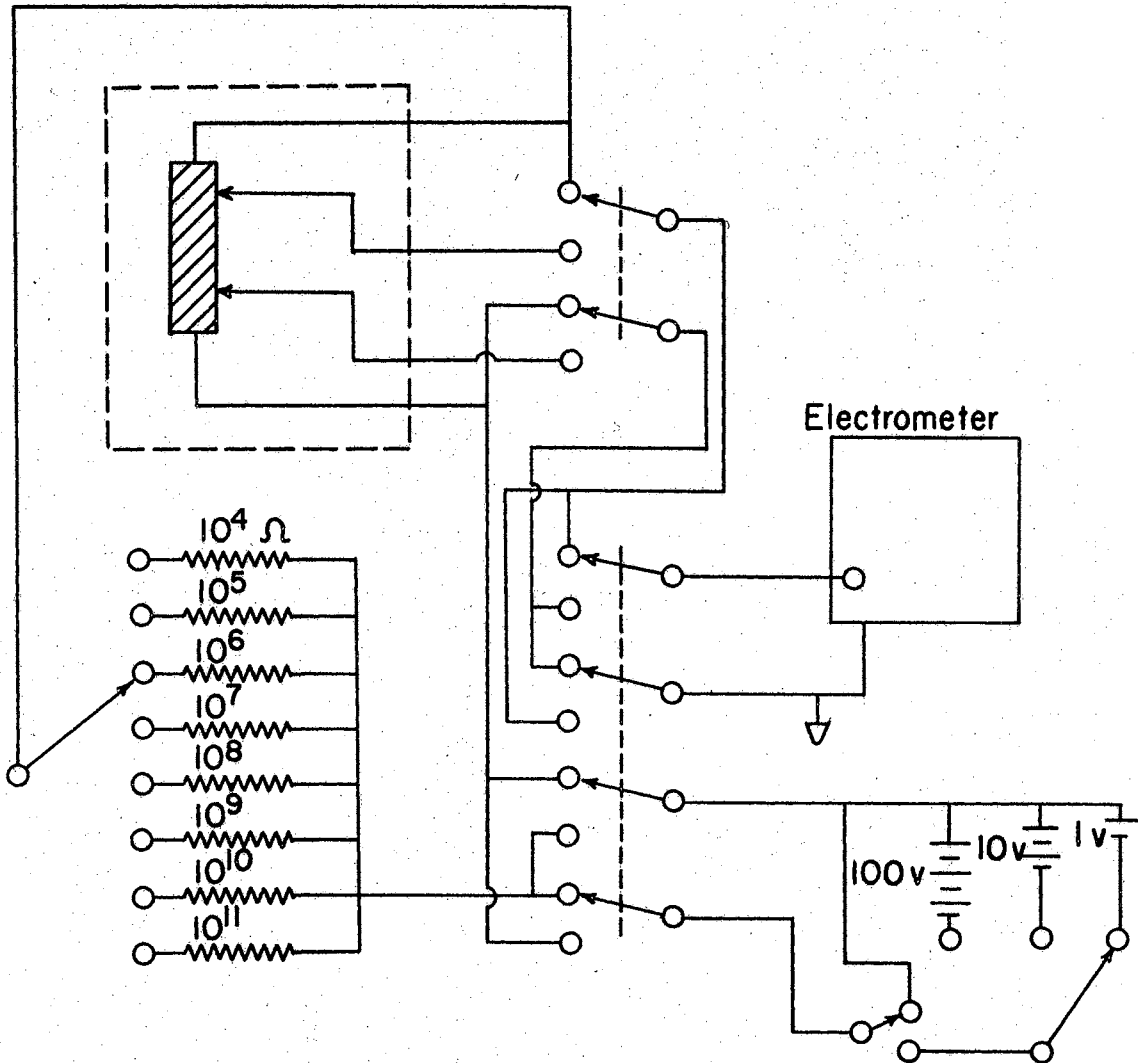
Figure 53. Proposed Electrical Circuitry for Two or Four Probe
Conductivity with Small Applied Potentials

BIBLIOGRAPHY

1. Verwey, E. J. W., Semiconducting Materials, ed. H. K. Henisch, Butterworths Scientific Publications Ltd., London (1951).

2. Gray, T. J., Semiconducting Materials, ed. H. K. Henisch, Butterworths Scientific Publications Ltd., London (1951).

3. Gray, T. J., Chemistry of the Solid State, ed. W. E. Garner, Butterworths Scientific Publications Ltd., London (1955).

4. Kingery, W. D., Introduction to Ceramics, John Wiley & Sons, Inc., New York (1960).

5. Coffeen, W. W., J. Am. Ceram. Soc., 36, 207 (1953).

6. U. S. Pat. 2,617,745 (Nov. 11, 1952) Pittsburgh Plate Glass Co.

7. Berkman, S., Morrell, J. C. and Engloff, G., Catalysis, Reinhold Publishing Corp., New York (1940).

8. Bauer, G., Ann. Physik., 30, 433 (1937).

9. Fisher, A., Z. Naturforsch, 9a, 508 (1954).

10. Foex, M., Bull. Soc. Chim. France, 11, 6 (1944).

11. LeBlanc, M. and Sache, H., Physik Z., 32, 887 (1931).

12. Loch, L. D., J. Electrochem. Soc., 110, 1081 (1963).

13. Kohnke, E. E., J. Phys. Chem. Solids, 23, 1557 (1962).

14. Kunkle, H. F., Unpublished Ph.D. dissertation, Oklahoma State University (1966).

15. Houston, J. E., Unpublished Ph.D. dissertation, Oklahoma State University (1965).

16. Marley, J. A. and MacAvoy, T. C., Investigations of the Mechanism of Single Crystal Growth in High Temperature Systems, Final Report, June 1961-June 1962, Contract No. AF 19(604)-8447.

17. Morgan, D. F. and Wright, D. A., Brit. J. Appl. Phys., 17, 337 (1966).

18. Nagasawa, M., Shionya, S. and Makishima, S., J. Phys. Soc. Japan,

20, 1093 (1965).

19. Marley, J. A. and Dockerty, R. C., Phys. Rev., 140, A304 (1965).

20. Johnson, V. A., Progress in Semiconductors Vol. I, Ed. A. F. Gibson, John Wiley & Sons, Inc., New York (1956).

21. Kittel, C., Introduction to Solid State Physics, John Wiley & Sons, Inc., New York (1956).

22. Kevane, C. J., Phys. Rev., 133, A1431 (1964).

23. Shockley, W., Electrons and Holes in Semiconductors, D. Van Nostrand Company, Inc., Princeton, New Jersey (1950).

24. Blakemore, J. S., Semiconductor Statistics, Pergamon Press, New York (1962).

25. Medved, D. B., J. Phys. Chem. Solids, 20, 255 (1961).

26. Vinetskii, V. L. and Kholodar, G. A., Phys. Stat. Sol., 19, 41 (1967).

27. Von Hippel, A., Kalnajs, J. and Westphal, W. B., J. Phys. Chem. Solids, 23, 779 (1962).

28. Lee, V. and Mason, D. R., J. Appl. Phys., 35, 1557 (1964).

29. Lee, V. and Mason, D. R., J. Appl. Phys., 34, 2660 (1963).

30. Seiwatz, R. and Green, M., J. Appl. Phys., 29, 1034 (1958).

31. Kingston, R. H. and Neustadter, S. F., J. Appl. Phys., 26, 718 (1955).

32. Glemza, R. and Kokes, R. J., J. Phys. Chem., 66, 566 (1962).

33. Saltzburg, H. and Snowden, D. P., J. Phys. Chem., 68, 2734 (1964).

34. Landsberg, P. T., J. Chem. Phys., 23,   (1955).

35. Kroger, F. A. and Vink, H. J., Solid State Physics, Advances in Research and Applications, Vol. III, Ed. F. Seitz and D. Turnball, Academic Press Inc., New York (1956).

36. Mitoff, S. P., J. Chem. Phys., 41, 2561 (1964).

37. Wagner, C., Z. Electrochem., 60, 4 (1956).

38. Vest, R. W., The Electrical Behavior of Refractory Oxides, Progress Report, Feb. 1961 - Feb. 1963 Contract No. AF 33(616)-7748.

39. Kunkle, H. F., J. Appl. Phys., 36, 1489 (1965).

40. Matthews, H. E., Unpublished Master's Thesis, Oklahoma State University (1965).

41. Summitt, R., Marley, J. A., and Borelli, N. F., J. Phys. Chem. Solids, 25, 1465 (1964).

42. Reddaway, S. F., and Wright, D. A., Brit. J. Appl. Phys., 16, 195 (1965).

43. Arai, T., J. Phys. Soc. Japan, 15, 916 (1960).

44. Blumenthal, R. N., and Pinz, B. A., J. Appl. Phys., 38, 2376 (1967).

VITA

James Luther Rutledge

Candidate for the Degree of

Doctor of Philosophy

Thesis: SEEBECK EFFECT AND ELECTRICAL CONDUCTIVITY OF STANNIC OXIDE AS A FUNCTION OF TEMPERATURE AND AMBIENT PRESSURE

Major Field: Physics

Biographical:

Personal Data: Born in Woodward County, Oklahoma, October 1, 1937, the son of Henry and Tena Rutledge.

Education: Graduated from Woodward High School in Woodward, Oklahoma, in 1955; received a Bachelor of Science degree from Oklahoma State University, with a major in Physics, in May, 1963; received a Master of Science degree from Oklahoma State University, with a major in Physics, in May, 1966; completed requirements for the Doctor of Philosophy degree in May, 1968.